

Insertion of Membrane Proteins in Artificial Polymer Membranes

Inauguraldissertation

zur

Erlangung der Würde eines Doktors der Philosophie

vorlegt der

Philosophisch-Naturwissenschaftlichen Fakultät

der Universität Basel

Von

Alexandra Graff

aus Colmar (Frankreich)

Basel, 2004

Genehmigt von der Philosophisch-Naturwissenschaftlichen Fakultät

Auf Antrag von

Herrn Prof. Dr. Wolfgang Meier (Universität Basel)

Herrn Prof. Dr. Mathias Winterhalter (Universität Bremen)

Herrn Prof. Dr. Hanspeter Huber (Universität Basel)

Basel, den 27.01.2004

Prof. Dr. Hans-Jakob Wirz

Dekan

Table of contents

Abstract

General Introduction	1
1. Stabilization Strategies of Model Membranes: Examples and Applications	5
2. Block Copolymers: Physico-Chemical Properties, Characteristics	9
2. 1. <i>A-B and A-B-A block copolymer molecular structures and superstructures organization</i>	
2. 2. <i>Self-assembly definitions and principles</i>	
2. 3. <i>Self-assembly of amphiphilic block-copolymer</i>	
3. Block Copolymer Vesicles: Principle of Formation and Applications	13
3. 1. <i>Principle of vesicle formation</i>	
3. 2. <i>Polymer vesicles properties</i>	
4. Presentation of The Membrane Protein-Porin Superfamily	20
4. 1. <i>Introduction to porin structure and function: The general diffusion pores (OmpF)</i>	
4. 2. <i>Maltoporin monomer structure</i>	
Chapter 1: Insertion of Proteins in Polymer-Stabilized Lipid Membranes	27
Summary	28
Publication 1: Stabilization of Planar Lipid Membranes: a Stratified Layer Approach	29

Publication 2: Nanoreactors from Polymer-Stabilized Liposomes	34
Additional results (Publication 2)	40
Chapter 2: Insertion of Membrane Proteins in Block Copolymer Membranes	42
Summary	43
Publication 3: Virus-Assisted Loading of Polymer Nanocontainers	44
Additional results (Publication 3)	50
1. <i>Infection of Lambda phage in polymerized ABA triblock copolymer vesicles</i>	
2. <i>Lambda phage DNA release from ABA triblock copolymer vesicles prepared with two different polymers: A comparative study</i>	
3. <i>DNA loading into lipid and ABA triblock copolymer vesicles: A comparative study</i>	
4. <i>Membrane protein titration assay into ABA triblock copolymer vesicles</i>	
Incorporation of Complex I in Block Copolymer Vesicles	58
1. <i>Structure and functions of NADH: ubiquinone oxidoreductase (complex I) from Escherichia coli</i>	
2. <i>Strategies for complex I incorporation in block copolymer vesicles</i>	
3. <i>Complex I functional incorporation: results and discussions</i>	
4. <i>Proton and electron transport across the polymer membrane:</i>	
5. <i>results and discussions</i>	
<i>Principle of electron transfer experiments</i>	
<i>Electron's pathway in complex I</i>	
<i>Principle of proton transfer experiments</i>	
6. Conclusion	

Reconstitution of The Membrane Protein Hemagglutinin in Block Copolymer Membranes	76
Summary	77
1. Structures and function of the flux membrane protein hemagglutinin	
2. Hemagglutinin (HA) insertion in block copolymer vesicles and induction of fusion with lipid membranes	
2. 1. <i>Results and discussions</i>	
2. 2. <i>Conclusion</i>	
Incorporation of FhuAΔ5-160 in Block Copolymer Vesicles	86
Summary	87
1. Structures and function of FhuAΔ5-160 from <i>Escherichia coli</i>	
2. FhuAΔ5-160 incorporation and functionality test: Results and discussions	
2. 1. <i>Conclusion</i>	
Summary	94
Materials and Methods	97
1. Lipids, enzymes and fluorescent probes	97
1. 1. <i>Commercial products</i>	
1. 2. <i>β-lactamase production and purification</i>	
2. Protein and phage purifications	98
2. 1. <i>The outer membrane protein OmpF</i>	
2. 1. 1 <i>Purification of plasmid DNA</i>	
2. 2. <i>LamB membrane protein</i>	
2. 3. <i>NADH:oxydo-reductase (complex I)</i>	

2. 4.	<i>Hemagglutinin (HA)</i>	
2. 4. 1	<i>Virus</i>	
2. 4. 2	<i>Preparation of HA Rosettes</i>	
2. 5.	<i>FhuA purification</i>	
2. 6.	<i>Preparation of phage λ</i>	
3.	<i>PMOXA-PDMS-PMOXA triblock copolymer synthesis and characteristics</i>	103
3. 1.	<i>Polymer used</i>	
3. 2.	<i>Polymer characterization</i>	
4.	<i>Membrane protein reconstitution in liposomes and triblock copolymer vesicles</i>	105
4. 1.	<i>Liposomes, proteoliposomes preparation</i>	
4. 1. 1	<i>OmpF and LamB reconstitution</i>	
4. 1. 2	<i>Complex I reconstitution</i>	
4. 1. 3	<i>Preparation of fluorescent labelled liposomes</i>	
4. 2.	<i>Protein reconstitution in triblock copolymer vesicles</i>	
4. 2. 2	<i>Triblock copolymer vesicles preparation and reconstitution of LamB</i>	
4. 2. 2. 1	<i>Triblock copolymer vesicles preparation</i>	
4. 2. 2. 2	<i>Reconstitution of LamB</i>	
4. 2. 3	<i>Complex I reconstitution</i>	
4. 2. 4	<i>Hemagglutinin reconstitution</i>	
4. 2. 5	<i>FhuA reconstitution</i>	
5.	<i>Dynamic light scattering (DLS)</i>	109
6.	<i>Langmuir film experiments</i>	109
6. 1.	<i>Surface pressure measurements</i>	
6. 2.	<i>Amphiphile spreading</i>	
6. 3.	<i>Isotherm measurements</i>	

7. Fluorescence spectroscopy	112
7. 1. <i>Steady-state fluorescence</i>	
7. 2. Fluorescence resonance energy transfer (FRET)	
7. 2. 1 Principle of FRET	
7. 2. 2 Prerequisites conditions for FRET	
7. 2. 3 Membrane fusion	
7. 2. 3. 1 General Principle	
7. 2. 3. 2 Fusion Assays	
8. Transmission electron microscopy (TEM)	115
8. 1. <i>Sample preparation</i>	
References	116

Abstract

The last few decades have seen a huge growth in research on “soft materials”. A large part of the research in this field was dedicated to the preparation of new types of artificial membranes, which behave similar to lipid or cell membranes. A particular challenge is the preparation of stabilized, flexible, adaptable and responsive materials. Similar to nature such systems can only be realized using hierarchically self-assembled systems.

In this context we have introduced a new way of stabilizing lipid-bilayers using hydrophobic polymer scaffold. In contrast to other approaches, presented by Ringsdorf *et al.*, 1988, the hydrophobic polymer scaffold allowed us to insert membrane proteins into the polymer stabilized membranes. One representative example of the functional insertion of a membrane protein into such stabilized membranes will be described in the present work.

In another approach we used the self assembling capacity of amphiphilic block copolymers to prepare stable biomimetic membranes. The last few years have seen considerable progress in the development of block copolymer chemistry. Particularly, a whole series of new amphiphilic block copolymers with low glass-transition temperatures have been introduced. The diversity of block copolymer chemistry allows to vary the chemical constitution, such as the nature and the sequence of the repeat unit (as mentioned in a later section), the length and the different structures of the different blocks and even the molecular architecture of the whole polymer, block, graft, star, etc. This may lead to the formation of new types of self-assembled superstructures that are not accessible to conventional low molar mass amphiphiles.

Recently our group introduced a new type of amphiphilic block copolymer composed of two hydrophilic side blocks poly-methyloxazoline (PMOXA) and one hydrophobic middle block poly-dimethylsiloxane (PDMS), forming an ABA triblock copolymer. The physico-chemical characterization of the ABA block copolymer has been described by Nardin *et al.*

Similar to conventional low molar mass amphiphiles (lipids, surfactants), this polymer self-assembles in aqueous media and forms well defined superstructures. Depending on its molecular composition and the experimental conditions various lyotropic mesophases, vesicles and nanotubes have been identified. Most interestingly it has been shown that membranes formed by such polymers could be used as a matrix for the incorporation of integral membrane proteins.

In the present work we developed new procedures for membrane proteins that are adapted and optimized with respect to the artificial polymer membranes. For that purpose we performed a series of experiments with different membrane proteins that have different structural properties and functionality. In all systems investigated we could successfully proof the incorporation and the functionality of the proteins.

For a first experiment we used well characterized and stable membrane proteins like bacterial porins. Porins are well characterized integral membrane proteins possessing interesting structural and physical properties, such as hydrophobic β -strands, which can interact and insert into the hydrophobic part of the block copolymer. Additionally, the porins form β -stranded pores, which allow a passive and selective transfer of small molecules across a membrane.

Then, more complex membrane proteins were used such as hemagglutinin or NADH:oxydoreductase. Both proteins are composed of a large soluble part which contributes to their structural and functional particularities. The globular part of hemagglutinin is involved in the fusion of two membranes whereas the soluble part of NADH:oxydoreductase is responsible for proton and electron transfer across the membrane.

The combination of natural proteins with artificial polymer membranes allows the formation of a new type of hybrid material combining the mechanical, chemical, and biological stability of the amphiphile block copolymer and the functional specificity of membrane proteins.

General Introduction

Biological membranes play a central role for the structure and function of cells. Their complex self assembled structure and composition is a prerequisite for the multiple functions that these membranes fulfil. Biological membranes act as a barrier that protects the inner space of a cell from the surrounding medium. Since the cell needs also to communicate and to interact with its surrounding a highly selective permeability is required that allows a molecular or signal exchange. Nature solved this by using a composite material formed by a lipid matrix in which highly specialized and optimised proteins fulfil the respective functions. These proteins may be divided structurally into two types: integral membrane proteins and peripheral membrane proteins as presented in Figure 1.

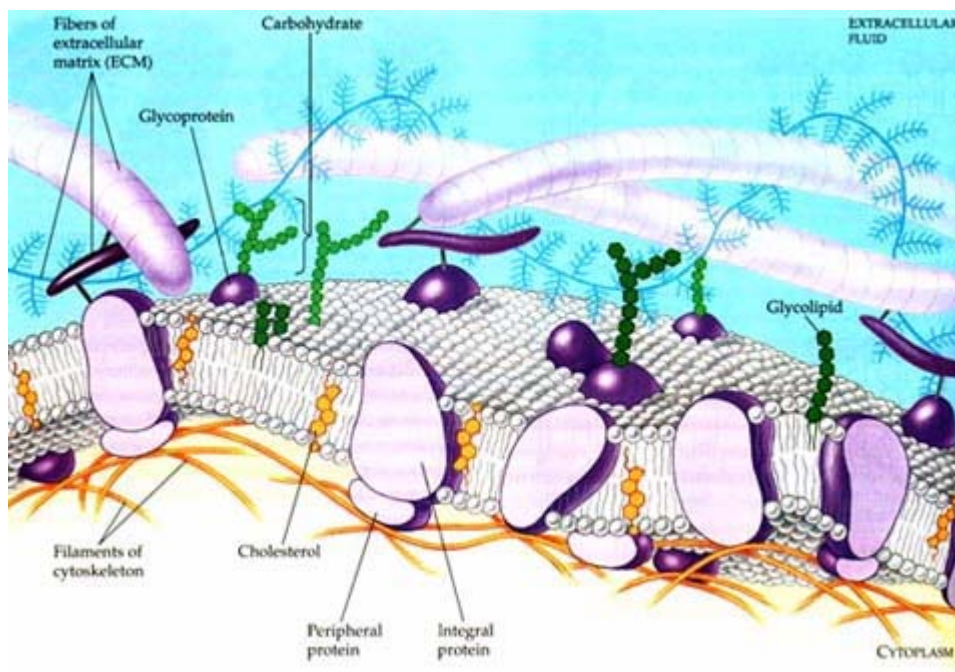


Figure 1. The detailed structure of animal plasma membrane, in cross section (@ Addison Wesley Longman, Inc).

The first type, integral proteins, are completely embedded into the lipid membrane whereas the second type, peripheral proteins, are partially inserted in the membrane and connected with a soluble part. They possess different functions, such as transport of molecules through the membrane (transporter), or anchoring point of cytoskeletal or extracellular elements (linker). They also allow selective receptivity and signal transduction (receptor) or are involved in enzymatic reactions (enzyme). Moreover, the cell membrane is involved in many different specialized processes like cell recognition and adhesion or immune reactions.

Figure 2 presents an overview of the various processes modulated by the cell membrane.

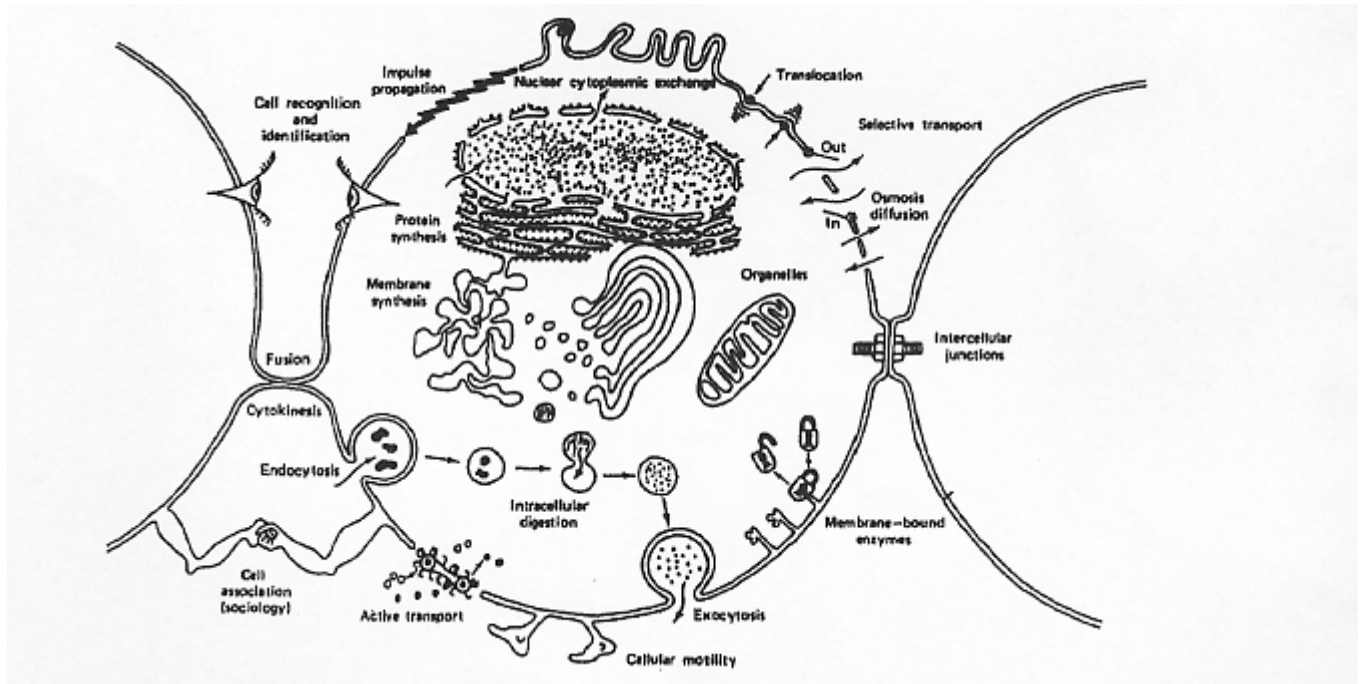


Figure 2: Cartoon of a typical cell, with emphasis on the various processes modulated by the cell membrane. (Jain and Wagner, 1980).

Furthermore, it has to be emphasized that biological membranes are able to self repair. It has also to be emphasized that many tissue environments generate and receive “physiological” levels of mechanical forces that impose shear, tensile, and compressive stresses on the constituent cells. In the course of such processes the integrity of biological membranes can be lost and hence disruption is a very common event found in many animal tissues. For example, plasma membrane disruption can be induced in muscles of cardiac and skeletal myocyte population during forced exercises or in various skin cells submitted to needle puncture, etc (Mc Neil and Khakee, 1992; Mc Neil and Ito, 1990). This induces an adaptive response of the cells which initiates an active repair-mechanism to restore or reseal the membrane. Recently it has been demonstrated that this repair process requires exocytotic events, which are largely mediated by a number of proteins. For example, Ca^{2+} -dependent exocytosis process utilizes vesicles docking/fusion SNARE (soluble N-ethylmaleimide-sensitive factor attachment protein receptor) proteins (Steinhardt *et al.*, 1994; Togo *et al.*, 1999).

Also new vesicle pools, which are necessary for cell repair, are generated via a protein kinase C (PKC)-dependent process (Togo *et al.*, 1999). Under certain conditions also artificial bilayers have the ability to self repair. In contrast to living cells this occurs as a purely passive process extensively, using giant liposomes and planar bilayers pores in lipid bilayers that are below a critical size will close rapidly if membrane tension is low. With increased membrane tension, the rate of resealing will be slowed, and, for larger tensions, pores grow and cause membrane lysis (Taupin *et al.*, 1975; Zhelev and Needham, 1993; Moroz and Nelson, 1997).

However, in contrast to biological membranes, artificial systems like liposomes do not possess the possibility to restore the membrane integrity after significant damage. This is due to the lack of an active self-repair.

Generally artificial lipid membranes are widely studied as a model system in different areas, such as theoretical physics, colloid and interface science over applied biochemistry (function of membrane proteins), to biology (excretion, cell function, trafficking and signaling, gene delivery, and function) (Lasic, 1993). Moreover, spherically closed lipid bilayers, so called liposomes have attracted considerable interest for applications, as controlled delivery devices for drugs (antifungal, anticancer agents, vaccines), non-viral gene delivery vectors, cosmetic formulations (skin-care products, shampoo) and diagnostic tools. Over the years, basic research led to further improvement of their formulation, mainly aimed at improving their stability and interaction characteristics (e.g., 'stealth' liposomes). However most of these technical application require a long term stability that cannot be reached with conventional lipids.

In the 1980's various stabilization strategies were developed (Ringsdorf *et al.*, 1988). Most of these strategies are based on the use of polymeric systems sketched as in Figure 3. These strategies will be presented further.

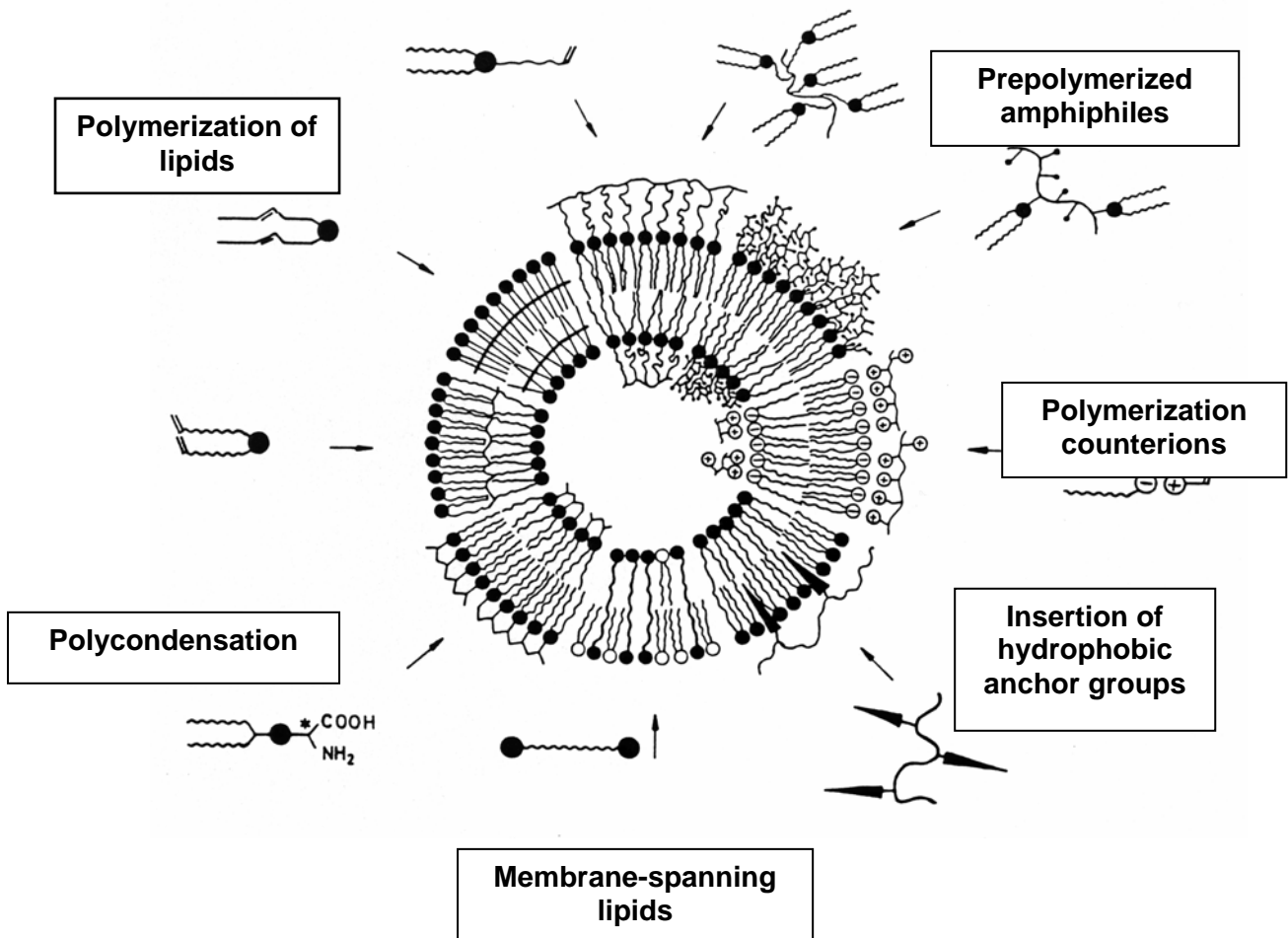


Figure 3: Strategies for the stabilization of lipid bilayer membranes (Ringsdorf *et al.*, 1988)

1. Stabilization Strategies of Model Membranes: Examples and Applications

In this section the different stabilization strategies and different types of polymeric model membranes are introduced. Stabilization of a membrane can be performed by using for example polymerizable amphiphile molecules (Figure 4) or by using prepolymerized lipids (Laschewsky *et al.*, 1987; Laschewsky *et al.*, 1986; Ringsdorf *et al.*, 1987; Frey *et al.*, 1987).

Polycondensation of liposomes is another possibility to prepare stable membranes. For example, lipids such as amino dicarboxylic acid lipids were used. This formation of stable polypeptide liposomes was described by Neumann *et al.* (Neumann and Ringsdorf, 1986; Neumann *et al.*, 1987).

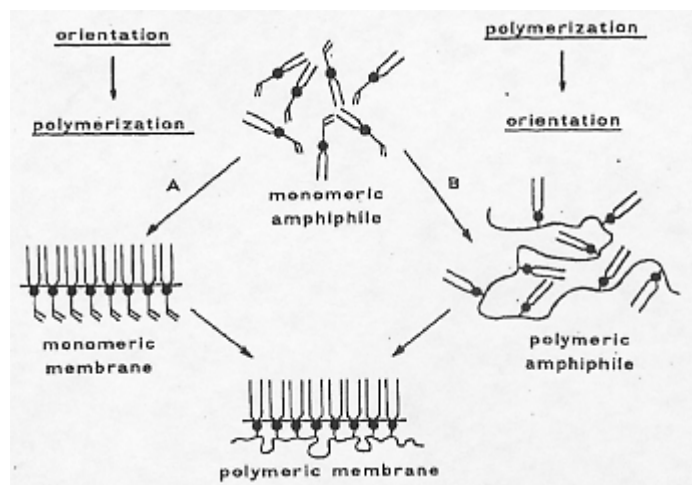


Figure 4: Strategies for the preparation of polymeric model membranes. A) Orientation of the monomers in model membranes with subsequent polymerization. B) Polymerization of the monomers in isotropic solution and subsequent orientation of the polymeric amphiphiles.

As demonstrated by the group of Okahata and Kunitake (Okahata and Kunitake, 1979) or the group of Fuhrhop (Fuhrhop *et al.*, 1982; Fuhrhop and Mathieu, 1983; Fuhrhop *et al.*, 1986; Fuhrhop and Fritsch, 1986) stable membrane can also be prepared from “mimetic” of membrane components of the archebacteria. The archebacteria can adapt to extreme conditions, like temperatures up to 110°C, pH values around 1 or saturated salt medium, thanks to their membrane components of unusually stable structure. From those components, so called bipolar lipids (that are structurally related to ABA-triblock copolymer), they prepared “monolayer” vesicle membranes (Fuhrhop and Mathieu, 1983). Membrane-spanning bipolar lipids, so-called “bola amphiphiles”, can also form for example small unilamellar vesicles with asymmetrical membrane orientation (Fuhrhop and Mathieu, 1983) when asymmetrical bipolar lipids are used. In addition this kind of membranes can be polymerized when they contain for example butadiene units as introduced by Bader *et al* (Bader and Ringsdorf, 1982).

A completely different approach is to stabilize the membranes by polymeric supports or “skeletons” that are attached to the membrane in different ways. A first approach was based on coating the membrane surface using either water-soluble polymers or water-soluble polymers containing hydrophobic anchor groups. For example, Tirrell *et al.* investigated the interaction

between synthetic polyelectrolytes and liposomal membranes (Borden *et al.*, 1987; Tirrell *et al.*, 1985; Seki and Tirrell, 1984, Takigawa and Tirrell, 1985) or Sunamoto's group showed that liposomes were stabilized using hydrophobically modified polysaccharides as a coating system (Takada *et al.*, 1984). This led to an artificial cell wall comparable to the cell-walls of plants.

Another approach involved a polymerization of the liposome surfaces. For this purpose, charged liposomes were prepared, then polymerizable counter ions were introduced to the inner, the outer or both surface sides of the vesicle membrane. After UV polymerization, the vesicle membranes are surrounded by asymmetric or symmetric polyelectrolyte chains bound via electrostatic interaction. This leads to the formation of a 2-D network (Torchilin *et al.*, 1987; Ringsdorf and Schlarb, 1986). Interestingly, this artificial cytoskeleton does not affect the membrane permeability, as shown by experiments with [³H]glucose (Ringsdorf *et al.*, 1988 a)).

These last studies dealt with vesicles stabilized by surface coating or surface polymerization. Despite the fact that the flexibility and stability were not affected, the encapsulation rate of compounds was reduced using this kind of stabilization.

One major drawback of all the stabilization strategies presented so far is that they did not preserve the mobility of the lipid molecules in the membrane. It as to be emphasized that such a mobility is a critical condition for the functionality of many membrane proteins.

In the present work we propose a new stabilization strategy where the lateral mobility of the lipids is preserved in the membrane. Similar to the previous approach we used the interaction of an independent 2D-polymer network with the lipid membrane. In contrast to previous studies we used hydrophobic interactions i. e. hydrophobic polymers that are dissolved in the hydrophobic part of the lipid membrane.

The enormous stabilization of a lipid bilayer by such "internal" polymer scaffolds could be demonstrated by electroporation experiments on free-standing film, so called black lipid membranes where short electric voltage pulses were applied across the membrane. The critical voltage leading to rupture is directly related to the stability of the "black lipid membrane".

Interestingly the polymer supported membranes required an extremely high energy for the formation of a defect that is large enough to induce breakdown of the entire membrane.

In the second step we incorporated this 2-D polymer networks also into the lipid bilayers of liposomes (Publication 2). Lysis experiments with detergents demonstrated again a drastic stabilization of the membranes. Moreover functionality of membrane proteins in the walls of

such liposomes was not affected. The results for such polymer-stabilized membranes are summarized in chapter 1.

Here we functionalized these membranes with OmpF membrane proteins. OmpF forms pores in the membrane and allows the passive diffusion of small solutes ($>400 \text{ g}\cdot\text{mol}^{-1}$). Structural and functional properties of OmpF will be presented in chapter 2.

The polymeric scaffold increased the colloidal stability of the liposomes considerably, but pharmaceutical or medical applications requires also biocompatibility and “protection” from the immune system. Generally, foreign particles are rapidly recognized and eliminated by macrophages. To overcome this problem sterically stabilized liposomes were developed, so called, “stealth” liposomes (Lasic and Martin, 1995). They consist of lipids which are grafted on their polar head with polyethylene glycol (PEG). These hydrophilic polymer chains enhance their stability and reduce their reactivity against plasma proteins and cell surface receptors. One main drawback of this approach is that it is still based on lipids which definitively limits the variability of chemical and physical properties.

Here the development of material science and its growing interest in new types of intelligent superstructures or materials has opened the opportunity for the development of amphiphilic materials that behave similar to lipids. In this field, block copolymers are of particular interest. The characteristics and properties of block copolymers will be described in detail, together with the principle of self-assembly. Attention will also be focused on various morphologies of polymer aggregates formed by self-organization. Even if self-assembly is considered as a universal process, we will focus mainly on the behavior of block copolymers in aqueous solution. Moreover, a particular section will be dedicated to.

Like conventional amphiphiles and lipids, amphiphilic block copolymers can form vesicles in aqueous solutions. Compared to phospholipids, polymer bilayers and vesicles not only have the advantage of higher stability and toughness, but, in addition, offer numerous possibilities for tailoring physical, chemical, and biological properties by variation of block lengths, chemical structure, and conjugation with biomolecules. Hence, vesicle research has been released from the constraints of natural lipids, extending potential experiments and applications to new functions, other solvents, other temperature ranges, etc. Also many functions can be integrated simultaneously either in a single polymer chain, or by simply admixing a polymer into the bilayer. This opens a broad field for functionalizing polymer vesicles for potential applications in pharmacy, agro-chemistry, sensors, and material synthesis.

2. Block Copolymers: Physico-Chemical Properties and Characteristics

2.1. A-B and A-B-A block copolymer molecular structures and superstructures organization

When a polymer is made by linking only one type of small molecules (monomer) together, it is called a **homopolymer**. When two different types of monomers are joined in the same polymer chain, the polymer is called a copolymer.

In these studies, block copolymers were used and are macromolecules consisting of at least two chemically different polymer chains that are covalently linked together. Due to the inherent incompatibility of different polymer chains individual molecules of block copolymers are integrated into larger functional units and structural hierarchies by self-organization. The principle of self-assembly will be described in the following paragraph.

2.2 Self-assembly definitions and principles

Definitions:

The term “self-assembly” does not have a precise definition, and, indeed, has often been abused. A wide variety of phenomena are regarded as self-organization in the various scientific disciplines, and the definitions applied differ.

For example in **chemistry**: well-defined structures result spontaneously from the components of a system by non covalent forces (self assembly), like in liquid crystals, micelles, oscillating reactions.

In **biology**, it is a spontaneous building-up of complex structures which takes place under adequate environmental conditions solely on the basis of the respective molecular property, namely, without the effect of external factors, for example, protein folding, formation of lipid double layers, morphogenesis.

In **physics** it is the spontaneous formation of new three-dimensional and temporal structures in complex systems which results from the cooperative effect of partial systems, for

example, ferromagnetism, superconductivity, convention cells (Falbe and Regitz, 1996; Anderson and Stein, 1987; *Lexikon der Biologie*, Spektrum, Heidelberg, 2000). Although there is different phenomena observed, there is a fundamental common mechanism.

As common definition, we can say that self-assembly does not refer to the formation of any assembly of atoms or molecules, rather to the reversible and cooperative assembly of predefined components into an ordered superstructure. Two types of self-assembly have been distinguished by Whitesides (Whitesides and Grzybowski, 2002). Static self-assembly involves systems at equilibrium that do not dissipate energy. The formation of a structure may require energy, but once formed it is stable. On the other hand, in dynamic self-assembly the formation of structure or patterns occurs when the system dissipates energy. Examples are patterns formed during reaction and diffusion processes in oscillating chemical reactions. Self-assembly of amphiphile block copolymers is driven by static self-assembly.

In the present work we were essentially interested in the formation of vesicular structures, even though many other superstructures can emerge from this principle. Some of these are presented in Figure 5 (Functional structural hierarchies from self-organizing polymers), which illustrates the different levels of polymer self-organization. This phenomenon can drive the block copolymer from a single molecular structure (AB or ABA block copolymer) to nanostructures like spherical micelle, worm-like micelle or vesicular structure.

Self-assembly:

As mentioned above, self-assembly is a “wide variety of phenomena” and was often described in the literature as a physical principle. The self-assembly or aggregation process will be mainly and in particular described for amphiphilic block copolymer in our studies.

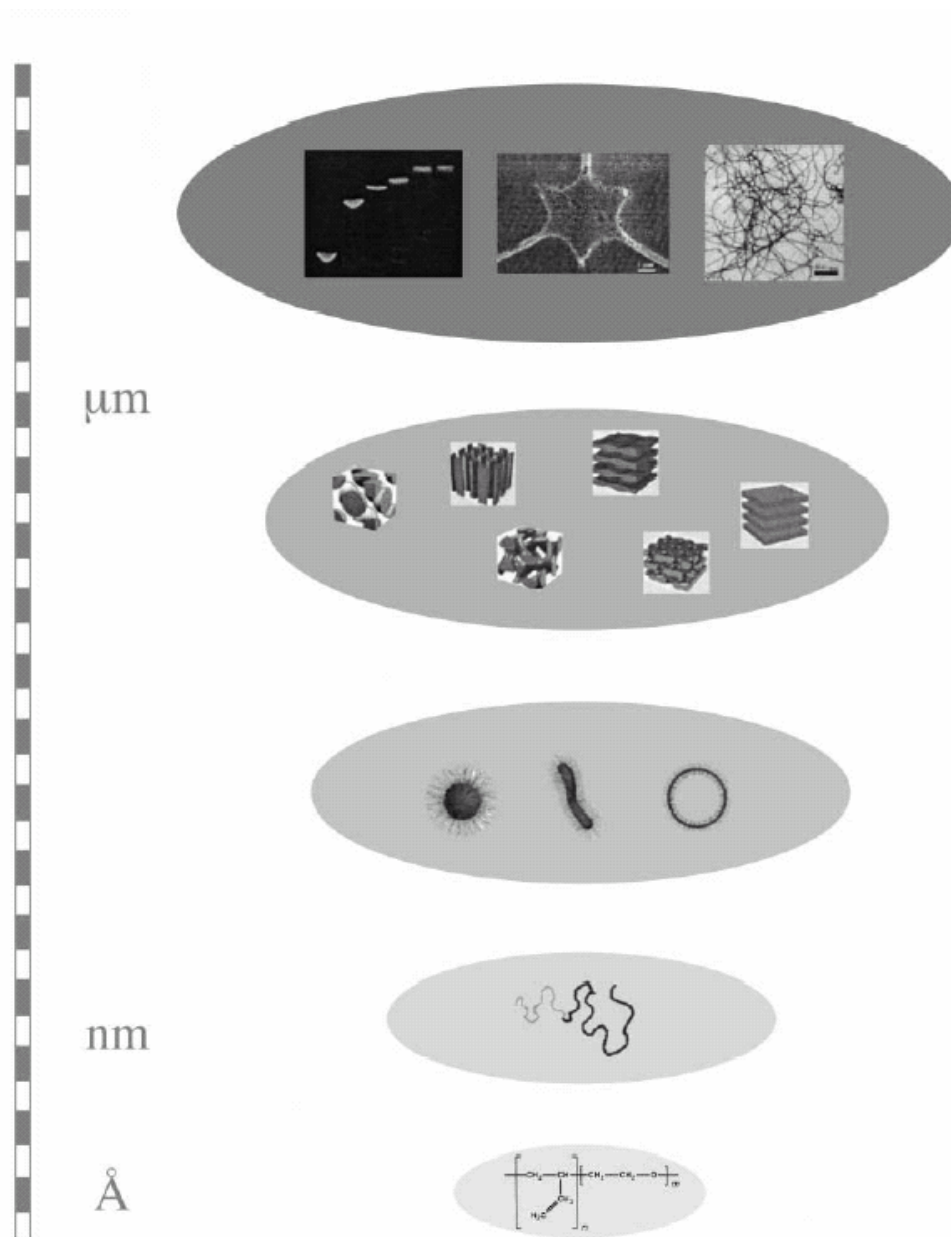


Figure 5. Functional structural hierarchies of self-organizing polymers (Förster and Plantenberg, 2002)

2.3 Self assembly of amphiphilic block-copolymer

Block copolymer self-organization can be controlled by using different parameters like temperature, block copolymer concentration, etc. For example, amphiphilic block copolymers, as well as surfactants, can form micelles (Tuzar and Kratochvil, 1993; Gast, 1998, Alexandridis, 1996; Selb and Gallot, 1985; Moffit *and al*, 1996) in dilute aqueous solutions. As the consequence of the chemical structure of the blocks, block copolymers form micelles not only in polar solvents, such as water, but also in highly non-polar media, such as fluorinated hydrocarbons or supercritical CO₂. Well-defined micelles have cores consisting of the insoluble A blocks and shells or coronas of the soluble B blocks (Figure 6).

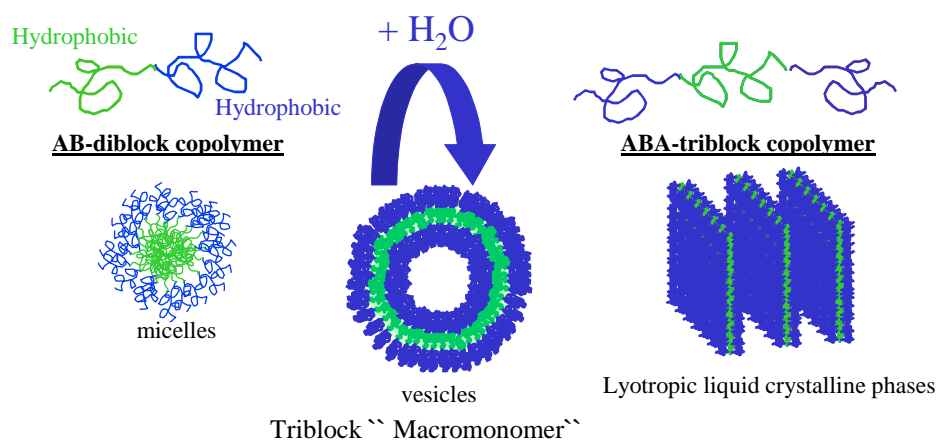


Figure 6. Amphiphilic block copolymer morphologies in aqueous dilute solution and with higher concentration of polymer.

Micelle formation is a simple and well-known example of polymer self-assembly. Block copolymers self-assemble into micelles with defined size and shape, whereby the size of the micelles depends on the length of the polymer blocks. The aggregation number Z (the number of block copolymer molecules in a micelle) and the size of the micelles can directly be set through the degree of polymerization of the blocks (Förster *et al.*, 1996). This is valid for the description of the formation of micelles made from diblock, triblock, graft, and heteroatom star copolymers, as well as for low molecular surfactants.

Frequently, the block lengths can also affect the shape of the micelles. Block copolymers with large soluble B blocks, that is, with small curvature radii R (Figure 6) preferably form spherical micelles, whereas cylindrical micelles or vesicles result from smaller soluble blocks, that is with greater curvature radii. Block copolymer vesicles were observed with diameters from 100 nm up to several micrometers. Polymer vesicles, also called polymersomes (Discher *et al.*, 1999) are mechanically and thermodynamically more stable than the well-known lipid vesicles, and are well suited for the encapsulation and the release of substances (Nardin *et al.*, 2000) (Figure 3)

3. Block Copolymer Vesicles: Principle of Formation and Applications

In this section, the process of vesicles formation will be described in more detail. These superstructures are of particular interest for many applications and especially for the design of new kinds of material.

3.1. Principle of vesicle formation

The formation of vesicles can be viewed as a two-step self-assembly process, in which the amphiphile first forms a bilayer, which then, in a second step, closes to form the vesicle. In the classical description, the factor determining the shape of self-assembled amphiphile structures is the size of the hydrophobic part relative to the hydrophilic part. It determines the curvature of the hydrophobic-hydrophilic interface. The curvature is related to the surfactant packing parameter. (Chiefari *et al.*, 1998). In order to obtain bilayers of a given block copolymer with a given volume v and length l one needs to adjust the interfacial area a until the surfactant parameter approaches unity (Figure 7).

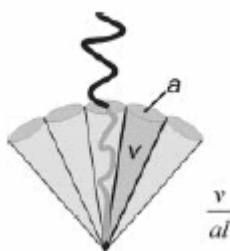


Figure 7. Description of amphiphile shape in terms of the surfactant parameter $v/(al)$ (Förster and Plantenberg, 2002).

An example is shown in Figure 8 for a series of poly(butadiene)-*b*-poly (ethylene oxide), PB-PEO, block copolymers, where the decrease of the hydrophilic/hydrophobic block ratio (as the interfacial area increases in proportion to the hydrophilic block length (Hawthorne *et al.*, 1999) leads to shape changes from spherical to cylindrical micelles and finally to vesicles.

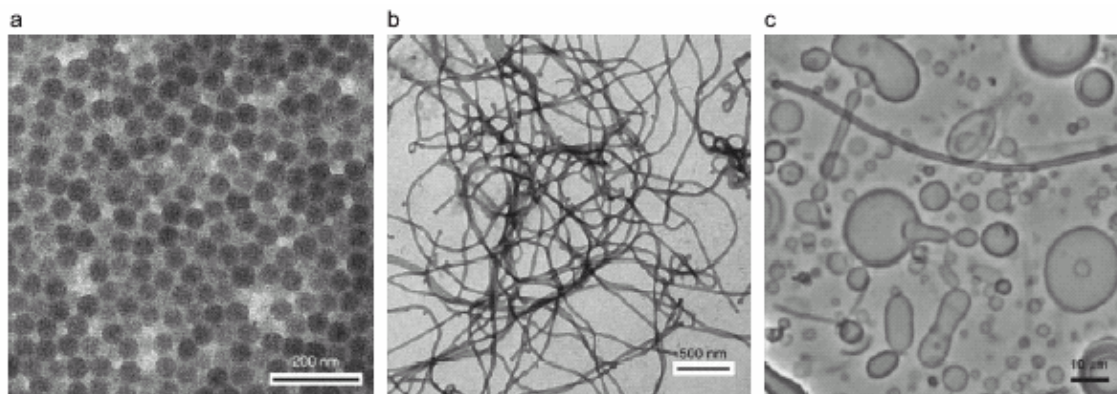


Figure 8. Transmission electron microscopy (TEM) images (a, b) and optical micrograph (c) of different shape of aggregate structures for a series of PB-PEO block copolymers ranging from spherical micelles (PB₂₀₀-PEO₃₆₀) via cylindrical micelles (PB₁₂₅-PEO₁₅₅) to vesicles (PB₃₇-PEO₄₀) (Förster and Plantenberg, 2002).

So far, the description of amphiphile aggregation has been purely geometric, yet thermodynamics also plays a role in the process. For an amphiphile, the two main contributions to the free energy are the interfacial energy of the hydrophobic-hydrophilic interface and the loss of entropy when a flexible surfactant or polymer chain is forced to fit into the aggregate microdomains. When the interfacial energy is large and the entropy loss is small, the minimization of the interfacial area dominates the association thermodynamics. Typical high-energy interfaces arranged in order of increasing interfacial energy are water-oil < water-silicon < water-fluorinated hydrocarbon. Polymers with low conformational entropy are typically stiff polymer chains with low internal degree of freedom. Under these conditions the amphiphile will associate into structures that minimize the interfacial area per unit volume. Many recent observations of bilayer or vesicle formation are that flexible alkyl chains, dendrimers, and amphiphiles need to have a very low spontaneous curvature to form bilayers.

3.2. Applications of polymer vesicles

The list of polymer vesicles applications is exhaustive, only some examples will be described in the following section.

Encapsulation and release of active compounds:

Vesicles are promising systems for the encapsulation of both hydrophilic and hydrophobic compounds. Hydrophobic compounds can be solubilized into the vesicle bilayer by stirring together with the vesicles solution or by dissolving the vesicles-forming polymer and the compound in an organic co-solvent with subsequent transfer to water. In Figure 9 a) polymer vesicles containing a fluorescent dye are presented. Other compounds of interest were encapsulated, such as carotene, vitamin E (for skin treatment and nutrition) and taxol for cancer therapy.

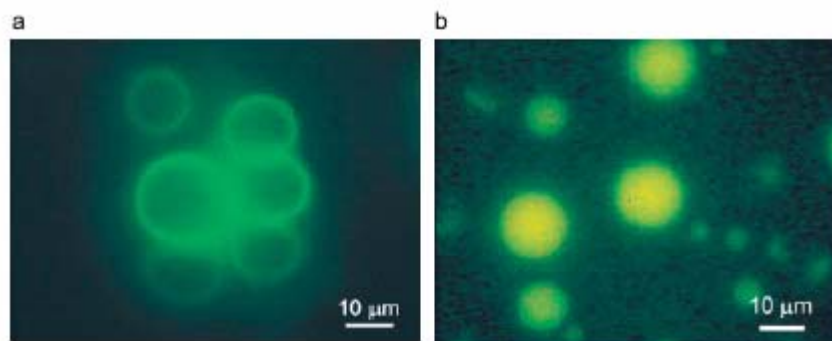


Figure 9. P2VP vesicles with luminescent CdTe quantum dots solubilized onto a vesicle bilayer (a) and encapsulated fluorescein in the interior (b) (Antonietti and Förster, 2003).

Hydrophilic molecules can be encapsulated by dissolving the block copolymer in the aqueous drug solution. Removal and recycling of non-encapsulated active substances is possible by ultra-filtration, gel filtration, or dialysis. Polymer vesicles can retain encapsulated molecules over periods of days to weeks. Figure 9 b) shows a fluorescent micrograph of polymer vesicles containing encapsulated fluorescein. Due to the larger thickness of polymer bilayers (5-20 nm) compared to lipid bilayers (3-5 nm) the permeation of molecules is much slower.

Recently the group of Nolte *et al* described the preparation of an amphiphile rod-coil diblock copolymer consisting of polystyrene and poly-3-(isocyano-L-alanyl-amino-ethyl)-thiophene (PS-PIAT). Due to a slight difference in polarity between the two blocks the diblock can behave as an amphiphile and form vesicles in both organic and aqueous solvents. The vesicles of PS-PIAT were loaded with *Candida antarctica* Lipase B (CALB) enzymes in order to form microreactors. The authors demonstrated the permeation of the enzymes substrate, 6,8-difluoro-4-methylumbelliferyl octanoate (DiFMUoctanoate) and its hydrolysis inside the vesicles by the enzyme CAL B (Vriezma *et al.*, 2003).

Interestingly, the resulting more polar product does not permeate the vesicles. Moreover, the thiophene groups located in the outer layer membrane of the aggregates can be coupled to give polymerized vesicles. The combination of polymerizable vesicles-forming diblock copolymers with the inclusion of enzymes opens the possibility to create stable micro-meter-sized reaction vessels.

Upon the designing of vesicles and triggering of solution conditions, the vesicles can also undergo spontaneous structural rearrangement to release the encapsulated substance. It is possible to prepare block copolymers forming vesicles where the solubilities of the different blocks respond to the pH, temperature, or ionic strength. For example, the pH response can be realized by using weak polybase blocks, which become protonated and water soluble at low pH. This could allow triggering the release of drugs and genes into the cytosol via endo-lysosomal acidification (Moffit *et al.*, 1996).

Additionally, it has to be emphasized that the stability of polymer vesicles against lysis by classical surfactants is much higher than that of liposomes. In contrast to lipid bilayers there is no quick dissolution of the bilayer due to the low entropy of mixing of polymers. All those properties render polymer vesicles interesting for the encapsulation and stabilization of active compounds (e.g., enzymes) in detergents and body-care products, for oral drugs that have to pass the bile system, etc.

Block copolymer-protein hybrid systems

The complexity of biological membranes in terms of their lipid, protein, and glycoprotein composition and the different nature of their functions leads naturally to the desire to separate their various components so they can be studied in simpler systems and possibly in isolation. The advent of liposomes and planar bilayer lipid membrane (BLMs) has led to the development of studies of membrane protein from structural and functional points of view. Recently, block copolymers consisting of hydrophilic and hydrophobic blocks which behave like conventional lipids, were presented (Nardin *et al.*, 2000). They can be regarded as mimetic of biological membranes and it has been shown that membrane proteins could be successfully reconstituted in such artificial polymer membranes. Surprisingly, these proteins remain functional despite the 2-3 fold larger thickness of the block copolymer membrane that does not match the hydrophobic-hydrophilic pattern of natural membrane proteins.

It seems that this requires a high flexibility of the hydrophobic blocks of the polymers that allows them to adapt to the specific geometric and dynamic requirements of membrane proteins. Under certain conditions (that is, polymerizable groups at the very ends of the hydrophilic blocks) the proteins survive even a subsequent polymerization of their block copolymer matrix

(Meier *et al*, 2000; Nardin *et al*, 2000). This leads to new polymer-protein chimeras combining the mechanical and chemical stability of block copolymer membranes with the selectivity and specificity of proteins. For instance, the outer membrane protein, OmpF, a channel protein extracted from the outer cell wall of Gram-negative bacteria has been used to control the permeability of block copolymer vesicles. Encapsulated enzymes inside such ‘nanoreactors’ showed full activity and were considerably stabilized against proteolysis and self-denaturation (Nardin *et al*, 2000). Moreover, it has been shown that a controlled transmembrane potential could be used to induce a reversible gating transition of the proteins. Since only the open channels allow the exchange of substrates and products between the container’s interior and the surrounding medium, such gating activates or deactivates the nanoreactors.

Generally, these systems have a great potential for applications in pharmacy, diagnostics and biotechnology. Suitably engineered channels for example could be used as prefilters to increase the selectivity of an encapsulated enzyme or as selective gates to trap bio-transformation products inside such nanocontainers, which could facilitate purification. In addition, due to their high mechanical and (bio-)chemical stability, the polymer containers provide a constant environment for encapsulated molecules which is of crucial importance for technical applications where storage of the systems over extended periods of time is required.

Polymers and gene therapy

Similarly to drug delivery, non-viral gene delivery consists of the transport of molecules that have a therapeutic effect on the cell. In the case of gene delivery, it can, for example, increase or decrease the expression of a specific gene, involved in a disease, using DNA, RNA, oligonucleotides or antisense sequences. Designing an optimized vector requires first the identification of the desired therapy pathway, i. e., cellular uptake *in vivo* or *in vitro* or directed to a specific tissue.

Gene therapy currently suffers from the lack of safe and efficient carriers. Genetically engineered viruses have high efficiency. However, they have only a limited genome size to insert the dedicated genes. In addition, safety issues emerging from the virus production itself and their potential immunogenicity and mutagenicity recently led to the development of various non-viral systems. Widely investigated is the complexation of DNA with cationic lipids, polycationic polymers and dendrimers (Azzam, 2002; Segura, 2001). However, *in vivo*, these vectors are affected by the interactions with the environmental components (serum, proteins) and show

only moderate transfection efficiency. Encapsulation in liposomes subsequent to precondensation reduces serum inhibition and enhances the transfection efficiency (Segura, 2001). However, the poor stability of the liposome in the blood stream is well-known. Therefore, polymer vectors allowing receptor mediated gene delivery seem to be more promising. Gene delivery using dendrimers as vehicles and a comparison with the classical techniques of gene transfer has been reviewed by Dennig and Duncan (Dennig and Duncan).

Due to their limited blood clearance and draining into the lymphatic system (in case of tissue injection), also suitable biocompatible block copolymer nanocontainers would enable a protection of the genetic material from endonucleases. In addition, block copolymer chemistry would allow preparing nanocontainers that have the potential for encapsulation of large quantities of guest molecules within their central cavity and that allow crossing the endothelium barrier. Eventually, as block copolymer chemistry allows to introduce a wide variety of moieties, cell targeting, endocytosis and nuclear uptake can be envisioned by specific targeting. Moreover, biocompatible and electrically neutral vectors based on amphiphilic block copolymers could be prepared that decrease the repulsion between the negatively charged plasmid DNA and the negatively charged cell membrane thus facilitating cellular uptake.

4. Presentation of The Membrane Protein-Porin Superfamily

Porins are found both in the outer membrane of Gram-negative bacteria and in the outer membrane of mitochondria. They are transmembrane proteins with a molecular weights from 30 to 50 kD. Porins form generally, non-specific channel pores that are regulated by environmental triggers. Additionally, they allow bacterial cells to interact with their environment through the passive diffusion of hydrophilic solutes with size exclusion limits between 400 and 6000 D. In membranes most of them arrange as trimers, such as OmpF and LamB, or monomers like FhuA.

A few porins display substrate-specificity in addition to their general diffusion properties. Maltoporin, or LamB, is among the best-studied examples of substrate-specific porins. It is responsible for the guided diffusion of maltose and maltodextrins into *E. coli* cells. Maltoporin is also one of the many porins that contain a bacteriophage recognition sequence.

4.1 Introduction to porin structure and function: The general diffusion pores (OmpF)

Interestingly, there is little to no sequence homology among porins. Nevertheless, they often share a strong structural resemblance. OmpF (for outer membrane protein f) is among the most simple *E. coli* porins and is, therefore, used as a reference in discussing the structures of more specific porins such as maltoporin. The active form of the OmpF protein is formed by linkage of three identical monomers. A major component of OmpF monomers is a 16-stranded antiparallel β -sheet barrel (Figure 1, purple) that encloses an elliptic channel 7 x 11 Å in diameter (Figure 1 a)). The channel is slightly cation selective. Successive β -strands are connected through periplasmic β -hairpin turns and long, tightly packed cell surface loops (pink loops) that differ in structure. The barrel is completed by a salt bridge-mediated linkage of the amino acid Ala and highly conserved Phe carboxyl termini in the last (16th) strand (yellow) (Figure 1 b)). The closed nature of the barrel keeps polar main chain atoms away from the membrane core by involving them in inter-strand H-bonds. Monomer barrels are further stabilized by internal loop structures and hydrogen bonding (yellow) created by Tyr residues on the barrel walls (Figure 1 c)).

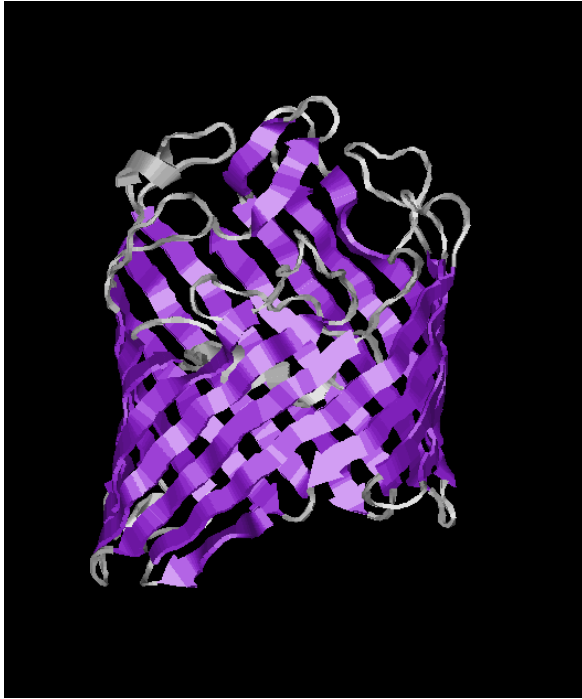


Figure 1 a). OmpF side view



Figure 1 b). OmpF side view

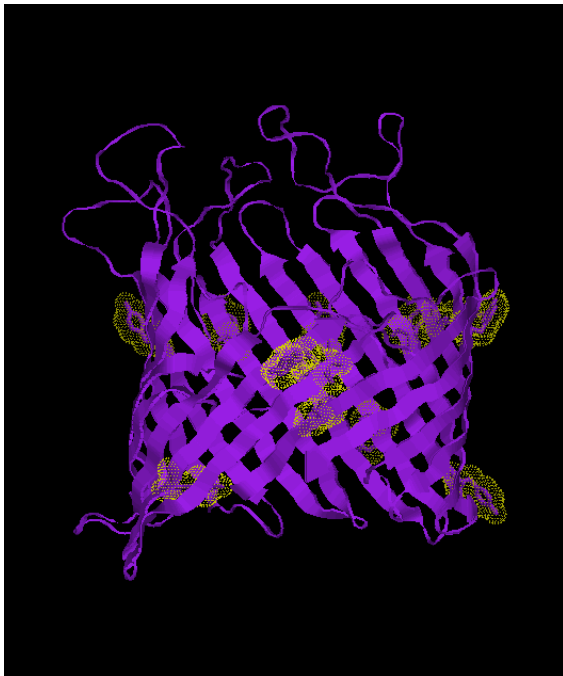


Figure 1 c). OmpF side view

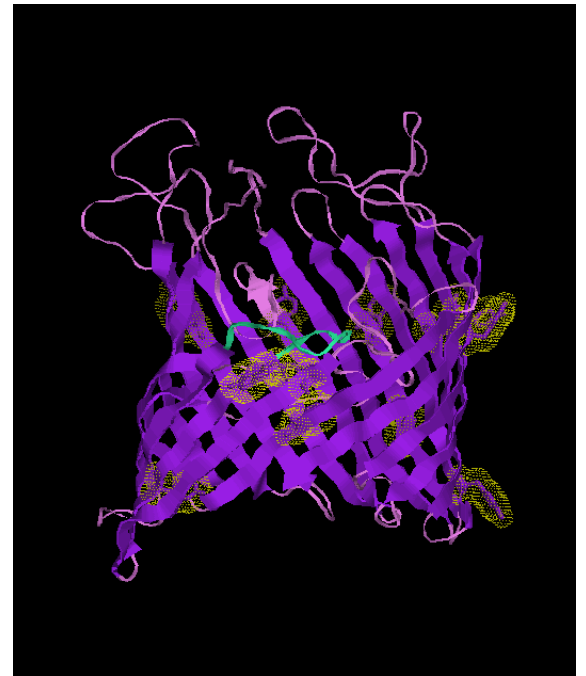


Figure 1 d). OmpF side view

Figure 1 a), b), c), d), e). OmpF is a 16-stranded antiparallel β -sheet barrel (purple) protein.

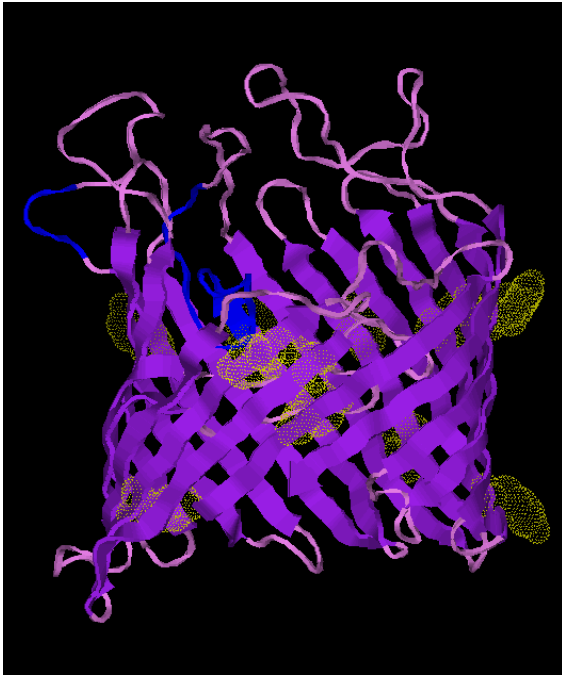


Figure 1 e). OmpF side view

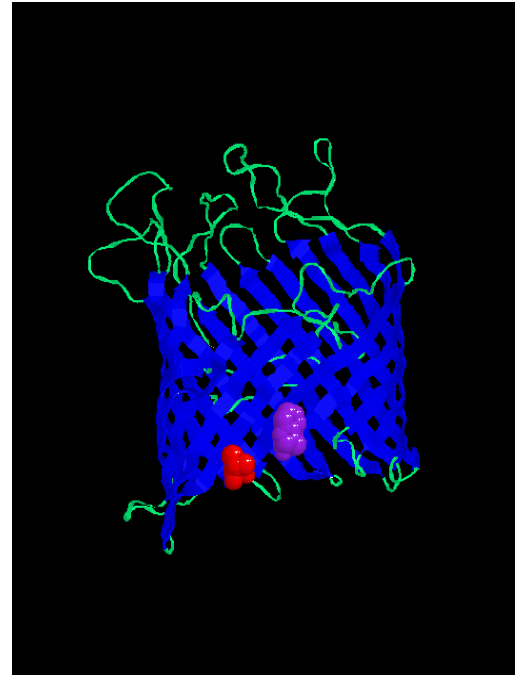
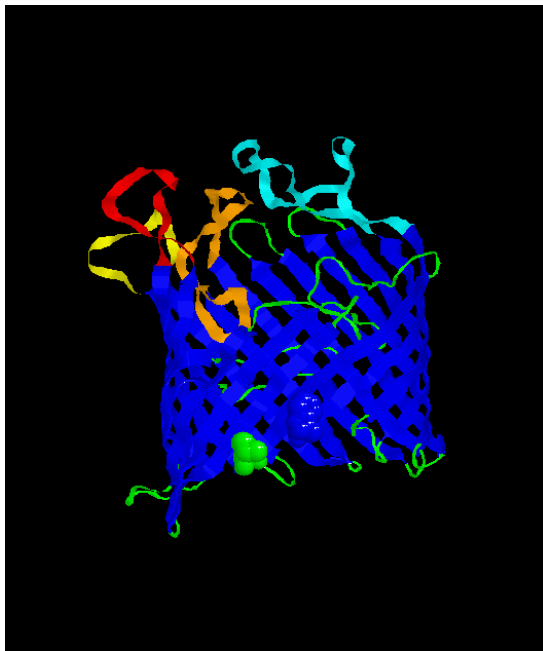
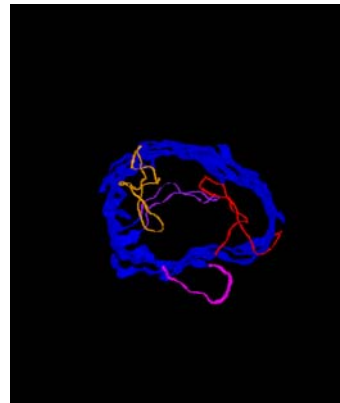


Figure 1 f). Maltoporin side view



(Figure 1 g)). Maltoporin side view



(Figure 1 h)).
LamB top view

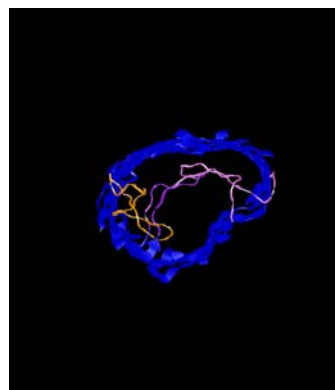


(Figure 1 i)).
LamB top view

The profound stability of porin trimers is a result of strong monomer interactions. The monomer interface contains an amino-carboxyl salt bridge and forms a hydrophobic core through extensive, mainly hydrophobic residue interactions (over 35% of the molecule). The C termini and strand 16 are essential to trimer formation. Points of contact include the barrel walls and peripheral contacts between loop 1 and loop 5. Cell surface loop 2 (light blue) increases trimer stability by folding into the channel of an adjacent monomer and hydrogen bonding to loops 2, 3, and 4. Salt bridges are also formed with arginines in loop 3 (Figure 1 d)).

Many of the channel's functional properties stem from its loops. Some loops pack (dark blue) together to form a hydrophilic umbrella structure over the channel opening. It is inferred that these loops protect the channel and screen solutes depending on their size and charge (Figure 1 e)).

Loop 3 folds into the channel and packs against the channel wall, forming a 9 Å constriction zone halfway through the barrel. Contributors to the constriction with the barrel wall are highly conserved Pro, Glu, Phe, Gly residues at the tip of loop 3 as well as Asp¹¹³ and Glu¹¹⁷. The constriction zone determines the pore selectivity and absolute solute size limitation. The channel diameter widens to 15 X 22 Å below the constriction (Branden and Tooze, 1991; Cowan et al., 1992; Hofnung, 1995).

4.2 Maltoporin monomer structure

Although there obviously exists no sequence homology between maltoporin and OmpF, there are a number of similarities in folding (Figure 1 f)). Maltoporin monomers are 80 residues longer and form 18-stranded β -barrels (blue) that enclose narrower channels, about 5-6 Å in diameter. The barrel is completed by a linking of the amino (Val¹) and carboxyl (Trp⁴²¹) termini in strand 18, and barrel stability and active trimer formation are influenced by many of the same types of residue interactions as described for OmpF. Successive stands are connected through periplasmic β -hairpin turns (green) and irregular cell surface loops. The loops found in maltoporin (Figure 1 g)) are considerably longer than those found in OmpF. Parts of loop 6 (orange), together with loop 4 (red), loop 5 (yellow), and loop 9 (light blue) form a protective compact structure over the channel entrance. In addition to loop 2 (pink) from an adjacent subunit, three monomer surface loops fold into the channel (Figure 1 h)). As in OmpF, aromatic and ionizable residues in loop 3 (blue) form a mid-channel constriction

zone with residues on the barrel wall. Additionally, residues from loop 1 (orange) and loop 6 (pink) narrow the channel entrance (Figure 1 i)).

Structure/Function Relationships in Maltoporin

Lambda phage receptor

An intact maltoporin trimer is required for lambda phage infection of *E. coli* (Figure 2 a), b), c), and d)). The monomer loops forming the protective structure (Figure 2 a)) (red) are the most variable regions among porins. This variability may serve to protect bacteria from infection. A number of surface point mutations in these regions (residues 154, 155, 164, 259, 382, 386, 387, 394, 401) (Figure 2 b)) (purple) have been shown to have no effect on sugar translocation while conferring lambda phage resistance.

Another series of resistance mutations occurs in sites 151, 152, 163, 245, 247, and 250 (Figure 2 c)) (yellow), all buried by loop compaction. These mutations may affect umbrella behavior or surface structure and have variable effects on sugar translocation. An additional mutation site (residue 18) (Figure 2 d)) (light blue) prevents translocation and is located on loop 1. The precise nature and structure of the lambda binding site is unclear.

Sugar translocation

Diffusion is influenced by residues from loop 3 (constriction zone) (blue), loop 1 (pink) and loop 6 (orange) (Figure 3 a)), which narrow the channel entrance, as well as by residues on the barrel walls. A series of aromatic residues (Tyr⁴¹, Tyr⁶, Trp⁴²⁰, Trp³⁵⁸, Phe²²⁷) forms a left-handed helical path down the channel lining. Trp⁷⁴ (orange residue) (Figure 3 b)) from an adjacent loop 2 adds to the top of this path.

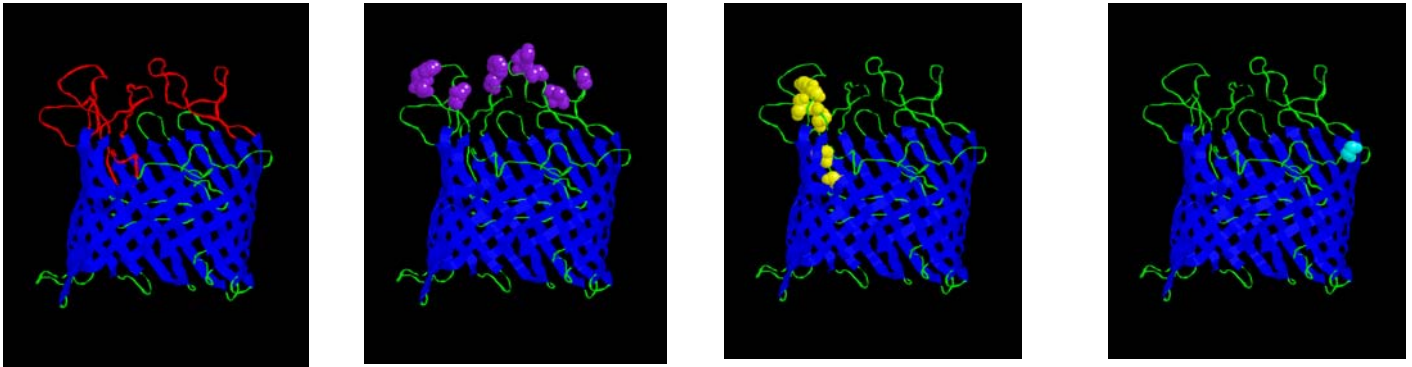


Figure 2 a), b), c), and d). LamB side view

These aromatic residues are spaced 6-7 Å apart and may stack with hydrophobic faces of sugar molecules, forming transient bonds to guide the sugar from the channel opening through the constriction zone.

This aromatic helical path, or "greasy slide", is surrounded by a number of ionizable residues (yellow) (Figure 3 b)) from the channel lining that are assumed to replace the hydration shells of diffusing molecules and convey sugar specificity to the channel.

Although the precise molecular mechanisms underlying maltoporin function are still unknown, translocation is currently modeled as follows. Residues from L1 and L6 serve to orient sugar molecules which are then guided through the constriction zone along the "greasy slide". Channel specificity is determined by residues in the channel lining (Branden and Tooze, 1991; Cowan *et al.*, 1992; Hofnung, 1995; Schirmer *et al.*, 1995).

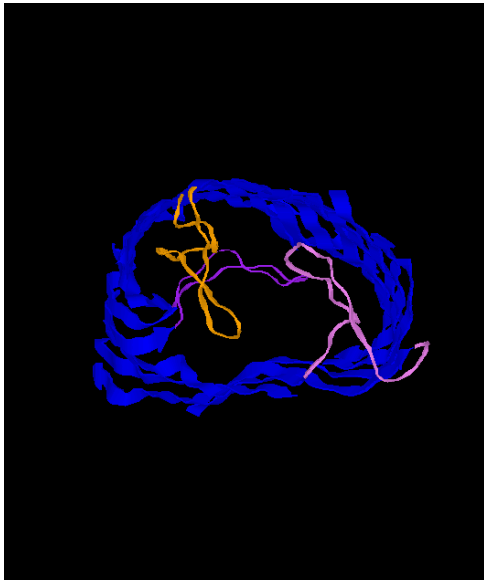


Figure 3 a). LamB top view

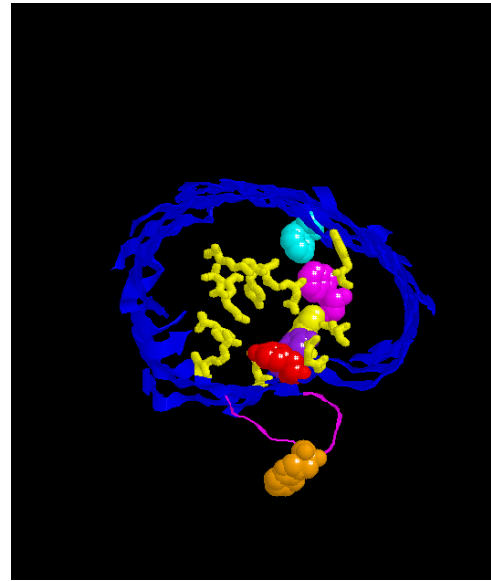


Figure 3 b). LamB top view

Figure 1 f), g), h), i), Figure 2 a), b), c), d) and Figure 3 a), b). LamB is a 18-stranded antiparallel β -sheet barrel (blue) protein.

Figures from OmpF and LamB are found on the webpage:

<http://www.clunet.edu/BioDev/omm/porins/frames/porintx.htm>

CHAPTER 1

***Insertion of Proteins in Polymer-Stabilized Lipid
Membranes***

Summary

We demonstrated in the first chapter that lipid membrane can be considerably stabilized by an “internal” polymer scaffold as long as the mesh-size of the polymer is not too high. As shown in the study above a certain crosslinking density the network induces small defects in the membrane.

Moreover, for appropriate crosslinking densities membrane proteins can be inserted and remain functional into this polymer supported lipid bilayer. To our knowledge it is the first report of a “polymerized” bilayer that allows protein reconstitution.

PUBLICATION 1

***Stabilization of Planar Lipid Membranes: A Stratified Layer
Approach***

Stabilization of planar lipid membranes: A stratified layer approach

Wolfgang Meier,^a Alexandra Graff,^a Anke Diederich^b and Mathias Winterhalter^{*c}

^a Department of Physical Chemistry, University of Basel, Klingelbergstrasse 80, CH-4056, Switzerland

^b Hoffmann–La Roche, CH-4002 Basel, Switzerland

^c IPBS-CNRS UPR 9062, University Paul Sabatier, 31077, Toulouse, France.
E-mail: winter@ipbs.fr

Received 22nd May 2000, Accepted 2nd August 2000

First published as an Advance Article on the web 15th September 2000

Here we briefly summarize our recent efforts in stabilization of giant planar lipid membranes and provide the first promising results achieved with a new technique. A water-soluble polymer can be coupled to lipid membranes either electrostatically or *via* a hydrophobic linker. Such coated membranes are significantly destabilized and the rupture process is slowed down. In contrast, partitioning of hydrophobic styrene monomer into the lipid membrane and its polymerization lead to an increase in stability. A short electric field pulse under controlled conditions was applied to quantify the stability. Voltages above 1.2 V are required to induce an electrical discharge. Within less than 100 μ s these defects reseal. However, after resealing, the stability of this particular lipid membrane corresponds to that of a lipid membrane without a 2-D polymer network. We suggest the use of this technique to stabilize self-assembled lipid membrane structures.

Introduction

Artificial lipid bilayer systems are often used to characterize membrane proteins or to study membrane active substances.^{1–3} Many of these substances are pharmacologically important or have biotechnological potential. Prior to an application, one has to immobilize them in an artificial membrane system to create a biosensor, which allows *e.g.* rapid drug screening.^{3–8} Established membrane models are black lipid membranes. Unlike liposomes these giant planar free-standing films have the advantage of direct access to both sides of the membrane. For example, this allows one to perform conductance measurements and to follow *e.g.* easy transport processes across membranes or to detect minor changes in reconstituted channel-forming membrane protein.^{1–3}

Since about 40 years ago several similar techniques have been developed to form free-standing planar lipid membranes.^{9,10} One technique is based on solvent-containing membrane.⁹ Here the lipid is dissolved in saturated hydrocarbon, mostly decane, and during the formation of a giant planar lipid bilayer small amounts of this hydrocarbon are trapped inside the lipid membrane. The larger the hydrocarbon length, the less solvent the membrane contains.

For a long time it has been tempting to use the large variety of natural specific channels to construct biosensors.^{3–7} Recently we have shown that, based on the structure, specific affinity sites can be engineered into such channels and the results can be tested by analysis of ion current fluctuation. The main difficulty in commercial application of these biosensors is the inherent instability of these free-standing films. This can be overcome by using a solid support, which reduces the sensitivity due to the interaction of the support, manifested on a larger scale in a higher background conductance.⁶ Currently we are working on strategies to stabilize free-

standing planar lipid bilayers and we will briefly outline the main features.

Materials and methods

Diphytanoyl-phosphatidylcholine (DPhPC), diphytanoyl-phosphatidylserine (DPhPS), 1-palmitoyl-2-oleoyl-*sn*-glycero-3-phosphocholine (POPC), and 1-palmitoyl-2-oleoyl-*sn*-glycero-3-(phospho-L-serine) (POPS) were purchased from Avanti Polar Lipids (Alabaster, Alabama) with purity >99% and were used without further purification. The electrolyte contained ion-exchanged water (NANOpure, Barnstead) with specific resistance >17 M Ω cm and specified amounts of KCl (p.a.) from Merck (Darmstadt, Germany). The membrane-forming solution contained 1 wt% lipid in *n*-decane (Fluka). In the case of POPS, we added small amounts of butan-1-ol (p.a.) from Merck for better solubilization of the lipids into the membrane-forming solution. The solution used for pre-painting contained 1 wt% lipid in chloroform (p.a.) obtained from Merck. In the series with styrene polymerization the protocol was slightly modified as the membrane-forming solution contained DPhPS/styrene/divinylbenzene 4 : 1 : 1(v/v/v) dissolved in 99% *n*-decane. All buffers must be carefully degassed. The polymerization was induced by a UV lamp for several minutes.

Black lipid membranes

Black lipid membranes (BLMs) of \sim 1 mm diameter were formed according to Mueller *et al.*^{9,11–15} Briefly, a Teflon cuvette containing two chambers was pre-painted around the hole connecting both chambers with about 1 μ l of the pre-painting solution. After allowing 20 min for drying, each

chamber was filled with 5 ml electrolyte. Then 1 μl of the membrane-forming solution was spread on a Teflon loop and painted across the hole, leading to the separation of the two chambers by a lipid membrane. The thinning of the membrane could be observed through a glass window in the front side of the cuvette by a microscope (60-fold magnification).

Electroporation setup

Membrane rupture was initiated as previously described and the basic features are shown in Fig. 1.^{11–14} The Ag/AgCl electrode in the *trans* compartment is connected to a fast pulse generator (Tektronix PG 507) through a diode (reverse resistance $\gg 10^{11} \Omega$). The voltage between the *cis* and *trans* electrode is recorded on a digital storage oscilloscope (LeCroy 9354A).

Prior to rupture, the membrane capacitance is determined by charging the BLM with a rectangular pulse of 10 μs duration to a voltage of about 100 mV. The value of the membrane capacitance is calculated from the RC time constant of the exponential discharge process of the membrane across the 10 M Ω resistance of the passive oscilloscope probe. Irreversible breakdown is initiated by charging the membrane with rectangular 250 to 1200 mV voltage pulses of 10 μs duration. In order to avoid the formation of multiple pores, we start to charge the membrane with a small voltage of 250 mV. Then we raise the applied voltage in 20 mV steps, applying at least five pulses per step until the membrane disrupts. In a typical rupture experiment about 20 to 200 pulses are applied prior to membrane rupture.

In Fig. 2(a) we show a typical recording of the time dependence of the transmembrane voltage. At a given time the pulse generator will raise the membrane voltage to a given value. After the onset the electrodes are used to read the transmembrane voltage. Due to the parallel resistor and the finite capacitance of the system, the membrane voltage relaxes. Instantaneously or after some lag time a defect occurs and the voltage suddenly drops superexponentially. In Fig. 2(a) the lag time is almost 100 μs after the maximum voltage is reached. According to previous discussion the critical voltage leading to rupture can be related to the stability of the BLM.^{11–14} In all investigated lipid membrane systems the voltage dropped down to zero, indicating an irreversible rupture. In Fig. 2(a) we show an exception. In this case the voltage relaxes not to zero but to a finite value, indicating a resealing of the defect. The capacitance measured shortly after the resealing revealed a similar value to that of the intact membrane prior to pulsing. As long as the defect is small relative to the total area

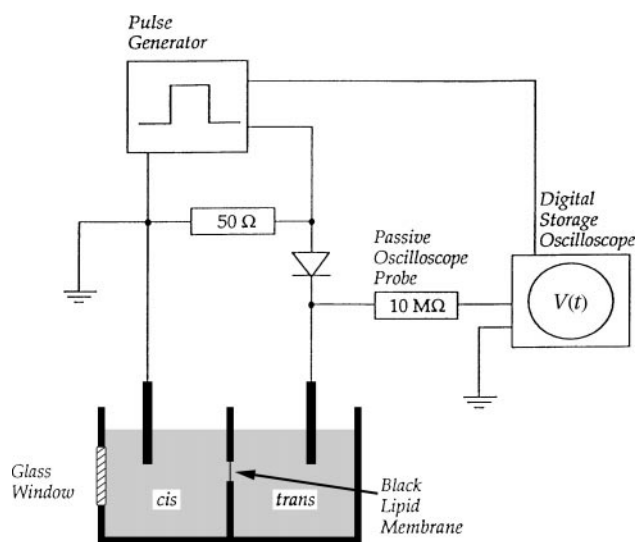


Fig. 1 Schematic view of the setup.

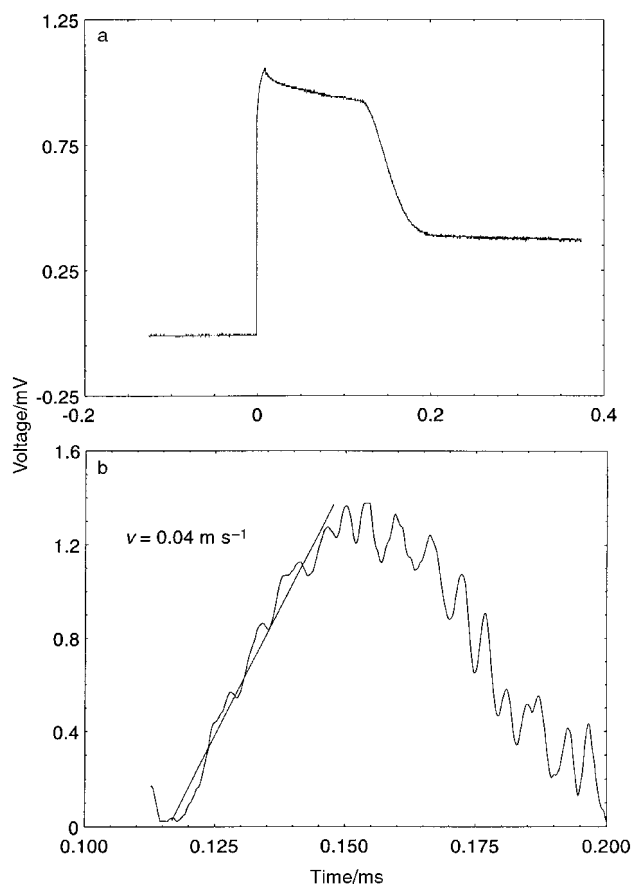


Fig. 2 (a) Time course of the transmembrane voltage during electric field-induced rupture of a DPhPS/styrene/divinylbenzene membrane. The length of the voltage pulse was 10 μs . The aqueous phase contained 100 mM KCl, $T = 295 \text{ K}$. (b) Analysis of the rapid voltage decay as suggested in the text. Under the assumption of a single defect we observe increasing pore size up to micrometre size, which reseals again. The original slope is $v = 0.04 \text{ m s}^{-1}$.

of the membrane, the bilayer capacitance can be considered as constant. Under this assumption the membrane conductance, $G(t)$, can be calculated via

$$\begin{aligned}
 G(t) &= \frac{I(t)}{U(t)} = \frac{1}{U(t)} \frac{dQ(t)}{dt} \\
 &= \frac{1}{U(t)} \frac{-d[CU(t)]}{dt} = \frac{-C}{U(t)} \frac{dU(t)}{dt} \\
 &= -C \frac{d \ln U(t)}{dt} \quad (1)
 \end{aligned}$$

where $I(t)$ is the discharge current over the defect, $U(t)$ the transmembrane voltage, $Q(t)$ the charge excess on one side of the membrane and C the membrane capacitance. The minus sign indicates discharging of the membrane.

Our interpretation of the presented data is based on the assumption that the voltage pulses trigger only the formation of one pore. We came to this conclusion from the following observations: Repeated determination of the conductance increase during membrane rupture under the same conditions yields a distribution around a minimal value and multiples of it. In a few cases we observed a sudden doubling of the conductance increase during membrane rupture. This we interpret as the occurrence of a second pore during the rupture process. If the conductance increase were due to the widening of a large number of pores, no distinct minimal value but rather a wide distribution should be observed. Moreover, we observe a very broad distribution of the delay between the end of the applied rectangular voltage pulse and membrane rupture. This

again suggests a single event rather than the formation of many pores.

In our experimental setup, we can detect a pore only from the point when the membrane resistance becomes smaller than 10 M Ω . In the case of a single pore, this pore has a large radius relative to the membrane thickness. Under these conditions the conductance $G_{\text{pore}}(t)$ of a pore can be approximated by the inverse access resistance

$$G_{\text{pore}}(t) = \frac{1}{R_{\text{pore}}} = 2\kappa a(t) \quad (2)$$

where κ is the specific conductivity of the electrolyte. The above equation relates the conductance to the widening of the pore with radius a . This is only strictly valid in the special case of a single circular defect. In the case of a non-circular defect or multiple pores we approximate this by an equivalent pore of circular area with radius a .

Pore widening in pure BLMs is driven by surface tension and is limited by the inertia of the film.^{11,14} The viscosity of the lipid film can in most cases be neglected.^{11–14} Balancing the decrease in elastic energy by inertia and dissipation during the widening of the pore yields a linear increase of the pore radius with time, $a(t) = vt$, with v as the rupture velocity.^{11–12}

In addition we measured the modification of the transmembrane voltages.^{12–15} This was necessary as in some experiments we applied different electrolyte concentrations on each side, causing a transmembrane potential. In the case of polylysine, the adsorption of the polymer on one side of the charged membrane caused screening, which resulted in a transmembrane potential. These potentials add or subtract to the externally applied potentials and apparently lead to stabilization or destabilization.

Results

We quantified the stability and kinetics of the rupture of surface-coated lipid membranes. In a first series we investigated the influence of surface charges on the rupture of black lipid membranes (BLMs).¹² Rupture is induced by short electric voltage pulses across the membrane. The average voltage necessary to induce breakdown gives information on the energy barrier of defect formation. In Table 1 we give the critical voltage leading to irreversible rupture for two different lipids with two different headgroups. The breakdown voltage is about the same for BLMs made of lipids with phosphatidylserine (PS) headgroups and for BLMs made of lipids with phosphatidylcholine (PC) headgroups. Moreover the breakdown voltage is independent of the ionic strength of the aqueous medium surrounding the BLMs. This indicates that the stability of the BLMs is not dominated by mutual electrostatic repulsion of the headgroups. However, the breakdown voltage depends on the type of hydrophobic chain of the lipids. Palmitoyl-oleoyl (PO) membranes require ~ 100 mV

Table 1 Average breakdown voltage and average rupture velocity for four different lipids

	2 M KCl	100 mM KCl	10 mM KCl
Rupture velocity/cm s ⁻¹			
POPC	455 \pm 7	400 \pm 6	420 \pm 23
POPS	480 \pm 20	410 \pm 20	435 \pm 25
DPhPC	527 \pm 2	546 \pm 15	565 \pm 25
DPhPS	525 \pm 25	530 \pm 15	530 \pm 25
Breakdown voltage/mV			
POPC	8 \pm 1	5 \pm 1	5 \pm 0.5
POPS	14 \pm 1	5 \pm 1	5 \pm 2
DPhPC	33 \pm 2	19 \pm 2	20 \pm 4
DPhPS	43 \pm 3	20 \pm 1.5	20 \pm 2

smaller breakdown voltages compared to diphytanoyl (DPh) membranes.

Rapid transmembrane voltage decay during rupture allows one to evaluate the kinetics of defect widening. Surprisingly the rupture kinetics depends on the hydrocarbon chains. It was found to be four times faster for DPh than for PO membranes and independent of the type of headgroup.¹²

In a second series we investigated the stability and rupture kinetics of planar lipid membranes covered with electrostatically coupled polyelectrolytes.¹³ After black lipid membranes were formed from negatively charged lipids, polylysines (PLs) of different molecular weights (MW) were added on one or on both sides of the membrane. The adsorption of PL was detected by recording changes of the transmembrane voltage. Adsorption of PL on one side of the membrane leads to an asymmetric transmembrane potential, which adds to the externally applied voltage. High-MW PL decreases the critical breakdown voltage of the membrane significantly as shown in Table 2. Interestingly the presence of polylysine also increases the delay time between the voltage pulse and pore formation. Adsorption of PL alters the time course of pore widening in a molecular-weight-dependent manner. Low-MW PL-decorated membranes and undecorated membranes show a fast rupture determined by inertia. In contrast, adsorption of high-MW PLs causes a significant decrease of the critical voltage leading to rupture.¹³

Lipid membranes can also be coated with water-soluble polymers linked by hydrophobic interaction.¹⁴ Here we covalently linked hydrophobic anchors to larger water-soluble dextran. Coating lipid membranes with dextran *via* a hydrophobic linker drastically destabilized the membrane as shown in Table 3. The density of the hydrophobic anchor groups along the polymer chains is found to be of considerable influence. While dextran with a low anchor group density slows down the inertia-driven rupture process of lipid membranes, dextran with higher anchor group density alters the kinetics and causes an exponential increase in membrane conductance, suggesting a viscosity-determined rupture process. Dextran derivatives of medium anchor group density show a transition from a viscosity- to an inertia-limited rupture.¹⁴

In a third series of experiments planar lipid membranes from DPhPS/styrene/divinylbenzene 4 : 1 : 1 were formed. Due to their low solubility in water, styrene and divinylbenzene are mainly dissolved within the hydrophobic part of the bilayer. After thinning, the capacitance of the monomer-swollen membranes was recorded, and no significant differences from pure DPhPS membranes were found. Subsequently rupture was induced and values similar to those for pure DPhPS membranes were observed. Polymerization of the styrene/divinylbenzene mixture in the hydrophobic part of the

Table 2 Average breakdown voltage for symmetrical addition of polylysine and 100 mM KCl

DPhPS alone	530 \pm 20 mV
+ PL MW 600	525 \pm 15 mV
+ PL MW 8000	540 \pm 24 mV
+ PL MW 42 000	500 \pm 26 mV
+ PL MW 420 000	426 \pm 20 mV

Table 3 Average breakdown voltage in the presence of dextran with different hydrophobic anchor and 100 mM KCl

DPhPS alone	530 \pm 20 mV
+ dextran	510 \pm 12 mV
+ dodecyl-dextran-1	416 \pm 24 mV
+ dodecyl-dextran-3	388 \pm 13 mV
+ dodecyl-dextran-6	310 \pm 11 mV

membrane could be induced by 10 min UV irradiation.^{16–17} Polymerization leads to the formation of a polymer network. This network causes a drastic change in the rupture behaviour. In about 50% of cases critical voltages above 1 V were necessary to induce an electrical discharge, which was characterized by a voltage relaxation to finite values [see Fig. 2(a)]. An analysis using eqn. (2) of the rapid voltage decay gives the apparent pore size. As shown in Fig. 2(b) the pore opens linearly up to micrometre size at about 0.04 m s^{-1} and reseals again. Capacitance measurements after the pulse revealed an intact membrane with capacitance similar to that before inducing rupture.

Discussion and conclusion

The main advantage of free-standing giant lipid membrane systems is their well-defined and defect-free structure, which allows the application of electrophysiological techniques. The most surprising result of our investigation concerning stability was the insensitivity of membrane stability to the ionic strength. For PC membranes this is somewhat expected, but not for PS headgroups. Assuming each PS headgroup to be dissociated gives a fairly high surface charge density. Calculating the surface potential based on Poisson–Boltzmann theory results in significantly higher voltages than the measured ones.¹⁵ Even using the lower experimental voltages observed gives rise to unreasonably high repulsive forces, which do not allow stable lamellar phases, as the additional repulsive forces are above the mechanical ones leading to rupture. The answer is likely an overestimation of the electrostatic forces within the first layer.

Adsorption of large polymers destabilizes giant soft planar lipid membranes. Adsorption can only occur at the cost of entropy which the polymer coil has to pay. This clearly gives rise to a destabilization effect in agreement with the observation.

A significant stabilization can be achieved with a 2-D polymer network formed inside the hydrophobic lipid layer as schematically shown in Fig. 3. Here the lipid preserves the fluidity necessary to reseal small defects occurring transiently due to external forces. For the polymer-containing mem-

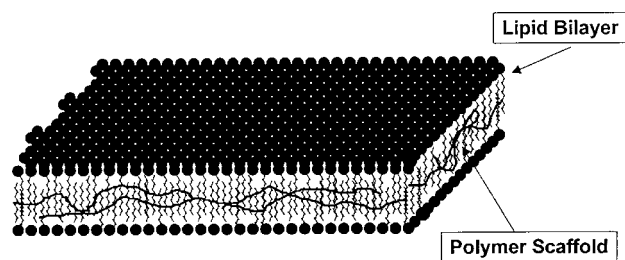


Fig. 3 Schematic sketch to illustrate a 2-D polymer network. The actual structure of the 2-D network is not yet resolved. A more detailed discussion may be found in ref. 17.

branes an additional dissipative mechanism has to be taken into account: During rupture of the membrane the polymer chains of the 2-D polymer network structure also have to be disrupted. Up to this point the underlying network chains are stretched elastically. As a result of the associated energy dissipation the velocity of defect growth decreases with time and finally stops. Subsequently the energetically favorable pore closes again due to lateral diffusion of the lipid molecules. Application of a second voltage pulse gave similar features to those of a pure DPhPC membrane concerning critical voltages and rupture velocities. Obviously, the polymer network structure is ‘pre-damaged’ during the first pulse and hence no longer able to dissipate enough energy to stop the growth of the defect.

We are currently investigating the extent to which this approach is compatible with functional reconstitution of membrane proteins. First results on a similar system were promising.¹⁸

Acknowledgements

We would like to thank the Swiss National Science Foundation and INTAS 96-1310 for financial support.

References

- 1 A. Charbit, C. Andersen, J. Wang, B. Schiffler, V. Michel, R. Benz and M. Hofnung, *Mol. Microbiol.*, 2000, **35**, 777.
- 2 T. K. Rostvtseva, T. T. Liu, M. Colombini, V. A. Parsegian and S. M. Bezrukov, *Proc. Nat. Acad. Sci. USA*, 2000, **97**, 7819.
- 3 M. Akeson, D. Branton, J. J. Kasianowicz, E. Brandin and D. W. Deamer, *Biophys. J.*, 1999, **77**, 3227.
- 4 B. A. Cornell, V. L. Braach-Maksvytis, L. G. King, P. D. Osman, B. Raguse, L. Wiczorek and R. J. Pace, *Nature*, 1997, **387**, 580.
- 5 S. Heyse, T. Stora, E. Schmid, J. H. Lakey and H. Vogel, *Biochim. Biophys. Acta*, 1998, **1376**, 319.
- 6 K. Seifert, K. Fendler and E. Bamberg, *Biophys. J.*, 1993, **64**, 384.
- 7 T. Stora, J. H. Lakey and H. Vogel, *Angew. Chem. Int. Ed. Engl.*, 1999, **38**, 389.
- 8 M. Winterhalter, *Colloids Surf. A*, 1999, **149**, 547.
- 9 P. Mueller, D. P. Rudi, H. T. Tien and W. C. Wescott, *J. Phys. Chem.*, 1963, **67**, 534.
- 10 M. Montal and P. Mueller, *Proc. Nat. Acad. Sci. USA*, 1979, **69**, 3561.
- 11 C. Wilhelm, M. Winterhalter, U. Zimmermann and R. Benz, *Biophys. J.*, 1993, **64**, 121.
- 12 A. Diederich, G. Bähr and M. Winterhalter, *Phys. Rev. E*, 1998, **58**, 4883.
- 13 A. Diederich, G. Bähr and M. Winterhalter, *Langmuir*, 1998, **14**, 4597.
- 14 A. Diederich, M. Strobel, W. Meier and M. Winterhalter, *J. Phys. Chem. B*, 1999, **103**, 1402.
- 15 G. Bähr, A. Diederich, G. Vergeres and M. Winterhalter, *Biochemistry*, 1998, **37**, 16252.
- 16 J. Hotz and W. Meier, *Langmuir*, 1998, **14**, 1031.
- 17 J. Hotz and W. Meier, *Adv. Mater.*, 1998, **10**, 1387.
- 18 C. Nardin, S. Thoeni, J. Widmer, M. Winterhalter and W. Meier, *Chem. Commun.*, 2000, 1433.

Stabilization of planar lipid membranes: A stratified layer approach

Wolfgang Meier,^a Alexandra Graff,^a Anke Diederich^b and Mathias Winterhalter^{*c}

^a Department of Physical Chemistry, University of Basel, Klingelbergstrasse 80, CH-4056, Switzerland

^b Hoffmann-La Roche, CH-4002 Basel, Switzerland

^c IPBS-CNRS UPR 9062, University Paul Sabatier, 31077, Toulouse, France.
E-mail: winter@ipbs.fr

Received 22nd May 2000, Accepted 2nd August 2000

First published as an Advance Article on the web 15th September 2000

Here we briefly summarize our recent efforts in stabilization of giant planar lipid membranes and provide the first promising results achieved with a new technique. A water-soluble polymer can be coupled to lipid membranes either electrostatically or *via* a hydrophobic linker. Such coated membranes are significantly destabilized and the rupture process is slowed down. In contrast, partitioning of hydrophobic styrene monomer into the lipid membrane and its polymerization lead to an increase in stability. A short electric field pulse under controlled conditions was applied to quantify the stability. Voltages above 1.2 V are required to induce an electrical discharge. Within less than 100 μ s these defects reseal. However, after resealing, the stability of this particular lipid membrane corresponds to that of a lipid membrane without a 2-D polymer network. We suggest the use of this technique to stabilize self-assembled lipid membrane structures.

Introduction

Artificial lipid bilayer systems are often used to characterize membrane proteins or to study membrane active substances.^{1–3} Many of these substances are pharmacologically important or have biotechnological potential. Prior to an application, one has to immobilize them in an artificial membrane system to create a biosensor, which allows *e.g.* rapid drug screening.^{3–8} Established membrane models are black lipid membranes. Unlike liposomes these giant planar free-standing films have the advantage of direct access to both sides of the membrane. For example, this allows one to perform conductance measurements and to follow *e.g.* easy transport processes across membranes or to detect minor changes in reconstituted channel-forming membrane protein.^{1–3}

Since about 40 years ago several similar techniques have been developed to form free-standing planar lipid membranes.^{9,10} One technique is based on solvent-containing membrane.⁹ Here the lipid is dissolved in saturated hydrocarbon, mostly decane, and during the formation of a giant planar lipid bilayer small amounts of this hydrocarbon are trapped inside the lipid membrane. The larger the hydrocarbon length, the less solvent the membrane contains.

For a long time it has been tempting to use the large variety of natural specific channels to construct biosensors.^{3–7} Recently we have shown that, based on the structure, specific affinity sites can be engineered into such channels and the results can be tested by analysis of ion current fluctuation. The main difficulty in commercial application of these biosensors is the inherent instability of these free-standing films. This can be overcome by using a solid support, which reduces the sensitivity due to the interaction of the support, manifested on a larger scale in a higher background conductance.⁶ Currently we are working on strategies to stabilize free-

standing planar lipid bilayers and we will briefly outline the main features.

Materials and methods

Diphytanoyl-phosphatidylcholine (DPhPC), diphytanoyl-phosphatidylserine (DPhPS), 1-palmitoyl-2-oleoyl-*sn*-glycero-3-phosphocholine (POPC), and 1-palmitoyl-2-oleoyl-*sn*-glycero-3-(phospho-L-serine) (POPS) were purchased from Avanti Polar Lipids (Alabaster, Alabama) with purity >99% and were used without further purification. The electrolyte contained ion-exchanged water (NANOpure, Barnstead) with specific resistance >17 M Ω cm and specified amounts of KCl (p.a.) from Merck (Darmstadt, Germany). The membrane-forming solution contained 1 wt% lipid in *n*-decane (Fluka). In the case of POPS, we added small amounts of butan-1-ol (p.a.) from Merck for better solubilization of the lipids into the membrane-forming solution. The solution used for pre-painting contained 1 wt% lipid in chloroform (p.a.) obtained from Merck. In the series with styrene polymerization the protocol was slightly modified as the membrane-forming solution contained DPhPS/styrene/divinylbenzene 4 : 1 : 1(v/v/v) dissolved in 99% *n*-decane. All buffers must be carefully degassed. The polymerization was induced by a UV lamp for several minutes.

Black lipid membranes

Black lipid membranes (BLMs) of \sim 1 mm diameter were formed according to Mueller *et al.*^{9,11–15} Briefly, a Teflon cuvette containing two chambers was pre-painted around the hole connecting both chambers with about 1 μ l of the pre-painting solution. After allowing 20 min for drying, each

chamber was filled with 5 ml electrolyte. Then 1 μl of the membrane-forming solution was spread on a Teflon loop and painted across the hole, leading to the separation of the two chambers by a lipid membrane. The thinning of the membrane could be observed through a glass window in the front side of the cuvette by a microscope (60-fold magnification).

Electroporation setup

Membrane rupture was initiated as previously described and the basic features are shown in Fig. 1.^{11–14} The Ag/AgCl electrode in the *trans* compartment is connected to a fast pulse generator (Tektronix PG 507) through a diode (reverse resistance $\gg 10^{11} \Omega$). The voltage between the *cis* and *trans* electrode is recorded on a digital storage oscilloscope (LeCroy 9354A).

Prior to rupture, the membrane capacitance is determined by charging the BLM with a rectangular pulse of 10 μs duration to a voltage of about 100 mV. The value of the membrane capacitance is calculated from the RC time constant of the exponential discharge process of the membrane across the 10 M Ω resistance of the passive oscilloscope probe. Irreversible breakdown is initiated by charging the membrane with rectangular 250 to 1200 mV voltage pulses of 10 μs duration. In order to avoid the formation of multiple pores, we start to charge the membrane with a small voltage of 250 mV. Then we raise the applied voltage in 20 mV steps, applying at least five pulses per step until the membrane disrupts. In a typical rupture experiment about 20 to 200 pulses are applied prior to membrane rupture.

In Fig. 2(a) we show a typical recording of the time dependence of the transmembrane voltage. At a given time the pulse generator will raise the membrane voltage to a given value. After the onset the electrodes are used to read the transmembrane voltage. Due to the parallel resistor and the finite capacitance of the system, the membrane voltage relaxes. Instantaneously or after some lag time a defect occurs and the voltage suddenly drops superexponentially. In Fig. 2(a) the lag time is almost 100 μs after the maximum voltage is reached. According to previous discussion the critical voltage leading to rupture can be related to the stability of the BLM.^{11–14} In all investigated lipid membrane systems the voltage dropped down to zero, indicating an irreversible rupture. In Fig. 2(a) we show an exception. In this case the voltage relaxes not to zero but to a finite value, indicating a resealing of the defect. The capacitance measured shortly after the resealing revealed a similar value to that of the intact membrane prior to pulsing. As long as the defect is small relative to the total area

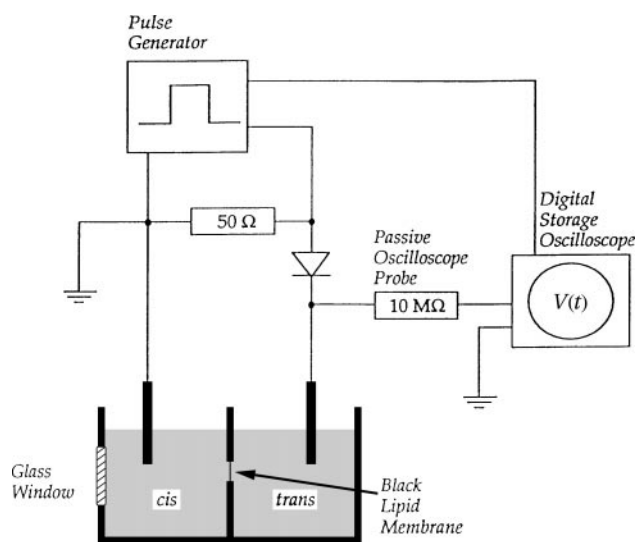


Fig. 1 Schematic view of the setup.

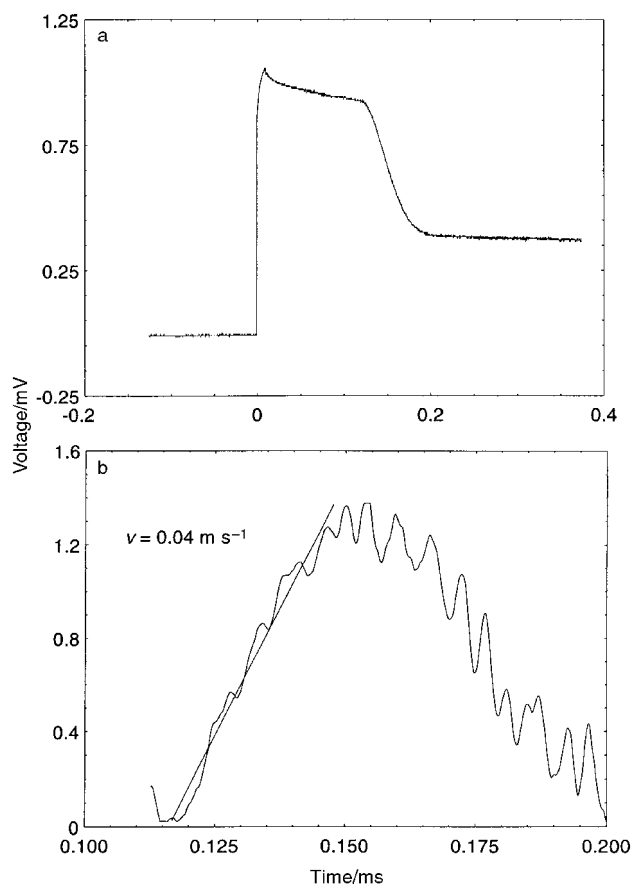


Fig. 2 (a) Time course of the transmembrane voltage during electric field-induced rupture of a DPhPS/styrene/divinylbenzene membrane. The length of the voltage pulse was 10 μs . The aqueous phase contained 100 mM KCl, $T = 295 \text{ K}$. (b) Analysis of the rapid voltage decay as suggested in the text. Under the assumption of a single defect we observe increasing pore size up to micrometre size, which reseals again. The original slope is $v = 0.04 \text{ m s}^{-1}$.

of the membrane, the bilayer capacitance can be considered as constant. Under this assumption the membrane conductance, $G(t)$, can be calculated via

$$\begin{aligned}
 G(t) &= \frac{I(t)}{U(t)} = \frac{1}{U(t)} \frac{dQ(t)}{dt} \\
 &= \frac{1}{U(t)} \frac{-d[CU(t)]}{dt} = \frac{-C}{U(t)} \frac{dU(t)}{dt} \\
 &= -C \frac{d \ln U(t)}{dt} \quad (1)
 \end{aligned}$$

where $I(t)$ is the discharge current over the defect, $U(t)$ the transmembrane voltage, $Q(t)$ the charge excess on one side of the membrane and C the membrane capacitance. The minus sign indicates discharging of the membrane.

Our interpretation of the presented data is based on the assumption that the voltage pulses trigger only the formation of one pore. We came to this conclusion from the following observations: Repeated determination of the conductance increase during membrane rupture under the same conditions yields a distribution around a minimal value and multiples of it. In a few cases we observed a sudden doubling of the conductance increase during membrane rupture. This we interpret as the occurrence of a second pore during the rupture process. If the conductance increase were due to the widening of a large number of pores, no distinct minimal value but rather a wide distribution should be observed. Moreover, we observe a very broad distribution of the delay between the end of the applied rectangular voltage pulse and membrane rupture. This

again suggests a single event rather than the formation of many pores.

In our experimental setup, we can detect a pore only from the point when the membrane resistance becomes smaller than 10 M Ω . In the case of a single pore, this pore has a large radius relative to the membrane thickness. Under these conditions the conductance $G_{\text{pore}}(t)$ of a pore can be approximated by the inverse access resistance

$$G_{\text{pore}}(t) = \frac{1}{R_{\text{pore}}} = 2\kappa a(t) \quad (2)$$

where κ is the specific conductivity of the electrolyte. The above equation relates the conductance to the widening of the pore with radius a . This is only strictly valid in the special case of a single circular defect. In the case of a non-circular defect or multiple pores we approximate this by an equivalent pore of circular area with radius a .

Pore widening in pure BLMs is driven by surface tension and is limited by the inertia of the film.^{11,14} The viscosity of the lipid film can in most cases be neglected.^{11–14} Balancing the decrease in elastic energy by inertia and dissipation during the widening of the pore yields a linear increase of the pore radius with time, $a(t) = vt$, with v as the rupture velocity.^{11–12}

In addition we measured the modification of the transmembrane voltages.^{12–15} This was necessary as in some experiments we applied different electrolyte concentrations on each side, causing a transmembrane potential. In the case of polylysine, the adsorption of the polymer on one side of the charged membrane caused screening, which resulted in a transmembrane potential. These potentials add or subtract to the externally applied potentials and apparently lead to stabilization or destabilization.

Results

We quantified the stability and kinetics of the rupture of surface-coated lipid membranes. In a first series we investigated the influence of surface charges on the rupture of black lipid membranes (BLMs).¹² Rupture is induced by short electric voltage pulses across the membrane. The average voltage necessary to induce breakdown gives information on the energy barrier of defect formation. In Table 1 we give the critical voltage leading to irreversible rupture for two different lipids with two different headgroups. The breakdown voltage is about the same for BLMs made of lipids with phosphatidylserine (PS) headgroups and for BLMs made of lipids with phosphatidylcholine (PC) headgroups. Moreover the breakdown voltage is independent of the ionic strength of the aqueous medium surrounding the BLMs. This indicates that the stability of the BLMs is not dominated by mutual electrostatic repulsion of the headgroups. However, the breakdown voltage depends on the type of hydrophobic chain of the lipids. Palmitoyl-oleoyl (PO) membranes require ~ 100 mV

Table 1 Average breakdown voltage and average rupture velocity for four different lipids

	2 M KCl	100 mM KCl	10 mM KCl
Rupture velocity/cm s ⁻¹			
POPC	455 \pm 7	400 \pm 6	420 \pm 23
POPS	480 \pm 20	410 \pm 20	435 \pm 25
DPhPC	527 \pm 2	546 \pm 15	565 \pm 25
DPhPS	525 \pm 25	530 \pm 15	530 \pm 25
Breakdown voltage/mV			
POPC	8 \pm 1	5 \pm 1	5 \pm 0.5
POPS	14 \pm 1	5 \pm 1	5 \pm 2
DPhPC	33 \pm 2	19 \pm 2	20 \pm 4
DPhPS	43 \pm 3	20 \pm 1.5	20 \pm 2

smaller breakdown voltages compared to diphytanoyl (DPh) membranes.

Rapid transmembrane voltage decay during rupture allows one to evaluate the kinetics of defect widening. Surprisingly the rupture kinetics depends on the hydrocarbon chains. It was found to be four times faster for DPh than for PO membranes and independent of the type of headgroup.¹²

In a second series we investigated the stability and rupture kinetics of planar lipid membranes covered with electrostatically coupled polyelectrolytes.¹³ After black lipid membranes were formed from negatively charged lipids, polylysines (PLs) of different molecular weights (MW) were added on one or on both sides of the membrane. The adsorption of PL was detected by recording changes of the transmembrane voltage. Adsorption of PL on one side of the membrane leads to an asymmetric transmembrane potential, which adds to the externally applied voltage. High-MW PL decreases the critical breakdown voltage of the membrane significantly as shown in Table 2. Interestingly the presence of polylysine also increases the delay time between the voltage pulse and pore formation. Adsorption of PL alters the time course of pore widening in a molecular-weight-dependent manner. Low-MW PL-decorated membranes and undecorated membranes show a fast rupture determined by inertia. In contrast, adsorption of high-MW PLs causes a significant decrease of the critical voltage leading to rupture.¹³

Lipid membranes can also be coated with water-soluble polymers linked by hydrophobic interaction.¹⁴ Here we covalently linked hydrophobic anchors to larger water-soluble dextran. Coating lipid membranes with dextran *via* a hydrophobic linker drastically destabilized the membrane as shown in Table 3. The density of the hydrophobic anchor groups along the polymer chains is found to be of considerable influence. While dextran with a low anchor group density slows down the inertia-driven rupture process of lipid membranes, dextran with higher anchor group density alters the kinetics and causes an exponential increase in membrane conductance, suggesting a viscosity-determined rupture process. Dextran derivatives of medium anchor group density show a transition from a viscosity- to an inertia-limited rupture.¹⁴

In a third series of experiments planar lipid membranes from DPhPS/styrene/divinylbenzene 4 : 1 : 1 were formed. Due to their low solubility in water, styrene and divinylbenzene are mainly dissolved within the hydrophobic part of the bilayer. After thinning, the capacitance of the monomer-swollen membranes was recorded, and no significant differences from pure DPhPS membranes were found. Subsequently rupture was induced and values similar to those for pure DPhPS membranes were observed. Polymerization of the styrene/divinylbenzene mixture in the hydrophobic part of the

Table 2 Average breakdown voltage for symmetrical addition of polylysine and 100 mM KCl

DPhPS alone	530 \pm 20 mV
+ PL MW 600	525 \pm 15 mV
+ PL MW 8000	540 \pm 24 mV
+ PL MW 42 000	500 \pm 26 mV
+ PL MW 420 000	426 \pm 20 mV

Table 3 Average breakdown voltage in the presence of dextran with different hydrophobic anchor and 100 mM KCl

DPhPS alone	530 \pm 20 mV
+ dextran	510 \pm 12 mV
+ dodecyl-dextran-1	416 \pm 24 mV
+ dodecyl-dextran-3	388 \pm 13 mV
+ dodecyl-dextran-6	310 \pm 11 mV

membrane could be induced by 10 min UV irradiation.^{16–17} Polymerization leads to the formation of a polymer network. This network causes a drastic change in the rupture behaviour. In about 50% of cases critical voltages above 1 V were necessary to induce an electrical discharge, which was characterized by a voltage relaxation to finite values [see Fig. 2(a)]. An analysis using eqn. (2) of the rapid voltage decay gives the apparent pore size. As shown in Fig. 2(b) the pore opens linearly up to micrometre size at about 0.04 m s^{-1} and reseals again. Capacitance measurements after the pulse revealed an intact membrane with capacitance similar to that before inducing rupture.

Discussion and conclusion

The main advantage of free-standing giant lipid membrane systems is their well-defined and defect-free structure, which allows the application of electrophysiological techniques. The most surprising result of our investigation concerning stability was the insensitivity of membrane stability to the ionic strength. For PC membranes this is somewhat expected, but not for PS headgroups. Assuming each PS headgroup to be dissociated gives a fairly high surface charge density. Calculating the surface potential based on Poisson–Boltzmann theory results in significantly higher voltages than the measured ones.¹⁵ Even using the lower experimental voltages observed gives rise to unreasonably high repulsive forces, which do not allow stable lamellar phases, as the additional repulsive forces are above the mechanical ones leading to rupture. The answer is likely an overestimation of the electrostatic forces within the first layer.

Adsorption of large polymers destabilizes giant soft planar lipid membranes. Adsorption can only occur at the cost of entropy which the polymer coil has to pay. This clearly gives rise to a destabilization effect in agreement with the observation.

A significant stabilization can be achieved with a 2-D polymer network formed inside the hydrophobic lipid layer as schematically shown in Fig. 3. Here the lipid preserves the fluidity necessary to reseal small defects occurring transiently due to external forces. For the polymer-containing mem-

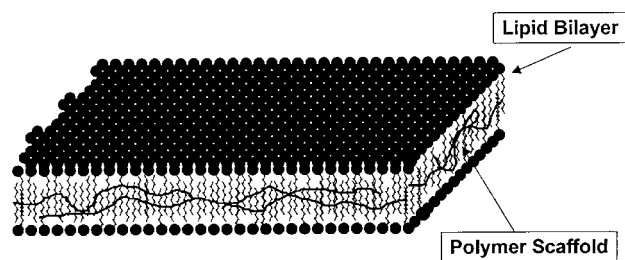


Fig. 3 Schematic sketch to illustrate a 2-D polymer network. The actual structure of the 2-D network is not yet resolved. A more detailed discussion may be found in ref. 17.

branes an additional dissipative mechanism has to be taken into account: During rupture of the membrane the polymer chains of the 2-D polymer network structure also have to be disrupted. Up to this point the underlying network chains are stretched elastically. As a result of the associated energy dissipation the velocity of defect growth decreases with time and finally stops. Subsequently the energetically favorable pore closes again due to lateral diffusion of the lipid molecules. Application of a second voltage pulse gave similar features to those of a pure DPhPC membrane concerning critical voltages and rupture velocities. Obviously, the polymer network structure is ‘pre-damaged’ during the first pulse and hence no longer able to dissipate enough energy to stop the growth of the defect.

We are currently investigating the extent to which this approach is compatible with functional reconstitution of membrane proteins. First results on a similar system were promising.¹⁸

Acknowledgements

We would like to thank the Swiss National Science Foundation and INTAS 96-1310 for financial support.

References

- 1 A. Charbit, C. Andersen, J. Wang, B. Schiffler, V. Michel, R. Benz and M. Hofnung, *Mol. Microbiol.*, 2000, **35**, 777.
- 2 T. K. Rostvtseva, T. T. Liu, M. Colombini, V. A. Parsegian and S. M. Bezrukov, *Proc. Nat. Acad. Sci. USA*, 2000, **97**, 7819.
- 3 M. Akeson, D. Branton, J. J. Kasianowicz, E. Brandin and D. W. Deamer, *Biophys. J.*, 1999, **77**, 3227.
- 4 B. A. Cornell, V. L. Braach-Maksvytis, L. G. King, P. D. Osman, B. Raguse, L. Wiczorek and R. J. Pace, *Nature*, 1997, **387**, 580.
- 5 S. Heyse, T. Stora, E. Schmid, J. H. Lakey and H. Vogel, *Biochim. Biophys. Acta*, 1998, **1376**, 319.
- 6 K. Seifert, K. Fendler and E. Bamberg, *Biophys. J.*, 1993, **64**, 384.
- 7 T. Stora, J. H. Lakey and H. Vogel, *Angew. Chem. Int. Ed. Engl.*, 1999, **38**, 389.
- 8 M. Winterhalter, *Colloids Surf. A*, 1999, **149**, 547.
- 9 P. Mueller, D. P. Rudi, H. T. Tien and W. C. Wescott, *J. Phys. Chem.*, 1963, **67**, 534.
- 10 M. Montal and P. Mueller, *Proc. Nat. Acad. Sci. USA*, 1979, **69**, 3561.
- 11 C. Wilhelm, M. Winterhalter, U. Zimmermann and R. Benz, *Biophys. J.*, 1993, **64**, 121.
- 12 A. Diederich, G. Bähr and M. Winterhalter, *Phys. Rev. E*, 1998, **58**, 4883.
- 13 A. Diederich, G. Bähr and M. Winterhalter, *Langmuir*, 1998, **14**, 4597.
- 14 A. Diederich, M. Strobel, W. Meier and M. Winterhalter, *J. Phys. Chem. B*, 1999, **103**, 1402.
- 15 G. Bähr, A. Diederich, G. Vergeres and M. Winterhalter, *Biochemistry*, 1998, **37**, 16252.
- 16 J. Hotz and W. Meier, *Langmuir*, 1998, **14**, 1031.
- 17 J. Hotz and W. Meier, *Adv. Mater.*, 1998, **10**, 1387.
- 18 C. Nardin, S. Thoeni, J. Widmer, M. Winterhalter and W. Meier, *Chem. Commun.*, 2000, 1433.

PUBLICATION 2

Nanoreactors From Polymer-Stabilized Liposomes

Nanoreactors from Polymer-Stabilized Liposomes

Alexandra Graff,[†] Mathias Winterhalter,[‡] and Wolfgang Meier^{*,†}

Department of Physical Chemistry, University of Basel, Klingelbergstrasse 80, CH-4056 Basel, Switzerland, and IPBS-CNRS UPR 9062, University Paul Sabatier, F-31077, Toulouse, France

Received September 12, 2000. In Final Form: November 13, 2000

We introduce new nanometer-sized bioreactors based on liposomes functionalized by incorporated natural channel proteins. Additionally the lipid bilayers of the underlying liposomes can be stabilized by a cross-linking polymerization of hydrophobic methacrylate monomers in the interior of the membranes. As a representative example we functionalize (polymer-stabilized) 1-palmitoyl-2-oleoyl-*sn*-glycero-3-phosphocholine liposomes by reconstituting a channel-forming protein from the outer cell wall of Gram-negative bacteria. The protein used (OmpF) acts as a size-selective filter, which allows only passage of molecules with a molecular weight below 400 g mol⁻¹. Substrates below this size may still have access to enzymes encapsulated in the nanocontainers. We demonstrate this using the enzyme β -lactamase, which is able to hydrolyze the antibiotic ampicillin. Interestingly the enzyme and the membrane channel preserve their activity even in the presence of the hydrophobic methacrylate monomers and after their cross-linking polymerization.

Introduction

A current research field in material science is to formulate new types of responsive materials on a nanometer-sized scale. Although it is quite a challenge in the laboratory, nature provides already optimized solutions for this. For example, the outer cell wall of bacteria, such as *Escherichia coli*, contains channel proteins that allow specific substrates to diffuse into the periplasmic space from where they are uptaken actively to the inside.¹ Bacteria can open and close these channels upon specific triggers,² and they have mechanisms to eject material outside. It is tempting to use such an optimized system to create a synthetic nanoreactor with controlled permeability and the ability to react on external stimuli.

A typical and widespread model system for nanocapsules are liposomes.^{3,4} They can easily be formulated using the extrusion technique. However, such liposomes are generally rather unstable.^{3,4} A stabilization of the liposomes by polymerization of reactive lipid molecules is feasible but destroys the lateral mobility of the lipids required for the functionality of certain membrane proteins. Recently it was shown that polyelectrolyte multilayer nanocapsules can be coated with lipid membranes.⁵ Such supported vesicles are more stable, but due to interactions with the underlying polyelectrolyte skeleton, their shells may have defects, i.e., not all of them are completely tight.⁵ Another solution is to formulate block copolymer vesicles which later can be cross-linked via polymerizable groups at the water-soluble blocks.^{6,7}

Here in this work we suggest a different type of stabilization. We add hydrophobic methacrylate monomers to aqueous liposome dispersions which penetrate into the hydrophobic interior of the lipid membranes (see for example refs 8–12). These monomers can easily be polymerized inside the membranes by an UV-induced free radical polymerization. As shown previously this may lead to the formation of a 2-D polymer network in the middle of the membrane on which the lipid molecules can freely glide.¹³ Similar to the network of erythrocytes the polymer acts as a scaffold which stabilizes the membrane. This has recently been quantified using giant, free-standing, planar lipid membranes which became extremely stable after polymerization.¹³

Here we demonstrate that inside such liposomes water-soluble enzymes can be encapsulated thereby leading to a small bioreactor. We chose β -lactamase as a model enzyme. β -Lactamase is part of the natural defense system of bacteria and hydrolyses β -lactam antibiotics such as ampicillin.^{14–16} However, the low permeability for substrates across lipid membranes limits drastically the turn over of encapsulated enzymes^{17–20} which have thus rather limited applications. To overcome this limit, we propose

* Corresponding author. Tel: ++41 61 2673835. Fax: ++41 61 2673855. E-mail: wolfgang.meier@unibas.ch.

[†] University of Basel.

[‡] University Paul Sabatier.

(1) Schirmer, T. *J. Struct. Biol.* **1998**, *121*, 101.

(2) Delcour, A. H. *FEMS Microbiol. Lett.* **1997**, *151*, 115. Van Gelder, P.; Dumas, F.; Winterhalter, M. *Biophys. Chem.* **2000**, *85*, 153.

(3) Lasic, D. D. *Liposomes: From Physics to Applications*; Elsevier Science Publications B.V.: Amsterdam, 1993.

(4) Ringsdorf, H.; Schlarb, B.; Venzmer, J. *Angew. Chem.* **1988**, *100*, 117.

(5) Moya, S.; Donath, E.; Sukhorukow, G. B.; Auch, M.; Bäuml, H.; Lichtenfeld, H.; Möhwald, H. *Macromolecules* **2000**, *33*, 4538.

(6) Nardin, C.; Hirt, T.; Leukel, J.; Meier, W. *Langmuir* **2000**, *16*, 1035.

(7) Nardin, C.; Thoeni, S.; Widmer, J.; Winterhalter, M.; Meier, W. *Chem. Commun.* **2000**, 1433.

(8) Murtagh, J.; Thomas, J. K. *Faraday Discuss. Chem. Soc.* **1986**, *81*, 127.

(9) Kurja, J.; Noelte, R. J. M.; Maxwell, I. A.; German, A. L. *Polymer* **1993**, *34*, 2045.

(10) Poulain, N.; Natache, E.; Pina, A.; Levesque, G. *J. Polym. Sci., Part A: Polym. Chem.* **1996**, *34*, 729.

(11) Morgan, J. D.; Johnson, C. A.; Kaler, E. W. *Langmuir* **1997**, *13*, 6447.

(12) Hotz, J.; Meier, W. *Langmuir* **1998**, *14*, 1031.

(13) Meier, W.; Graff, A.; Diederich, A.; Winterhalter, M. *Phys. Chem. Chem. Phys.* **2000**, *2*, 4559.

(14) Zimmermann, W.; Rosselet, A. *Antimicrob. Agents Chemother.* **1977**, *12*, 368.

(15) Nikaido, H.; Rosenberg, E. *J. Bacteriol.* **1983**, *153*, 241.

(16) Nikaido, H.; Rosenberg, E.; Foulds, J. *J. Bacteriol.* **1983**, *153*, 232.

(17) Kato, Y.; Hosokawa, T.; Hayakawa, E.; Ito, K. *Biol. Pharm. Bull.* **1993**, *16*, 740.

(18) Shimizu, M.; Miwa, Y.; Hashimoto, K.; Goto, A. *Biosci. Biotechnol. Biochem.* **1993**, *57*, 1445.

(19) Nema, S.; Kiick, D. M.; Avis, K. E. *PDA J. Pharm. Sci. Technol.* **1994**, *48*, 231.

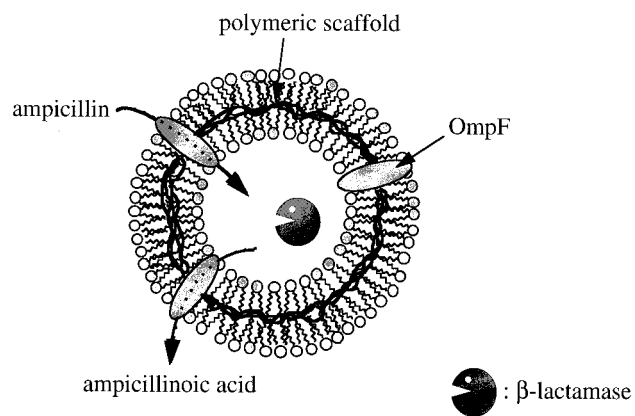


Figure 1. Schematic representation of a polymer-stabilized nanoreactor with encapsulated enzyme.

a novel technique to control the permeability of the liposomes using naturally occurring membrane channels with selected features. As an example we use OmpF, a channel protein from the outer cell wall of *E. coli*. The resulting nanoreactors are stabilized by polymerization of hydrophobic monomers inside their lipid bilayers. A schematic representation of the resulting nanoreactors is shown in Figure 1. The influence of the presence of hydrophobic monomers and subsequent free-radical polymerization on the functionality of the channel proteins and the enzyme activity is quantified.

Experimental Section

Materials. The lipid, 1-palmitoyl-2-oleoyl-*sn*-glycero-3-phosphocholine (POPC), was purchased from Avanti Polar Lipids Inc. (Birmingham, AL). The monomers, *n*-butyl methacrylate (BMA, Fluka) and ethylene glycol dimethacrylate (EGDMA, Fluka) were distilled over calcium hydride and stored at $-4\text{ }^{\circ}\text{C}$. The β -lactamase was obtained from Fluka and stored at $-20\text{ }^{\circ}\text{C}$ under argon. Ampicillin was purchased from Sigma and used without further purification. The protein, OmpF from the outer membrane of *E. coli* was purified according to previous protocols²¹ and stored at 1 mg mL^{-1} in 1% octyl-POE detergent (Alexis, Lauchringen, Switzerland).

Preparation of OmpF-Containing Liposomes and Encapsulation of the β -Lactamase. Two milliliters of a POPC stock solution in chloroform (10 mg mL^{-1}) was evaporated under high vacuum over 6 h. Afterward $20\text{ }\mu\text{L}$ of a 1 mg mL^{-1} stock solution of OmpF in 1% detergent octyl-POE (OPOE) was added, vortexed to provide a homogeneous mixture, and dried again for a short period (molar ratio POPC:OmpF $\approx 5 \times 10^4$). The dry mixed POPC/protein film was dispersed in 1 mL of buffer containing 10 mM Hepes, 100 mM NaCl, and 0.11 mg mL^{-1} β -lactamase at pH 7.4. This yields a dispersion containing multilamellar, polydisperse liposomes. A freeze-thaw cycle was applied to the dispersion consisting of five cycles of freezing in liquid nitrogen and thawing in a water bath at $30\text{ }^{\circ}\text{C}$. To obtain unilamellar liposomes of rather uniform size the dispersion was repeatedly extruded through polycarbonate filters (Nucleopore filters (Millipore)) with a pore size of 200 nm. Nonencapsulated β -lactamase was removed chromatographically (Sephadex G-150, Pharmacia) from the porin-containing liposomes.

Dynamic light scattering showed that generally the resulting liposomes (with and without OmpF and/or β -lactamase) had a unimodal size distribution with a polydispersity of about 20%, in good agreement with previously reported values on extruded liposomes.^{22–24} Their average hydrodynamic radius was typically around 150 nm.

Polymerization of Hydrophobic Monomers inside the Lipid Membranes. Five milliliters (2 mg mL^{-1} with respect to the lipid) of the liposome solution was mixed with 1.01 mg ($9 \times 10^{-4}\text{ mol}$) of BMA and 0.7 mg ($4.5 \times 10^{-4}\text{ mol}$) of the cross-linking agent EGDMA. Purified argon was bubbled through the solution to eliminate oxygen. The polymerization was initiated by UV-irradiation (Ultratech 400W, $\lambda = 254\text{ nm}$, Osram AG) for 30 min. Previous investigations showed a nearly complete conversion of the monomers under these conditions.¹² A schematic representation of the resulting polymer-stabilized nanoreactors is shown in Figure 1.

β -Lactamase Assay. The enzyme β -lactamase is able to hydrolyze β -lactam antibiotics such as ampicillin. The activity of the enzyme can be quantified via a secondary reaction. In contrast to ampicillin the product of the hydrolysis, the ampicillinoic acid, can reduce iodine to iodide. This can readily be monitored by iodometry, i.e., via the decolorization of a starch-iodine complex.^{25,26} To check the functionality of the system, we added $5\text{ }\mu\text{L}$ of a 20 mM ampicillin solution (in 10 mM Hepes, 100 mM NaCl, pH 7.4) to 0.5 mL of the nanoreactor dispersion and incubated the resulting mixture for the desired time interval. Starch-iodine reagent was prepared by mixing 5 mL of a 8 mM iodine, 320 mM potassium iodide solution with 20 mL 1 M sodium wolframate, and 50 mL of 2 M acid acetic and then adding 5 mL of 2 wt % soluble starch which had been dissolved in 1 M acetic acid by gentle boiling for 3 min. The hydrolysis reaction was stopped by adding 0.5 mL of this starch-iodine reagent to the reaction mixture,²⁵ and the absorbance of the starch-iodine complex at 623 nm (where the complex shows an absorption maximum) was measured as a function of time using a Hewlett-Packard 8452A spectrophotometer. The standard curve for the assay was linear over the relevant ampicillinoic acid concentration range from 0.1 to $50\text{ }\mu\text{M}$ (see also refs 25 and 26). To convert the rates of decolorization of the starch-iodine complex into enzyme reaction velocities, the iodine consumption of the system after the respective incubation time was determined using the Beer-Lambert law.²⁶

Dynamic Light Scattering. Dynamic light scattering experiments were performed using a commercial goniometer ALV-Langen equipped with a frequency-doubled Nd:YAG laser (ADLAS, $\lambda = 532\text{ nm}$ at $20\text{ }^{\circ}\text{C}$). An ALV-5000/E correlator calculates the photon intensity autocorrelation function $g_2(t)$. The samples were prepared by filtering through Millipore filters ($0.22\text{ }\mu\text{m}$, Millex GV for aqueous solutions). The data were analyzed using CONTIN. Dynamic light scattering investigations were routinely employed to determine the hydrodynamic radius of the samples.

In agreement with previous investigations, the polymerization did not lead to any measurable changes in size and size distribution of the liposomes.¹² To demonstrate the polymer-scaffold-induced stabilization of the liposomes, we performed lysis experiments with the detergent OPOE. Prior to the light scattering investigations, the liposomes were incubated for 12 h at room temperature with OPOE. Additional control measurements after 48 and 72 h generally reproduced the results. The data for the liposomes before and after polymerization are shown in Figure 2. A titration of the POPC liposomes leads to a rapid breakdown, and above a molar ratio OPOE/POPC of about 5:1, only mixed surfactant-lipid micelles are detected with a hydrodynamic radius of $R_h = 15\text{ nm}$. In contrast to that, the polymer-containing liposomes are resistant to lysis and their hydrodynamic radius remained constant at 168 nm at least up to a molar ratio of OPOE: POPC of 40:1 where we stopped the experiment. This is expected since the polymer shells formed inside the lipid bilayers have approximately the same dimensions as the liposomes.

It has to be emphasized that the polymer-containing liposomes can be isolated from the aqueous phase by lyophilization. The resulting white powder can subsequently be redispersed in

(20) Schumacher, I.; Arad, A.; Margalit, R. *Biotechnol. Appl. Biochem.* **1999**, *30*, 225.

(21) Saint, N.; Lou, K. L.; Widmer, C.; Luckey, M.; Schirmer, T.; Rosenbusch, J. P. *J. Biol. Chem.* **1996**, *271*, 20676.

(22) van Zanten, J. In *Vesicles*; Rosoff, M., Ed.; Marcel Dekker: New York, 1996; Vol. 62, p 240.

(23) van Zanten, J. H.; Monbouquet, H. G. *J. Colloid Interface Sci.* **1991**, *146*, 330.

(24) Ruf, H.; Georgalis, Y.; Grell, E. *Methods Enzymol.* **1989**, *172*, 364.

(25) Zimmermann, W.; Rosselet, A. *Antimicrob. Agents Chemother.* **1977**, *12* (3), 368.

(26) Novick, R. P. *Biochem. J.* **1962**, *83*, 236.

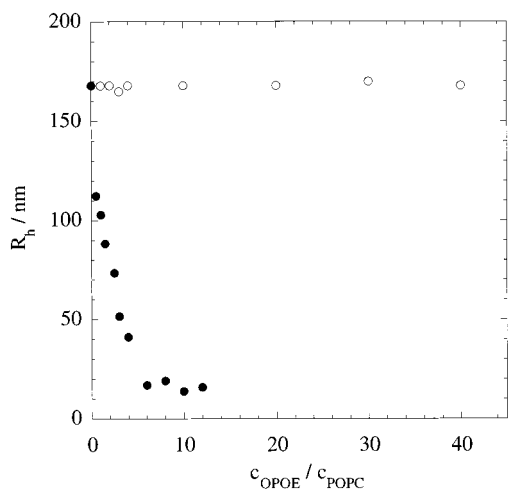


Figure 2. Hydrodynamic radius R_h as a function of the molar ratio of surfactant (OPOE) to lipid (POPC), $c_{\text{OPOE}}/c_{\text{POPC}}$.

aqueous media by sonification thus yielding particles of the same size as the original liposomes. Obviously the polymer-stabilized liposomes preserve their hollow sphere morphology even in the dry state.

Permeability of the Lipid Bilayers. We tested the permeability of the liposomes before and after polymerization to ensure tightness of their shells. Here we encapsulated the fluorescent dye 6-carboxyfluorescein (10 μM) and added Co^{2+} ions (500 μM) to the external aqueous phase. It is well-known that Co^{2+} acts as a quencher for 6-carboxyfluorescein. Hence permeation of either Co^{2+} ions or the dye across the membranes would cause a reduction in fluorescence intensity. Generally the fluorescence intensity (excitation wavelength 490 nm, measuring wavelength 520 nm) remained constant for at least 2 days after addition of Co^{2+} ; i.e., the shells of the particles are completely impermeable on this time scale. If the liposomes are destroyed by addition of OPOE, the fluorescence intensity decreases within a few seconds to zero. It is interesting to note that the fluorescence of the polymer-containing liposomes was also quenched in the presence of OPOE. Obviously the particles become leaky in the presence of the surfactant despite their morphological stabilization (see above).

Results and Discussion

To control the permeability of liposomes, we propose to insert naturally occurring membrane channels with selected features into their shells. As an example we use the porin OmpF, a channel from the outer cell wall of *E. coli*. It has the advantage to be extremely stable and available in large enough quantities to allow technological applications. Generally, porins are transmembrane proteins that form trimeric channels in the outer membrane of Gram-negative bacteria.²⁷ These water-filled channels allow passive diffusion of small solutes such as ions, nutrients, or antibiotics across the biological membrane. Molecules with a molecular weight above 400 g mol^{-1} are sterically excluded from the OmpF channels.²⁷

For our experiments we encapsulated the enzyme β -lactamase (M_w 50 000 g mol^{-1}) in the aqueous core domain of POPC liposomes. β -Lactamase hydrolyzes β -lactam antibiotics such as ampicillin (M_w 349 g mol^{-1}). The activity of the enzyme reaction can be monitored via a secondary reaction. In contrast to ampicillin, the product of the hydrolysis, the ampicillinoic acid, can reduce iodine to iodide. This can readily be monitored after quenching the hydrolysis reaction by iodometry, i.e., via the decolorization of a starch-iodine complex.^{25,26} The results are shown in Figure 3 together with the control experiments

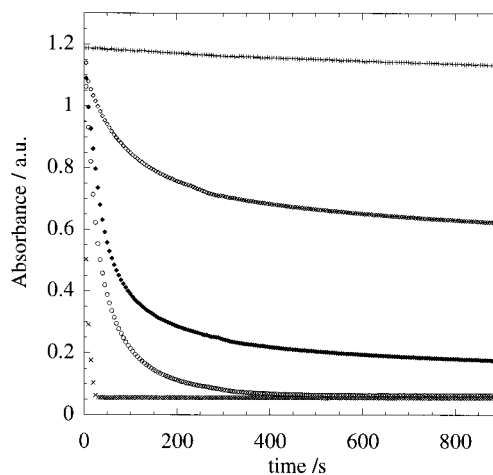


Figure 3. Time profile of the absorbance of the starch-iodine complex at 550 nm after incubation in the presence of 10 μL of a 1 mM ampicillin solution (10 mM Hepes, 100 mM NaCl, pH 7.4): \times , control with free, nonencapsulated enzyme; $+$, control with POPC liposomes without OmpF channels. OmpF-containing POPC liposomes incubated with ampicillin for (\diamond) 10 min, (\blacklozenge) 20 min, and (\circ) 30 min.

for the free, nonencapsulated enzyme and liposomes in the absence of OmpF channels. For liposomes made in the absence of porin, the absorbance remained constant on the time scale of the experiment. As expected the ampicillin is not able to diffuse across the lipid membranes of the liposomes. Therefore it is not hydrolyzed by the enzyme and the iodine is not reduced. In contrast to that for the OmpF-containing liposomes the absorbance of the complex decreases with time due to the reduction of the iodine by the ampicillinoic acid present in the system. The saturation values reflect the overall amount of ampicillinoic acid produced during the respective incubation time. Furthermore, inspection of Figure 3 shows that for a given incubation time the amount of hydrolyzed ampicillin and, hence, the reaction rate of encapsulated enzyme is lower than that in the control experiment using the free enzyme under the given conditions. This is due to the slow diffusion of ampicillin and ampicillinoic acid through the rather limited number of narrow OmpF channels in the membranes of the liposomes. (An estimation of the amount of lipid added and the number of liposomes formed versus the amount of OmpF protein added yields approximately 2 OmpF trimers per liposome!)

From these data it is possible to calculate the amount of hydrolyzed ampicillin. For comparison we take the amount of ampicillin hydrolyzed by the free enzyme under these conditions as a reference (i.e., 1 $\mu\text{mol mg}^{-1} \text{min}^{-1}$). Figure 4 shows the results for the nanoreactors at various external substrate concentrations together with that for the free enzyme and the liposomes without reconstituted channel proteins. Obviously below an external ampicillin concentration of about 0.5 μM the relative activity (expressed as the ratio of hydrolysis rates) of the OmpF-containing liposomes is considerably decreased compared to the free enzyme (i.e., $58 \pm 10\%$ and $86 \pm 10\%$ for 0.2 and 0.4 μM , respectively). This suggests that the turnover of the enzyme is limited at these concentrations by the translocation through the channels. At higher substrate concentrations, however, this difference vanishes, demonstrating clearly the absence of the membrane as a permeation barrier. Translocation of ampicillin through the channels is proportional to the ampicillin concentration. Hence, at higher concentrations β -lactam hydrolysis

(27) Nikaido, H. *Mol. Microbiol.* **1992**, 6 (4), 435.

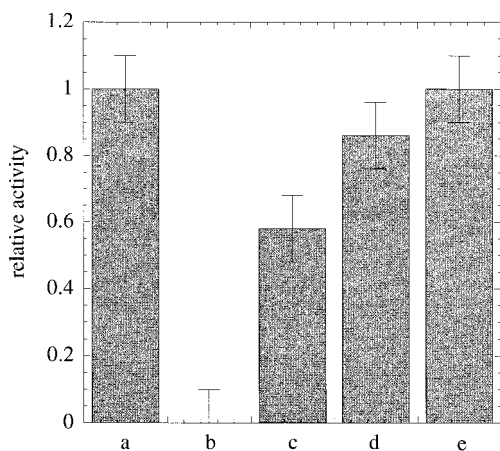


Figure 4. Relative activity (hydrolyzed ampicillin/hydrolyzed ampicillin by the free enzyme) of the encapsulated enzyme in liposomes and OmpF-containing liposomes ($c_{\text{ampicillin}}$, external ampicillin concentration): a, free enzyme; b, liposomes without OmpF; c, liposomes with OmpF (at $c_{\text{ampicillin}} = 0.2 \mu\text{M}$); d, liposomes with OmpF (at $c_{\text{ampicillin}} = 0.4 \mu\text{M}$); e, liposomes with OmpF (at $c_{\text{ampicillin}} = 0.8 \mu\text{M}$).

is no longer limited by the rate of antibiotics diffusion through the OmpF channels.

These results indicate clearly that the permeability of the shells of liposomes can be controlled by channel proteins. This suggests use of such functionalized liposomes for protection of sensitive enzymes against a hostile outside environment (e.g., protease). However, due to the noncovalent interactions responsible for their formation the underlying liposomes have only a limited stability and may undergo structural changes.³ Many applications require more stable particles. Therefore, in a second set of experiments we investigate whether such functionalized liposomes can be stabilized by a polymeric scaffold without loss of their activity. Hence we swell their lipid bilayers with a mixture of *n*-butyl methacrylate (BMA) and the cross-linker ethylene glycole dimethacrylate (EGDMA) (molar ratio BMA:EGDMA = 2:1), which can subsequently be polymerized by a UV-induced free radical polymerization.¹² Previous investigations have shown that the polymerization leads to the formation of a 2-D polymer network structure inside lipid bilayers without disrupting their structure (see also Figure 1 for a schematic representation).^{12,13} Moreover polymer-containing liposomes are considerably stabilized against surfactant lysis and are able to preserve their hollow sphere morphology even after lyophilization and redispersion in aqueous buffers (for details see Experimental Section).

Figure 5 shows the relative activity (i.e., ratio of reaction rates) of the functionalized liposomes in the presence of the hydrophobic monomers and after the cross-linking polymerization together with the control experiments for the corresponding systems without reconstituted OmpF. For the monomer-swollen and polymer-stabilized liposomes made in the absence of porin, no activity can be detected since the ampicillin cannot diffuse across the shells of the reactors. In the presence of reconstituted OmpF, the activity of the monomer swollen nanoreactors is always the same as that of the monomer-free system within the experimental error. Again above approximately $0.5 \mu\text{M}$ ampicillin the nanoreactors adopt the same activity as the free enzyme. This clearly indicates that the monomers do not denature the proteins or inhibit their function.

After polymerization, however, the activity of the functionalized liposomes decreases considerably. Since the

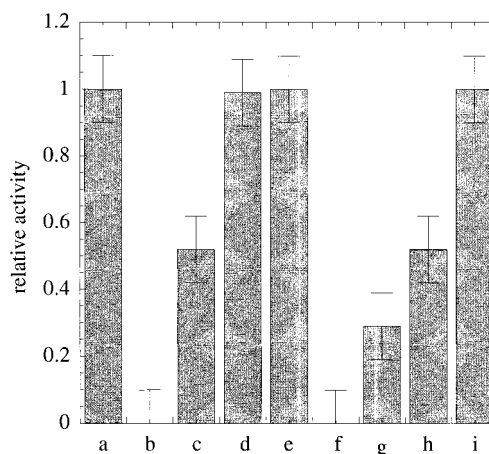


Figure 5. Relative activity (hydrolyzed ampicillin/hydrolyzed ampicillin by the free enzyme) of the encapsulated enzyme in monomer-containing and polymerized nanoreactors ($c_{\text{ampicillin}}$, external ampicillin concentration): a, free enzyme; b, monomer-swollen liposomes without OmpF; c, monomer-swollen liposomes with OmpF (at $c_{\text{ampicillin}} = 0.2 \mu\text{M}$); d, monomer-swollen liposomes with OmpF (at $c_{\text{ampicillin}} = 0.4 \mu\text{M}$); e, monomer-swollen liposomes with OmpF (at $c_{\text{ampicillin}} = 0.8 \mu\text{M}$); f, polymer-stabilized liposomes without OmpF; g, polymer-stabilized liposomes with OmpF (at $c_{\text{ampicillin}} = 0.2 \mu\text{M}$); h, polymer-stabilized liposomes with OmpF (at $c_{\text{ampicillin}} = 0.4 \mu\text{M}$); i, polymer-stabilized liposomes with OmpF (at $c_{\text{ampicillin}} = 0.8 \mu\text{M}$).

polymerization conditions (i.e., incubation of 5 mL of the β -lactamase stock solution in the presence of 1.01 mg of BMA and 0.7 mg of EGDMA for 1 h at room temperature and 30 min of UV-irradiation) do not lead to any detectable reduction of the activity of the free enzyme, this effect seems to originate from the OmpF channels. This is in agreement with a recent study on amphiphilic block copolymer membranes with reconstituted OmpF.²⁸ There it was shown that a polymerization may induce a closure or an expulsion of some of the reconstituted channels during the cross-linking reaction, probably due to internal stress occurring in the membrane in the course of the polymer chain reaction.²⁸

To quantify the time dependence of ampicillin hydrolysis by the nanoreactors, the decolorization was measured after different incubation times for a given ampicillin concentration. The results for the nanoreactors, the nanoreactors in the presence of the hydrophobic monomers and after polymerization, are shown in Figure 6. As can directly be seen after a lag time of about 10 min,²⁶ the hydrolysis rate was linear corresponding to a reaction kinetics of zero order. Since the same lag time is also observed in the case of the nonencapsulated enzyme, it seems to be related to the priming of the enzymatic reaction. Obviously for a given ampicillin concentration outside the nanoreactors, a steady state is rapidly established at which the rate of antibiotic diffusion through the OmpF channels and the β -lactam hydrolysis are equal thus resulting in a constant ampicillinic acid release. While this release is the same for the monomer-free and the monomer-swollen nanoreactors, that for the polymerized system is decreased by a factor of 1.7 due to partial closure of OmpF channels. Nevertheless the results indicate that the nanoreactors are interesting as a new type of delivery device for applications in pharmacy and diagnostics. Especially as such systems often require a constant release of substances over an extended period of time.

(28) Nardin, C.; Winterhalter, M.; Meier, W. *Angew. Chem.* **2000**, *112*, 4747. *Angew. Chem., Int. Ed.* **2000**, *39*, 4599.

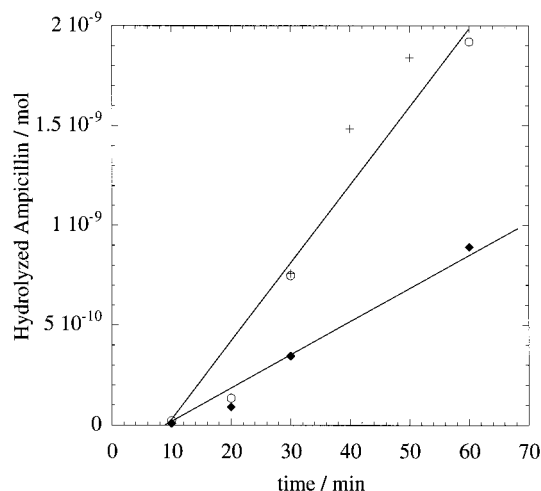


Figure 6. Amount of hydrolyzed ampicillin as a function of time: +, liposomes with OmpF; O, monomer-swollen liposomes with OmpF; ♦, polymer-stabilized liposomes with OmpF.

Conclusions

We have presented a route to prepare a new kind of effective bioreactor. As a representative example we incorporated the bacterial channel protein OmpF into the shells of POPC liposomes. The lipid membranes of the system can subsequently be stabilized by polymerization of hydrophobic monomers inside the lipid bilayers. This leads to the formation of a 2-D polymer network structure in the interior of the bilayers without disrupting the integrity of the membranes. Interestingly the functionality of the membrane protein is preserved despite the artificial surrounding within monomer-containing and/or polymer-stabilized membranes. For solutes with a molecular weight

below 400 g mol^{-1} , the incorporated channels allow a free molecular exchange between the interior of the resulting nanocapsules and the bulk medium.

In our present study we encapsulated the enzyme β -lactamase in the interior of the liposomes. It is important to note that this enzyme preserves its full activity in the presence of the hydrophobic methacrylate monomers and even after their cross-linking polymerization inside the lipid bilayers. Due to their size selectivity the functionalized shells of the (polymer-stabilized) liposomes provide a selective permeability, which allows protecting of the guest enzyme against a hostile outside environment (e.g., protease) and simultaneously controls the diffusion of substrates and products.

Moreover, it has to be emphasized that the system introduced in the current study is a representative example of this new type of nanometer sized bioreactors. In fact, nature provides many more specific, unspecific, or ligand gated channels which can be reconstituted in the same way providing a unique tool to control the permeation across nanoreactor shells. We believe that the principle of using the protective ability of such nanoreactors in combination with controlled permeability either by natural or genetically modified channels or pumps will have many future applications. For example, the encapsulation could be extended to antibodies and then decrease the immunogenicity of the enzyme when injected in plasma. This allows using enzymes designated to have a therapeutic role from various sources.

Acknowledgment. We thank F. Dumas, C. Nardin, and P. Van Gelder and for valuable advice and the Swiss National Science Foundation for financial support.

LA001306M

Additional results (publication 2)

To check the influence of crosslinking density on stability and integrity of the polymer stabilized liposomes we prepared particles with different crosslinking density controlled by the molar ratio of the crosslinker (EGDMA), to monomer (BMA). The two molar ratios used were EGDMA:BMA=2:1 and 1:1, respectively (Figure 1).

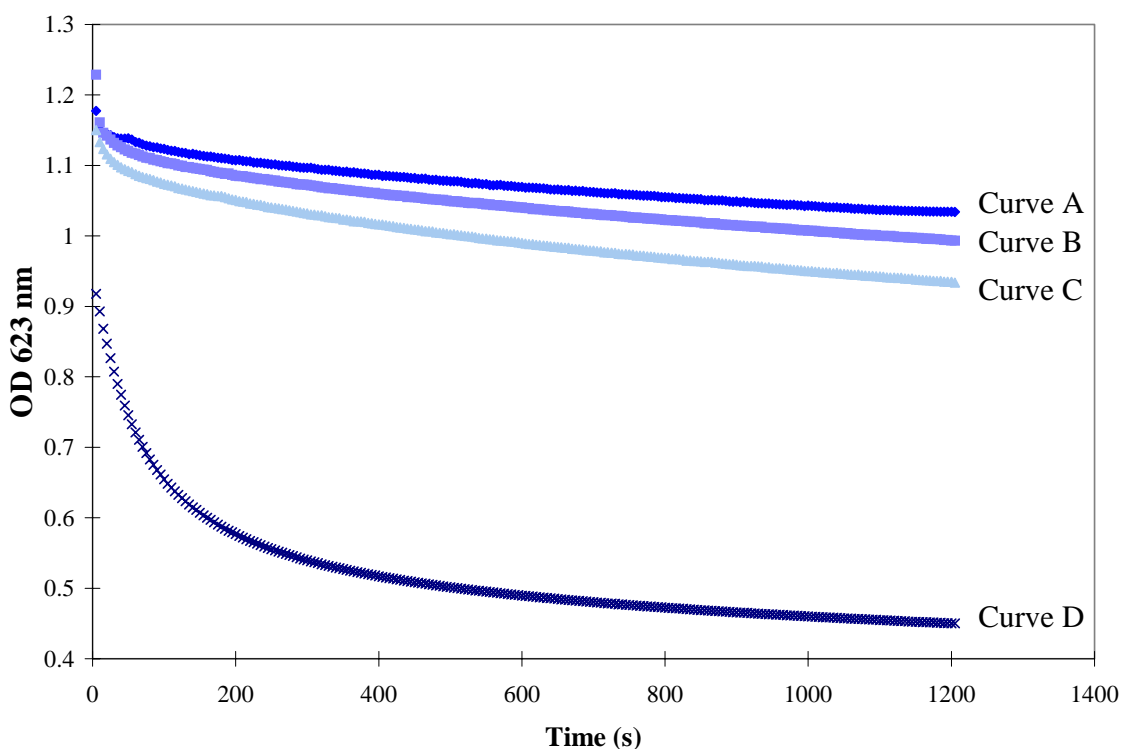


Figure 1. Time profile of the absorbance of the starch-iodine complex at 623 nm after incubation in the presence of 10 μ l of a 1 mM ampicillin solution (10 mM HEPES, 100 mM NaCl, pH 7.4): Curve A represents the control sample containing liposomes without polymer stabilization. Curve B and C represent respectively liposomes prepared with EGDMA:BMA ratio of 2:1, with and without polymerization. Curve D represents stabilized liposomes containing EGDMA:BMA ratio of 1:1 without UV polymerization.

As shown in Figure 1 inside the nanocapsule we encapsulated as described in the publication 2 the β -lactamase and added ampicillin to the external solution.

Obviously for higher crosslinking density the liposomes are not tight. In contrast to the control experiments we observed here considerably hydrolysis of the penicillin which indicates that the substrate had direct access to the enzyme inside the containers. Inside the lipid bilayer the stabilized polymer network is forced into a nearly 2-D configuration. The associated loss of entropy lead to mechanical stress acting against the confinement of the network inside the lipid bilayer. With increasing crosslinking density the elastic modulus of the network increase and hence also the mechanical stress on the membrane. Above a certain threshold stress the polymer network can therefore induce defects in the membrane that allow the passage of penicillin

CHAPTER 2:

***Insertion of Membrane Proteins in Block Copolymer
Membranes***

Summary

It has been demonstrated that membrane proteins could be successfully reconstituted in block copolymer membranes. Interestingly, these proteins remain functional despite the 2-3 higher thickness of the block copolymer membrane compared to lipid bilayers. In addition, under specific conditions (polymerizable groups at the ends of the hydrophilic blocks) the proteins can even survive subsequent polymerization of the block copolymer matrix (Meier, 2000; Nardin and Meier, 2000).

Following those preliminary studies on membrane protein insertion we proposed in the present work a systematic study of different membrane proteins reconstituted in block copolymer membranes. The studies were performed using different functional test showing the functional reconstitution of different membrane proteins.

PUBLICATION 3

Virus-Assisted Loading of Polymer Nanocontainers

Virus-assisted loading of polymer nanocontainer

Alexandra Graff*, Marc Sauer*, Patrick Van Gelder†, and Wolfgang Meier**§

*Department of Physical Chemistry, University of Basel, Klingelbergstrasse 80, CH-4056 Basel, Switzerland; †Department of Ultrastructure, Vrije Universiteit Brussel, Paardestraat 65, B-1640 Sint-Genesius-Rode, Belgium; and ‡School of Engineering and Science, International University of Bremen, Campus Ring 1, 28759 Bremen, Germany

Edited by Jack Halpern, University of Chicago, Chicago, IL, and approved January 18, 2002 (received for review December 7, 2001)

We present a DNA-containing polymeric nanocontainer using the self-assembled superstructure of amphiphilic block copolymers in aqueous solutions. To demonstrate that DNA translocation is possible across a completely synthetic block copolymer membrane, we have used a phage transfection strategy as a DNA-transfer model system. For this purpose the bacterial channel forming protein LamB was reconstituted in ABA-triblock copolymer vesicles. The outer membrane protein LamB is a specific transporter for maltodextrins but also serves as a receptor for λ phage to trigger the ejection of λ phage DNA. We demonstrate that the functionality of the LamB protein is fully preserved despite the artificial surrounding. This leads to a type of polymeric vehicle for DNA that could be useful for gene therapy.

It is well known that, similar to conventional lipids, appropriate amphiphilic block copolymers may self-assemble in aqueous media to membrane-like superstructures (e.g., vesicular aggregates; refs. 1–3). As a typical example, we introduced recently amphiphilic ABA-triblock copolymers consisting of a hydrophobic, highly flexible poly(dimethylsiloxane) (PDMS) middle block and two water-soluble poly(2-methyloxazoline) (PMOXA) side blocks that spontaneously form unilamellar vesicles in water (4). These block copolymer vesicles were found to be considerably more stable than, for example, conventional low molar mass lipid vesicles, reflected by the fact that they are stable over several years and do not show any changes in size or size distribution during that time within experimental error. Moreover, if the polymers carry additionally polymerizable end groups, these self-assembled superstructures can be frozen during a subsequent crosslinking polymerization. The resulting polymerized vesicles then have solid-state properties such as shape persistence because of their crosslinked nature and preserve their hollow sphere structure even after their isolation from aqueous phase (4).

Recently we demonstrated that despite their considerably higher thickness and mechanical stability the underlying polymer membranes can be regarded as mimetics of biological membranes that allow reconstitution of membrane proteins (5, 6). Interestingly the membrane proteins remained fully functional despite this artificial environment, even after a subsequent polymerization of their reactive block copolymer matrix. This combination leads to new types of polymer protein systems that are potentially interesting for applications in areas such as diagnostics or pharmacology.

The outside of such polymeric containers is covered completely by the hydrophilic PMOXA blocks of the triblock copolymers, which are known to prevent an unspecific protein adsorption (7). Therefore we expected, at least for long enough hydrophilic blocks, receptors in the walls of such vesicles to be hidden below a hydrophilic polymer layer such that larger ligands would not have access to them. This could be particularly interesting for use of such nanocontainers as intravascular drug delivery devices. We chose the bacterial receptor protein LamB as a model system for our investigations. This protein forms trimeric channels in the outer cell wall of Gram-negative bacteria that allow a specific transport of maltose and maltodextrins (8, 9). Simultaneously, it serves as a receptor for phage λ (10, 11). Because during infection the phages transfer their genome into

the host cells, it has been proposed that the channels of LamB could be a major intrusion path for the viral DNA (12). Interestingly, it has been shown that although LamB from both *Escherichia coli* and *Shigella sonnei* induce binding of λ phages, only the *Shigella* protein efficiently triggers the ejection and successful translocation of DNA (13, 14).

Here we report the insertion of LamB into the artificial shells of nanometer-sized triblock copolymer vesicles and its binding to phage λ (Fig. 1). The transfer of DNA into the polymeric nanocontainers was quantified following a recently established procedure via labeling the viral DNA with the fluorescent dye YO-PRO-1.

Materials and Methods

Preparation of Phage λ . Phage λ was isolated from an infected culture of *E. coli* JM109, which was grown in Luria–Bertani medium supplemented with 0.5% maltose. After an overnight infection, uninfected *E. coli* cells and cell fragments were removed as described (15).

Phages were collected from the cleared supernatant by ultracentrifugation at $75,000 \times g$ for 3 h at 4°C. The glassy pellet was resuspended in a buffer containing 10 mM MgCl₂ and 10 mM Tris-HCl, pH 8. Typically this method yielded a concentrated phage stock of 10^{11} – 10^{12} plaque-forming units·ml⁻¹.

Purification of LamB Protein. The LamB from *S. sonnei* was produced using *E. coli* strain pop 154, a derivative of *E. coli* K12, carrying the *malB* gene of *S. sonnei* 3070 (14).

The protein was solubilized from the outer membrane by using octyl-polyoxyethylene (octyl-POE, Alexis, Läufelfingen, Switzerland; ref. 1) as the detergent and purified in a procedure analogous to that used for porins from *E. coli* (16).

Preparation of PMOXA–PDMS–PMOXA Triblock Copolymer Vesicles and Proteovesicles. The PMOXA–PDMS–PMOXA triblock copolymer (M_n , PMOXA = 1,800 g·mol⁻¹, M_n , PDMS = 5,400 g·mol⁻¹; M_w/M_n = 1.7) used was described previously (4). The formation of small unilamellar vesicles from the triblock copolymer could be achieved according to the following procedure. The polymer was dissolved in ethanol to yield a clear, homogeneous solution containing 17 wt% polymer. This solution was added dropwise under vigorous stirring to the respective volume of a 100 mM KCl/5 mM MgCl₂/1 mM CaCl₂/10 mM Tris-HCl, pH 7.5 buffer solution. The procedure leads to a dispersion of triblock copolymer vesicles of a rather broad size distribution. Similar to lipid molecules, the vesicle size could be controlled by repeated extrusion through Nucleopore filters (Millipore) with defined pore size. For example, a pore diameter of 200 nm yields vesicles with a diameter of approximately 250 nm.

The vesicles containing the *Shigella* receptor were prepared by mixing a stock solution of the purified LamB (3 mg·ml⁻¹ 1% Octyl-POE/NaCl 100 mM/20 mM NaH₂PO₄, pH 7.5) with a 17

This paper was submitted directly (Track II) to the PNAS office.

Abbreviations: PDMS, poly(dimethylsiloxane); PMOXA, poly(2-methyloxazoline); octyl-POE, octyl-polyoxyethylene.

§To whom reprint requests should be addressed. E-mail: w.meier@iu-bremen.de.

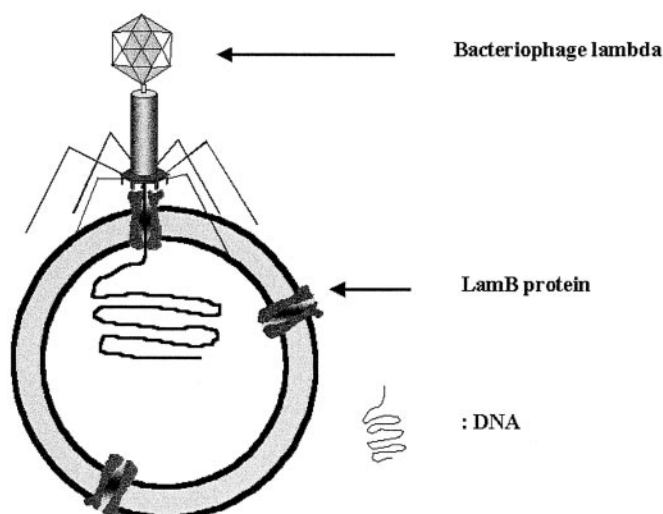


Fig. 1. Schematic representation of a DNA-loaded PMOXA-PDMS-PMOXA vesicle. λ phage binds a LamB protein, and the DNA is transferred across the block copolymer membrane.

wt% solution of the triblock copolymer in ethanol. Afterward, this mixture was added to the buffer solution as described previously.

The non-incorporated proteins were removed by gel filtration chromatography on a 1×55 -cm Sepharose 4 B (Sigma) column using the Tris-HCl buffer mentioned previously.

Fluorescence Experiments. Ejection of phage DNA was measured with a spectrofluorimeter Jasco F-P-773 in a 1×0.4 -cm cuvette thermostated at 37°C using a fluorescent quaternary ammonium dye derivative (YO-PRO-1, Molecular Probes), which intercalates into double-stranded DNA (17, 18). Excitation and emission wavelengths were set at 491 and 509 nm, respectively, and slits were 3 nm for excitation and 10 nm for emission. The final concentration of YO-PRO-1 was $8 \mu\text{M}$, and the final volume of the sample was 1 ml.

Reconstituted LamB was mixed with 3.10^9 phage λ in 1 ml of Tris-HCl buffer containing 5 mM MgCl_2 , 1 mM CaCl_2 , and $8 \mu\text{M}$ YO-PRO-1. The increase of the fluorescence signal was recorded as a function of time. To solubilize the proteovesicles, octyl-POE was added to a final concentration of 1%. In one control experiment, vesicles devoid of LamB protein were used. In another control, $1 \mu\text{g}$ of detergent-solubilized LamB protein was used in 1% octyl-POE.

Transmission Electron Microscopy Experiments. Five microliters of the phage-receptor complexes were adsorbed to carbon parlodion composite film on copper grids and negatively stained with 2% uranyl acetate solution as described by Engel and coworkers (19). The grids were allowed to dry in air and examined in a Phillips EM 400 with a magnification of $\times 55,000$.

Langmuir Trough Experiments. The protein-polymer and protein-lipid interactions were measured using the monolayer technique.

The surface pressure was measured by the Wilhelmy plate method (20, 21).

Both triblock copolymer and the lipid monolayers were spread from a chloroform solution ($1 \text{ mg}\cdot\text{ml}^{-1}$) at the air-water interface in a Teflon dish to give an initial surface pressure of $9 \text{ mN}\cdot\text{m}^{-1}$.

The LamB protein was injected with a microsyringe directly to the subphase composed of a 100 mM KCl/5 mM MgCl_2 /1 mM CaCl_2 /10 mM Tris-HCl, pH 7.5, buffer solution.

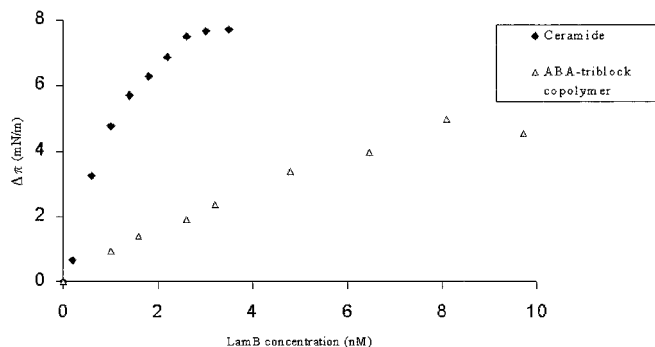


Fig. 2. Influence of LamB protein on a ceramide and triblock copolymer monolayer. The surface pressure increases as a function of protein concentration because of increasing protein insertion.

Measurements were started 30 min after protein injection. The resulting compression isotherm curves of lipids and triblock copolymers were recorded in the absence or presence of different amounts of purified LamB.

Results and Discussion

LamB Protein Insertion in a PMOXA-PDMS-PMOXA Triblock Copolymer Monolayer. The interaction of the membrane protein LamB with the block copolymer was studied by injecting the protein beneath the block copolymer film and then measuring the consequent changes of monolayer surface pressure. In parallel we performed the same study with a lipid film to compare the LamB protein behavior in both systems. Because of the non-charged block copolymer characteristic, we chose ceramide to avoid interference of electrostatic effects.

In each experiment LamB was added to the subphase at an initial pressure of $9 \text{ mN}\cdot\text{m}^{-1}$. The addition of LamB to the subphase of the monolayer film induced a shift toward higher surface pressure and larger effective area per lipid per polymer molecule in the compression isotherms, indicative of LamB-monolayer interaction (data not shown). Furthermore, the surface-pressure increase was protein concentration-dependent (Fig. 2).

A maximum surface pressure of 7.7 mN/m was reached at 3.5 nM LamB for the ceramide films. In contrast, for the polymer film at the same concentration of LamB, only $\approx 2.5 \text{ mN/m}$ was obtained. Thus in the latter case seven times more LamB protein had to be added to induce a similar surface-pressure increase. Compared with the ceramide film, a lower but still substantial fraction of protein inserts in the block copolymer film. Consequently, this lower insertion reflects directly the higher stability of block copolymer films. Indeed, the triblock copolymer films are considerably thicker than conventional low molecular weight lipid films. As described previously (22), the energy required for defect formation in the polymer membrane is approximately four times higher than for lipid membranes.

Reconstituted LamB in PMOXA-PDMS-PMOXA Triblock Copolymer Vesicles Still Functions as a Phage Receptor. The LamB protein was reconstituted into the membrane of triblock copolymer vesicles. The nonincorporated proteins were removed by gel-filtration chromatography to avoid interaction of the phage with the free proteins. To check whether the phages are still able to bind to the LamB in the walls of the polymeric nanocontainers, we incubated the particles with phage λ (10^{10} particles). As shown directly by the transmission electron micrograph of Fig. 3, the phages clearly bind the receptors in the walls of the amphiphilic block copolymer nanocontainers via their tails.

Moreover, the enormous size difference of the phage as

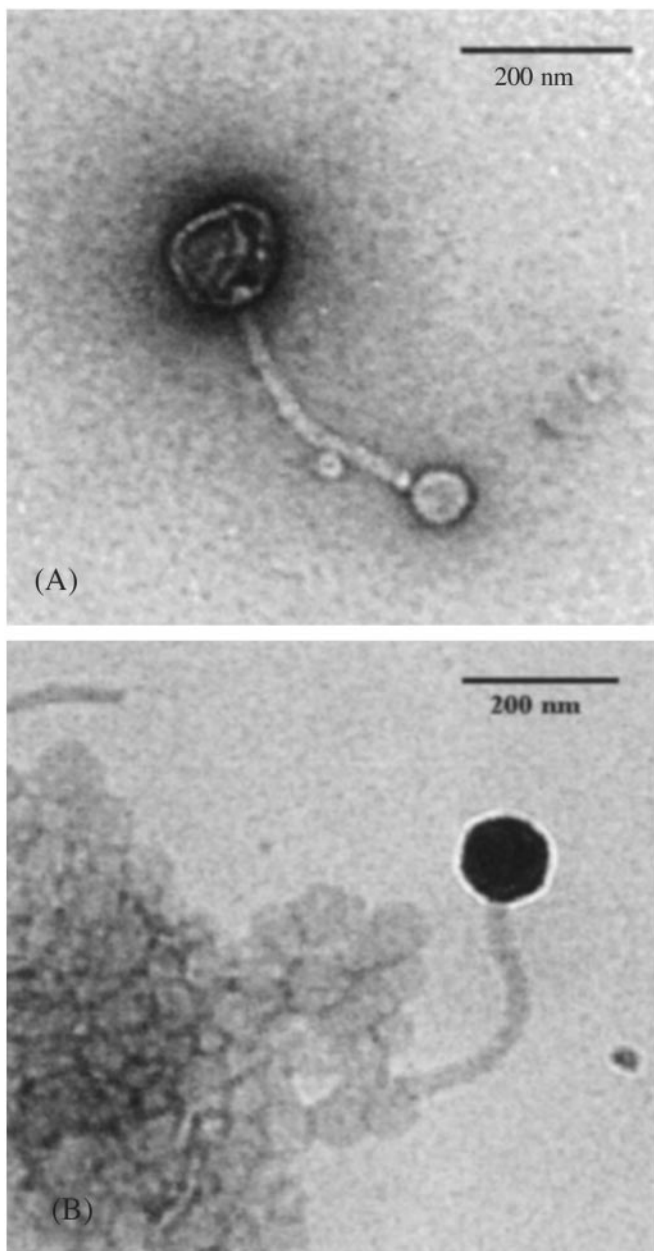


Fig. 3. Electron micrograph of negatively stained complexes formed between λ phage and vesicles bearing LamB protein at 37°C. (A) λ phage is attached to one vesicle via its tail. (B) A λ phage bound to a vesicle aggregate bearing LamB protein.

compared with the LamB protein-vesicle complex suggests that the interaction of both structures is sufficiently strong. No phage interaction was detected with non-LamB-containing vesicles (data not shown).

PMOXA-PDMS-PMOXA Triblock Copolymer Vesicles Can Be Loaded with DNA. In nature, after receptor recognition, the phage λ genome is injected into the cell, which then is turned into a phage-producing machinery. This fact immediately raises the question of whether the functionality of the protein is preserved also in the artificial block copolymer membranes, i.e., whether it is still able to induce the injection of the viral DNA into the nanocontainers. The injection can be followed with the help of the dye YO-PRO-1, which intercalates into double-stranded

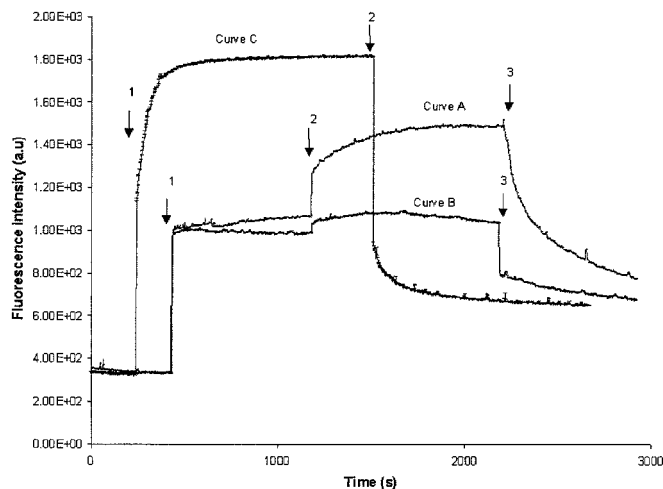


Fig. 4. Infection of λ phage DNA in PMOXA-PDMS-PMOXA triblock copolymer vesicles reconstituted with LamB receptor. The time course of the fluorescent dye YO-PRO-1 interacting with DNA is shown. Curve A corresponds to LamB-containing vesicles, curve B corresponds to a control experiment with vesicles without LamB, and curve C corresponds to a control with the detergent-solubilized LamB protein (no block copolymer was present in the solution). Arrow 1 corresponds to the addition of λ phage (10^{10} particles) into the respective buffer containing additional $8 \mu\text{M}$ fluorescent dye [buffer and vesicles bearing LamB or no LamB or the detergent-solubilized LamB ($3 \mu\text{g}$)]. Arrow 2 corresponds to solubilization of the vesicles by the addition of 1% octyl-POE, and arrow 3 indicates the addition of DNase I ($15 \mu\text{g}/\text{ml}$).

DNA and forms a fluorescent complex (17, 18). After the addition of λ phage ($3 \cdot 10^9$ particles), a steep increase in the fluorescence intensity was observed (Fig. 4). This increase can be attributed to the presence of naked DNA from lysed or broken phages (curves A and B). An additional increase is obtained with purified LamB (curve C), caused by ejected DNA after interaction of the phages with free receptor molecules. Although both control experiments (curves B and C) show a fast-establishing plateau, the signal of the proteovesicles (curve A) slowly increases. This obviously is because of ejection of phage DNA into the YO-PRO-1-containing medium caused by an inappropriate interaction between the phage and the receptor (23).

After the fluorescence intensity reached a plateau, we added the detergent Octyl-POE up to a concentration of 1% (see Fig. 4, arrow 2) to solubilize the vesicles. This treatment caused a rapid increase of fluorescence intensity by $\approx 40\%$ (curve A). This increase is caused by the encapsulated DNA that is released into the medium after solubilization of the block copolymer vesicles and not by DNA released from detergent-solubilized phage heads. This cause is documented by the control experiment of curve B, which remained virtually unaffected. To prove that the detergent-induced increase was caused by released DNA, we subsequently added DNase I (Fig. 4, arrow 3). The fluorescence signal dropped dramatically (curves A) because of enzymatic hydrolysis of the free DNA in the medium. In both control experiments, the initially naked DNA present in the phage stock (curves B and C) and the ejected DNA (curve C) were equally well digested by DNase I treatment.

An additional treatment with the DNase did not affect the fluorescence intensity (data not shown). Because the fluorescence signal never reached the baseline, quantification of the DNA ejected in the medium proved to be difficult. This residual fluorescence, observed in all curves, has to be attributed to remaining oligonucleotides that cannot be hydrolyzed further by DNase I (24) but are still able to interact with YO-PRO-1.

Interestingly, the fluorescence intensity decrease for free, nonencapsulated DNA is considerably faster than for the DNA

released from the interior of the nanocontainers. It seems that the small volume within the aqueous core of the block copolymer vesicles (diameter, ≈ 250 nm) accessible to the DNA forces it into a very compact, condensed conformation. After solubilization of the polymer shell, the released DNA has then first to “unfold” to be hydrolyzed by the DNase.

Alternatively, the DNA might be protected by interactions with the triblock copolymer. Pure phages (in a polymer- and protein-free solution) revealed similar kinetics to those of protein-free vesicles (data not shown).

The same preparation, vesicles containing LamB protein, was polymerized with UV light (data not shown). Because of their covalently crosslinked nature, the polymerized vesicles are resistant to detergent solubilization. Thus, after the addition of Octyl-POE no DNA was released. The small increase in fluorescence intensity probably is caused by DNA ejection induced by LamB proteins that have been released from the polymeric membrane during the crosslinking reaction. This result is a consequence of the internal stress occurring in the membrane during the polymer chain reaction, which may lead to a steric contraction of the PMOXA part of the polymer (4, 5). Similarly, part of the OmpF channel reconstituted into planar freestanding PMOXA-PDMS-PMOXA triblock copolymer membranes could be expelled after UV crosslinking of the triblock copolymer (5).

DNA Inside PMOXA-PDMS-PMOXA Triblock Copolymer Vesicles Is Protected from Hydrolysis. In another approach (Fig. 5A and B), we added DNase I before solubilization of the vesicles (Fig. 5A, arrow 2) to remove the DNA present in the external solution. Thus DNase treatment caused a rapid decrease of the fluorescence signal. The DNA entrapped in the vesicles was not accessible to the large enzyme (which is not able to enter their interior). In a following step (Fig. 5A, arrow 3) we released the entrapped DNA from the vesicles by detergent solubilization. An instantaneous increase of the fluorescence was observed as the released DNA came in contact with the fluorescent dye. This fluorescence increase was followed immediately by a decrease that can be explained by the presence of active DNase I in the medium, which hydrolyses the released DNA.

Part of the ejected DNA was DNase I-resistant. Nevertheless, the results show clearly that the phage DNA had been injected originally into the inner aqueous cavity of the vesicles where it is protected from externally added DNase. Subsequent disruption of the vesicles with detergent rendered the entrapped DNA sensitive to degradation by DNase.

The same experiment was done with an excess of LamB to prevent new phage binding and DNA ejection after vesicle solubilization. Thus, after vesicle solubilization (Fig. 5B, arrow 3) we observed an increase of the fluorescence intensity. This increase is only because of entrapped DNA in the vesicles.

Conclusion and Outlook

In conclusion, our investigations show that the conformation of the receptor LamB is not affected by the artificial block copolymer membrane used in this study, and its functionality is preserved fully. Similar observations have been made also with other membrane proteins. Here we demonstrated that DNA translocation mediated by the λ phage receptor LamB is possible across a completely synthetic block copolymer membrane. This phage-mediated loading of polymer nanocontainers with DNA

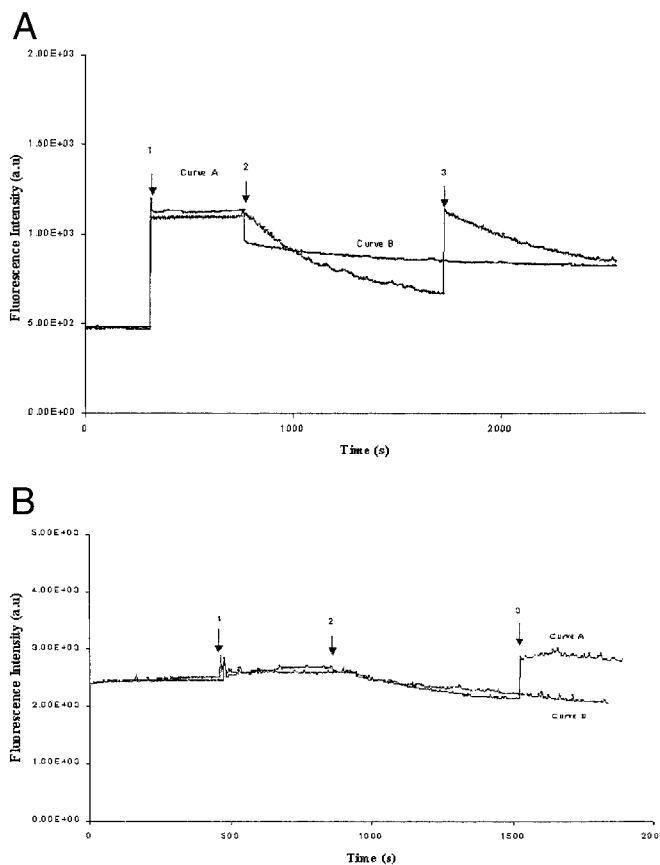


Fig. 5. λ phage DNA release from the triblock copolymer vesicles. (A) Curve A corresponds to LamB-containing vesicles, and curve B is the control experiment with protein-free block copolymer vesicles. Arrow 1 corresponds to the addition of λ phage (10^{10} particles) to the vesicle dispersion in the presence of $8 \mu\text{M}$ fluorescent dye YO-PRO-1, arrow 2 corresponds to the addition of DNase I ($15 \mu\text{g}/\text{ml}$), and arrow 3 indicates the solubilization of the vesicles by the detergent octyl-POE (1%). (B) Curve A corresponds to LamB-containing vesicles, and curve B is the control. Arrow 1 corresponds to the addition of LamB in excess ($1 \mu\text{g}$) to the vesicles' dispersion in the presence of $8 \mu\text{M}$ fluorescent dye YO-PRO-1 and λ phage (10^{10} particles). Arrow 2 indicates the addition of DNase I ($15 \mu\text{g}/\text{ml}$), and arrow 3 corresponds to the solubilization of the vesicles by addition of 1% octyl-POE.

represents a very stable model system to investigate the transport of foreign genes into eukaryotic cells. Possible applications of such DNA-loaded nanoparticles in the area of gene therapy are obvious. One major problem in this field is how to find efficient and biocompatible vectors that are able to transport the gene specifically into the desired target cells. Here particularly the high diversity of block copolymer chemistry (i.e., the possibility to modify their chemical constitution, block lengths, architecture, etc. . .) could be interesting, because it allows for the optimization of these systems with respect to a desired application.

We thank Dr. T. Pugsley for providing the strain pop 154 and Pr. M. Winterhalter for the Monolayer setup. We also thank Y. Rohrer for his contribution to the experimental part. The Swiss National Science Foundation is gratefully acknowledged for financial support.

- Wanka, G., Hoffmann, H. & Ulbricht, W. (1994) *Macromolecules* **27**, 4145–4149.
- Svensson, P., Alexandridis, P. & Linse, P. (1999) *Macromolecules* **32**, 637–645.
- Förster, S., Zisenis, M., Wenz, E. & Antonietti, M. (1996) *J. Chem. Phys.* **104**, 9956–9970.
- Nardin, C., Hirt, T., Leukel, J. & Meier, W. (2000) *Langmuir* **16**, 1035–1041.

- Meier, W., Nardin, C. & Winterhalter, M. (2000) *Angew. Chem. Int. Ed. Engl.* **39**, 4599–4602.
- Nardin, C., Widmer, J., Winterhalter, M. & Meier, W. (2001) *Eur. Phys. J. E* **4**, 403–410.
- Lasic, D. D. (1993) *Liposomes: From Physics to Applications* (Elsevier Science, Amsterdam), pp. 287–289.

8. Szmecman, S. & Hoffnung, M. (1975) *J. Bacteriol.* **124**, 112–118.
9. Schirmer, T. (1998) *J. Struct. Biol.* **121**, 101–109.
10. Randall-Hazelbauer, L. & Schwartz, M. (1973) *J. Bacteriol.* **116**, 1436–1446.
11. Schwartz, M. (1976) *J. Mol. Biol.* **103**, 521–536.
12. Mackay, D. J. & Bode, V. C. (1976) *Virology* **72**, 154–166.
13. Schwartz, M. & Le Minor, L. (1975) *J. Virol.* **15**, 679–685.
14. Roa, M. & Scandella, D. (1976) *Virology* **72**, 182–194.
15. Sambrook, J., Frisch, E. F. & Maniatis, T. (1989) in *Molecular Cloning: A Laboratory Manual* (Cold Spring Harbor Lab. Press, Plainview, NY), 2nd Ed.
16. Prilipov, A., Phale, P. S., Van Gelder, P., Rosenbusch, J. P. & Koebnik, R. (1998) *FEMS Microbiol. Lett.* **163**, 65–72.
17. Marie, D., Vaulot, D. & Partensky, F. (1996) *Appl. Environ. Microbiol.* **62**, 1649–1655.
18. Boulanger, P., le Maire, M., Dubois, S., Desmadril, M. & Letellier, L. (1996) *Biochemistry* **35**, 14216–14224.
19. Ringler, P., Heymann, B. J. & Engel A. (2000) in *Membrane Transport*, ed. Baldwin, S. A. (Oxford Univ. Press, Oxford), pp. 229–268.
20. Martin, P. & Szablewski, M. (1995) in *Tensiometers and Langmuir-Blodgett Throughs Operating Manual* (Nima, Cranfield University Milton Keynes, England).
21. Demes, R. A. (1974) *Methods Ezymol.* **32**, 539–545.
22. Nardin, C., Winterhalter, M. & Meier W. (2000) *Langmuir* **16**, 7708–7712.
23. Plangon, L., Chamis, M. & Letellier, L. (1997) *J. Biol. Chem.* **272**, 16868–16872.
24. Holloman, W. K. (1973) *J. Biol. Chem.* **248**, 8114–8119.

Additional results (publication 3)

As already described, triblock copolymer vesicles can be stabilized by additional polymerization of the two end groups of the side chains. It was also demonstrated that this polymerization process has no influence on the vesicle structure and did not disturb the function of the incorporated membrane proteins (Nardin *et al.*, 2000, Meier *et al.*, 2000)

1. Infection of lambda phage in polymerized ABA triblock copolymer vesicles

To check whether the polymerization influences the ligand-receptor interaction between the phages and LamB we polymerized the vesicles by UV-irradiation. Then the infection activity of the phages was examined. This activity was followed by fluorescence experiments (Figure 3) as described the publication 3.

The original solution was divided into two aliquots. One of them was polymerized by UV irradiation. Afterwards, all samples investigated, control vesicles (curve C), proteovesicles (curve A), and polymerized proteovesicles (curve B) were treated the same way (details in publication 3). First, lambda phages were added to all samples. Then, in a second step, the vesicles were destabilized by adding detergent to deliver DNA into the external medium containing the fluorescent probe. To complete the experiment, DNA was enzymatically digested by DNase. The delivery of DNA from the stabilized vesicles (curve B) was clearly less efficient, since the polymerization process added further stability (Meier *et al.*, 2000). However, as shown in the graph, a part of the injected DNA was released (curve B and C) and then enzymatically degraded. This can be explained by the fact that either the polymerization process was not complete for the vesicle population, i. e., some vesicles were not completely detergent resistant, or that during the polymerization process some LamB proteins were ejected from the vesicles. Also, LamB proteins could have reorganized into the vesicle membranes in a way that the DNA can be ejected into the surrounded medium. Such an “inappropriate” interaction between the phage and the receptor was already discussed in publication 3.

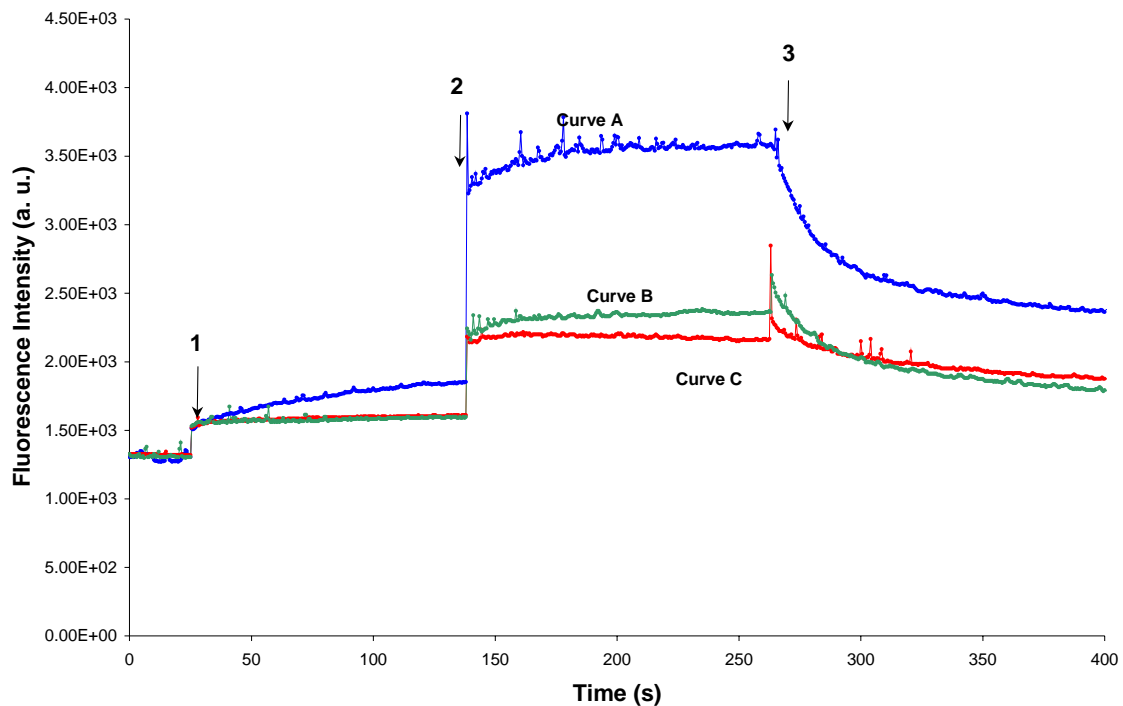


Figure 3. Infection of λ phageDNA in polymerized triblock copolymer vesicles containing with LamB receptor. The time course of the fluorescent dye YO-PRO 1 interacting with DNA is shown. Curve A corresponds to the non-polymerized LamB containing vesicles, curve B correspond to the polymerized LamB containing vesicles, and curve C corresponds to the control experiment with vesicles without LamB. Arrow 1 corresponds to the addition of λ phage (10^{10} particles), arrow 2 corresponds to the detergent solubilization (1% octyl-POE as the final concentration in the sample), and arrow 3 indicates the addition of DNase (15 $\mu\text{g/ml}$).

HP708 had a larger hydrophobic PDMS middle block which leads also to a higher hydrophobic thickness of the membranes in addition we tested the influence of the molecular weight of the block copolymer on the insertion and “activity” of LamB receptors.

2. Lambda phage DNA release from ABA triblock copolymer vesicles prepared with two different polymers: A comparative study.

The LamB receptor was prepared and incorporated into two different polymer vesicles.

One of the vesicle sample series was prepared with the polymer HP708 ($M_n = 9000 \text{ g mol}^{-1}$, $M_{\text{PDMS}} = 5400 \text{ g mol}^{-1}$ and $M_{\text{PMOXA}} = 1800 \text{ g mol}^{-1}$) the second sample series was prepared with the polymer called JW03 ($M_n = 4151 \text{ g mol}^{-1}$, $M_{\text{PDMS}} = 1941 \text{ g mol}^{-1}$ and $M_{\text{PMOXA}} = 1105 \text{ g mol}^{-1}$). The hydrophobic/hydrophilic ratio is $M_{\text{PDMS}}/M_{\text{PMOXA}} = 1.5$ for HP708 and for JW03 is $M_{\text{PDMS}}/M_{\text{PMOXA}} = 0.9$. Hence JW03 has a tendency to form aggregate of higher curvature and therefore less stable membranes. The fluorescence measurements presented in Figure 4, were performed on vesicles containing the LamB receptor as described in publication 3. In contrast to previous experiments, the DNase I was added before solubilization of the vesicles (Figure 3) to remove any DNA present in the external solution.

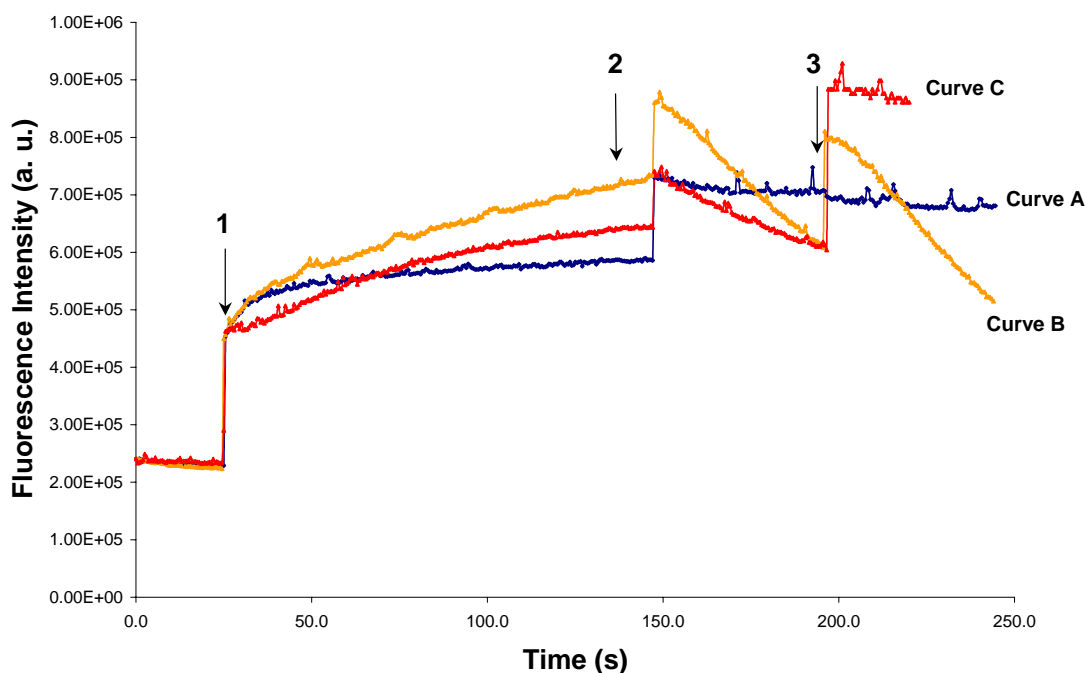


Figure 4. Infection of λ phage DNA in JW03 and HP708 triblock copolymer vesicles reconstituted with LamB receptor: a comparative study. The time course of the fluorescent dye YO-PRO 1 interacting with DNA is shown. Curve B corresponds to the JW03-LamB containing vesicles, curve C corresponds to the HP708-LamB containing vesicles, and curve A corresponds to the control experiment with vesicles without LamB. Arrow 1 indicates the addition of λ phage (10^{10} particles), arrow 2 corresponds to the detergent solubilization (1% octyl-POE as the final concentration in the sample), and arrow 3 indicates the addition of DNase (15 $\mu\text{g/ml}$).

In a following step the entrapped DNA was released from the vesicles by detergent solubilization. An instantaneous increase of the fluorescence was observed as the released DNA came in contact with the fluorescent probe. Then, followed a fast signal decrease that could be explained by the presence of DNase I in the solution, which hydrolyses the -released DNA. As already described before in publication 3 the residual fluorescence intensity was due partial DNase I-resistance of the ejected DNA. All these treatments were performed on both HP708 and JW03 vesicles containing LamB membrane protein and controls without the protein. Obviously the phages injected their DNA into both systems. As already observed in the previous measurements, after the phage addition the signals slowly increased (curve B and C). This was not observed for the control vesicles or the “free” LamB protein where a fast plateau was set up. This phenomenon could be explained by the fact that ejection of phage DNA into the medium can be caused by the interaction between the phage and the receptor (publication 3).

In a second step DNase I was added to the medium and a fast fluorescence decrease was observed for the two proteovesicle solutions (curve B and C), but not for the control vesicle solution. This is probably due to a lower amount of DNA in the medium. Finally, the entrapped DNA was released from the vesicles and an instantaneous fluorescence increase was observed for the two proteovesicle populations (curve B and C). As observed in the graph this increase is more important for the HP708 vesicle solution (curve C) than for the JW03 vesicles (curve B). It has to be emphasized that after phage addition we could also observe more DNA ejection into the medium in the case of the JW03 vesicles compared to for the HP708 vesicles. This explains why afterwards lower DNA release was observed. This is presumably because the critical aggregation concentration (cac) for JW03 which is higher than for HP708. Hence, there are less vesicles and more free polymer into the solution. The consequence was that they were less vesicles for the DNA injection. Moreover, as a result of its small hydrophobic to hydrophilic block length ratio JW03 can be expected to have a strong tendency to form aggregation of higher curvature, e. g micelles. If we assume an equilibrium between micelles and vesicles one has to take into account that the proteins might be solubilized in both species. This would also explain, that for JW03 a larger fraction of DNA was directly ejected into the medium.

3. DNA loading into lipid and ABA triblock copolymer vesicles: A comparative study.

Proteovesicles and proteoliposomes were prepared according to the description in the Materials and Methods section. Both samples were prepared with the same mass ratio amphiphile/protein. The amount of LamB was 300 μg and 150 μg for the lipid and polymer vesicles respectively. The lipid:LamB and polymer:LamB molar ratio was $\sim 333:1$ in both cases. The experiments were monitored as already described before. To compare the amount of DNA injected into the vesicles, both samples were submitted to detergent solubilization (Figure 5, arrow 2).

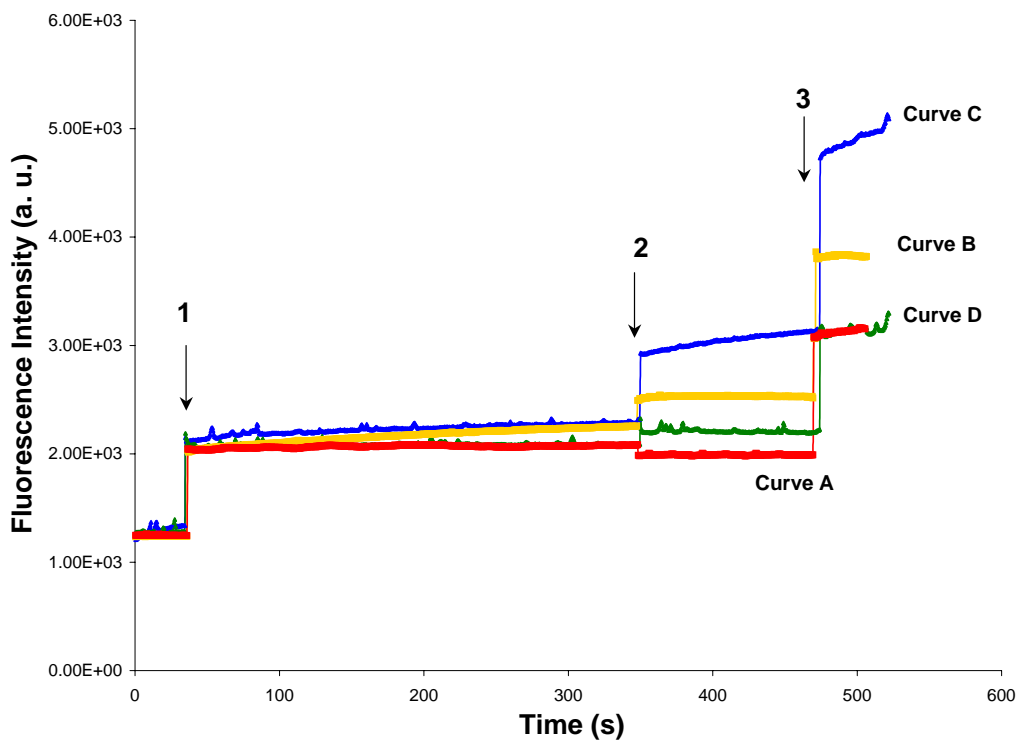


Figure 5. Infection of λ phage DNA in lipid vesicles and in HP708 triblock copolymer vesicles, both reconstituted with LamB receptor: a comparative study. The time course of the fluorescent dye YO-PRO 1 interacting with DNA is shown. Curve B correspond to the polymer LamB containing vesicles, curve C correspond to the lipid LamB containing vesicles, and curves A and D correspond to the control experiments with vesicles without LamB. Arrow 1 corresponds to the addition of λ phage (10^{10} particles), arrow 2 corresponds to the detergent solubilization (1% octyl-POE as the final concentration in the sample), and arrow 3 indicates the addition of EDTA (0.1 M as a final concentration).

A fast increase of the fluorescence signal was observed for the proteoliposomes and the proteovesicles. This increase is higher for the proteoliposomes than for the proteovesicles. The amount of DNA injected into the lipid system was higher. This can be explained by the fact that there is more protein incorporated or that there is an higher amount of well-oriented protein, with the phage binding sequence oriented towards the outer medium in the case lipid vesicles. Finally, the addition of EDTA destroys the residual unbound phages, which results in a fluorescence signal of the total amount of added phages DNA. This shows clearly that the membrane protein insertion was more effective in lipid monolayers. This lower fraction of protein inserted into polymer membranes is a direct consequence of the stability of the polymer membrane. Here, insertion of membrane proteins requires more energy compared to a lipid membrane. Nevertheless also for the polymer membrane effective insertions were observed without affecting the protein and its function.

4. Membrane protein titration assay into ABA triblock copolymer vesicles

In order to quantify the amount of membrane protein inserted into the triblock copolymer vesicles, a test was designed which followed the same procedure as in the previous experiments: addition of phages and then addition of detergent to deliver the DNA into the medium (Figure 6 a) and b)).

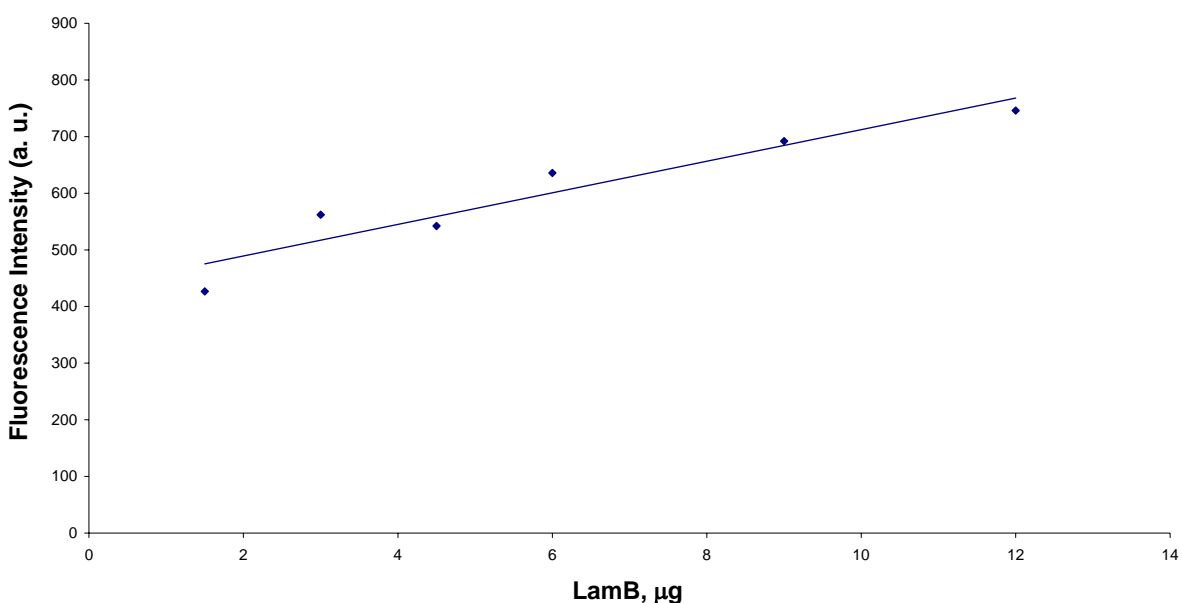


Figure 6 a). Titration curve with increasing LamB protein quantity.

The fluorescence signal induced by the DNA delivery into the surrounding medium is the reference for this assay. For this purpose, we had to prepare a reference curve for different LamB concentrations (Figure 6 a)). Here, the sample contained just the protein with the octyl-POE detergent and the YO-PRO dye, and then the phages were added to the solution.

The DNA ejection into the medium was instantaneous. As expected the fluorescence signal increase was proportional to the amount of LamB present the solution (Figure 6 a)). The experiment was repeated with different amounts of proteovesicles (Figure 6 b)).

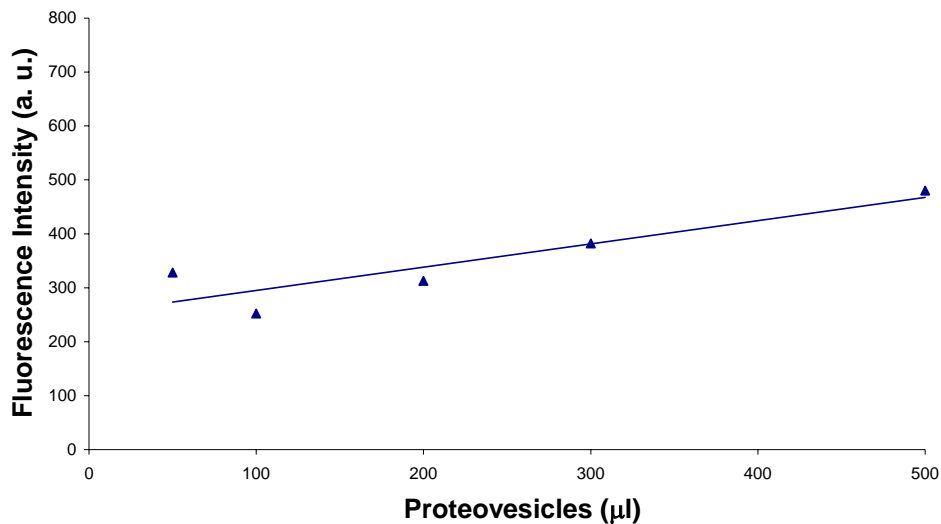


Figure 6 b). Titration of the LamB protein containing polymer vesicles

The phages were added to the polymer vesicles solution and subsequently we destabilized the vesicles by the detergent treatment. We could determine the fraction of LamB incorporated within the polymer vesicles for increasing concentration of proteovesicles solution. As shown in the (Figure 6 a)), the fluorescence intensity is proportional to the volume of proteovesicles solution. For 500 µl of the proteovesicles solution, 1.6 µg of LamB protein incorporated into the vesicles population. The proteovesicles were prepared with 150 µg of LamB. After cleaning and dilution, 7.5 µg of LamB should be detected in the 500 µl fraction of proteovesicles. As a consequence 42% of LamB inserted the polymer vesicles. Usually , 50% of the total amount of the inserted proteins are considered to be functional because they are

accessible for the phage binding. Finally, only 21% of LamB are accessible for the phages. The proteoliposomes were prepared with 300µg of LamB. After cleaning and dilution, 12 µg of LamB should be detected in the 200 µl fraction of proteoliposomes. We could conclude that 92% and finally, 46% of LamB were accessible for the phages (Figure 5). Compare to lipid membranes they was 2.2 times less LamB protein inserted in block copolymer membrane. This is explained that protein need higher energy for their insertion into block copolymer membrane.

Incorporation of Complex I in Block Copolymer Vesicles

1. Structure and functions of NADH: ubiquinone oxidoreductase (complex I) from *Escherichia coli*

NADH:ubiquinone oxidoreductase or also called NADH dehydrogenase, is homologous to the mitochondrial complex I and therefore is also called complex I. For our studies, complex I was expressed and purified from *Escherichia coli*. Complex I is much more difficult to study than other complexes of the respiratory chain: it consists of up to 45 different subunits and has a total mass of almost 1000 kDa. Mitochondrial complex I is one of the biggest and most complicated membrane protein complexes known. The prokaryotic counterpart is still rather big and complex with a molar mass of 500 kDa and of 14 subunits. Generally, bacterial enzymes tend to be extremely unstable. So far complex I from *Escherichia coli* and the closely related *Klebsiella pneumoniae* are the only bacterial enzymes that could be purified in intact form (Leif *et al.*, 1995; Krebs *et al.*, 1999).

The aerobic respiratory chain of *Escherichia coli* contains several primary dehydrogenases, including NADH dehydrogenase, succinate dehydrogenase, and D-lactate dehydrogenase, which oxidize organic substrates and transfer the electrons to membrane-bound ubiquinone-8 to (Figure 1).

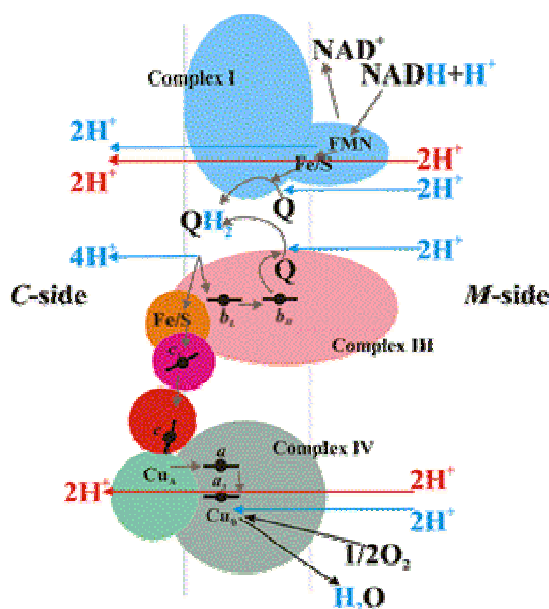
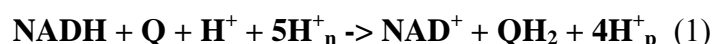


Figure 1. Cartoon of the different complexes involved in the aerobic respiratory chain of *E. coli* and proton translocations. Cartoon from the webpage of the group of Marten Wikstrom from University of Helsinki.

The resulting ubiquinol is then reoxidized by reductases, and the terminal oxidases. This exergonic process is coupled to endergonic translocation of protons across the cytoplasmic membrane. The resulting membrane potential is used to drive energy-consuming processes like ATP synthesis, solute transport and flagellar motion (Anraku, 1988; Anraku and Gennis, 1987).

Like the mitochondrial complex, it is a multi-subunit enzyme and couples electron transfer from NADH to ubiquinone with a proton translocation according to the overall equation:



Where Q refers to ubiquinone, and H_{n}^+ and H_{p}^+ to the protons taken up from the negative inner side of the membrane and delivered to the positive outer side. The complex 1 is also characterized by its prosthetic groups, namely 1 flavin mononucleotide (FMN) and up to 9 iron-sulphur (FeS) clusters.

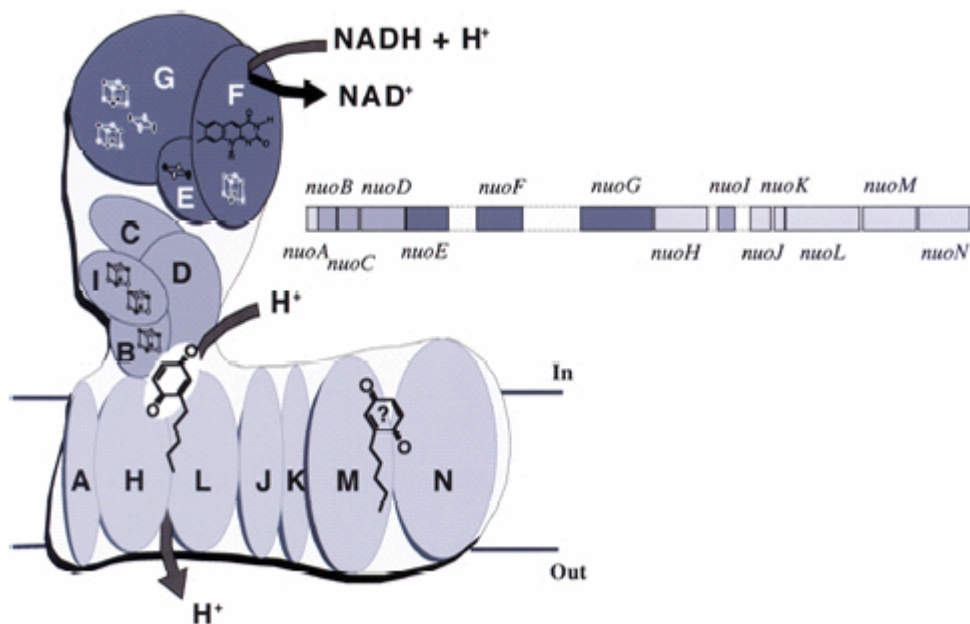


Figure 2. The bacterial complex I. Both in the operon and in the schematic structure of the enzyme, the subunits of the NADH-oxidizing domain (NUOE, -F, -G) are drawn in dark gray. The subunits comprised in the connecting fragment (NUOB, -C, -D, -I) are in the medium gray and the subunits located in the membrane-embedded arm (NUOA, -H, -J, -K, -L, -M, and -N) are in light gray (Dupuis *et al.*, 2001).

Moreover both mitochondrial and bacterial complex I share the remarkable conservation of the characteristic “L”-shaped quaternary structure (Figure 2).

In bacteria, the membrane embedded arm of the “L” is a module constituted mainly of seven hydrophobic proteins called subunits NUO-H, -N, -A, -M, -K, -L, and -J. The protruding arm, pointing out of the membrane, contains all the identified prosthetic groups of complex I except quinones. This arm is composed of two modules: the first one, the NADH-oxidizing unit, is composed of subunits NUO-E, -F, -G in the bacterial enzyme. The arm contains at least one FMN and four [Fe-S] clusters and is able to catalyze the oxidation of NADH by artificial electron acceptors like ferricyanide or ruthenium (III) hexamine. The second module is constituted of four proteins, namely, NUO-B, -C, -D, and -I. It connects the NADH-oxidizing unit to the membrane arm (Figure 1).

Complex I contains hydrogen (FMN and ubiquinone) and electron carriers ([Fe-S] clusters). According to the classical cycle process, the association of these two types of carriers allows a net transport of protons finally resulting from the transfer of two hydrogens across the membrane and the return of two electrons.

The NADH-oxidizing unit, which is the best understood part of the enzyme, appears to be an interchangeable input module (Dupuis *et al.*, 2001) and is not directly involved in the coupling mechanism of complex I (Scheide *et al.*, 2000). On the other hand, the membrane module has to be involved in vectorial proton transfer, but its hydrophobic nature and the absence of any enzymatic activity do not allow for characterization of the module. Finally, although the connecting module has no measurable catalytic activity, the presence of two to three [Fe-S] clusters and its clear phylogenetic relation with the multi-subunits [NiFe] hydrogenase indicate this module being a strategic crossing point for the electrons and the protons.

Numerous hypotheses have been suggested giving more detailed description of complex I mechanism and function (Brandt, 1997).

2. Strategies for complex I incorporation in block copolymer vesicles

Complex I containing polymer vesicles were prepared using the “ethanol method” and the “direct dissolution method” (Materials and Methods). The first method was directly inspired by the method used for the incorporation of porins. Instead of dissolving directly the protein in the polymer/ethanol mixture, the protein was incorporated drop by drop in parallel with the

addition of the polymer/ethanol mixture into the solution. We assumed that the protein was inserted into the polymer membrane during the formation of the vesicles. The vesicle formation kinetics is slow enough to allow for the protein insertion process. In the second insertion procedure, no organic solvent was used for the protein/ polymer vesicle preparation. Here, the polymer vesicle solution was used directly. To allow a protein insertion we destabilized vesicles membrane by the addition of surfactant. The mixed containing polymer/surfactant membranes are more flexible and allow a direct insertion of membrane proteins. Moreover Rigaud et al demonstrated in the case of lipids that the mechanism by which proteins associate with these mixed membrane has a critical effect on the final orientation of the protein in the bilayer. A higher asymmetrical orientation and hence also higher activities were observed for samples reconstituted by incorporation of the protein into preformed liposome. Optimal unidirectional orientations up to 70% to 80% were obtained upon triton X-100 mediated reconstitution in which, the starting detergent-lipid mixtures contained a large amount of preformed detergent doped liposomes. Afterwards, the surfactant is removed from the vesicle preparations using biobeads (Materials and Methods).

3. Complex I functional incorporation: results and discussions

NADH: ferricyanide activity of complex I

As described previously, complex I is considered as a highly asymmetric membrane protein compared to porins. The insertion process of this protein is more delicate than for porins. For those reasons it had to be demonstrated that the complex I was inserted into the membrane vesicles in the desired orientation. In the cell membrane, the hydrophilic part containing the NADH-oxidizing unit is oriented to the cytoplasmic side, whereas the membrane arm, which allows for the proton transport is located on the periplasmic side. The membrane module has to be involved in vectorial proton transfer from the cytoplasm to the periplasmic side, however its hydrophobic nature and the absence of any associated enzymatic activity do not allow for precise characterization of this part of complex I.

As mentioned above the water-soluble NADH dehydrogenase fragment is capable of transferring electrons from NADH to ferricyanide, which is an artificial electron acceptor. The enzymatic activity was used to demonstrate the complex I functionality. The same enzymatic activity measurements were performed using complex I reconstituted in the

polymer vesicles. As a control experiment, the same measurements were repeated with polymer vesicles without complex I.

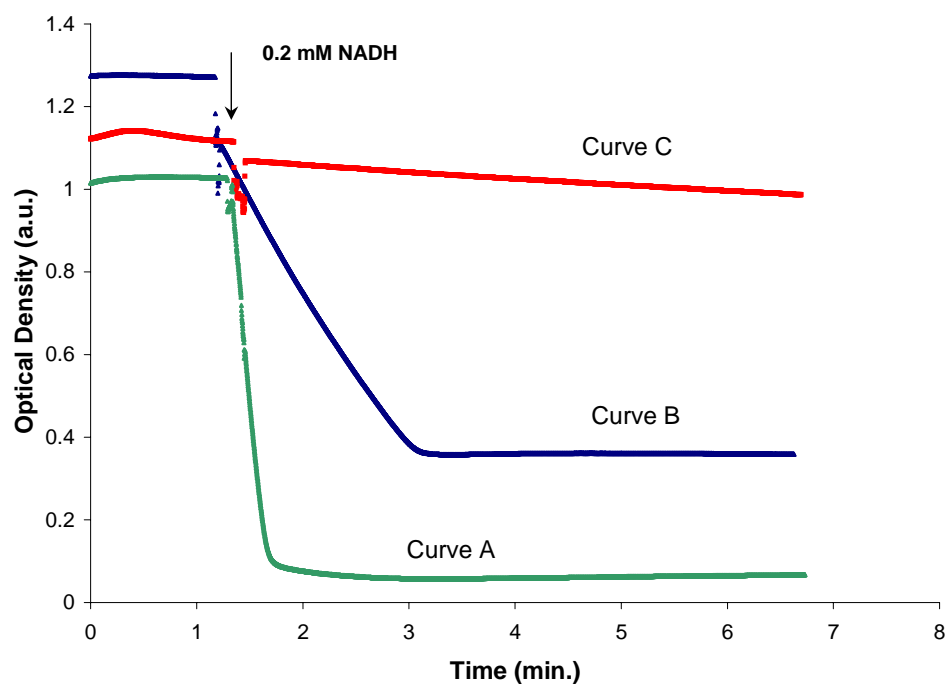


Figure 3. Time profile of the absorbance of ferricyanide solution reduced by NADH at 410 nm at 25 ° C. The reduction of ferricyanide started after NADH addition to the different samples containing or not the complex I. Curve A correspond to the “free” enzyme in solution whereas curve B correspond to the reconstituted complex I in polymer vesicles solution. The control vesicle solution containing no complex I is represented by curve C.

The results are reported in Figure 3. As shown in the Figure 3, the NADH: ferricyanide activity was preserved after reconstitution of complex I. Moreover, the results demonstrated that complex I was in the desired orientation. This mean that the hydrophilic arm of complex I was oriented towards the outer side when complex is reconstituted in the polymer membrane. Complex I reconstitution was repeated several times using different complex I concentrations

or biobeads incubation times. Only the optimized conditions for the complex I reconstitution were reported in the materials and methods part and in the results part (Figure 3).

We could demonstrate that the membrane protein complex I was still functional after reconstitution in polymer vesicles. Moreover, the biobead method inspired by the method of Rigaud et al allowed us to prepare complex I in polymer vesicles with the “desired” orientation. As demonstrated in Figure 3 the method is efficient. This reconstitution procedure using biobeads was already reported for complex I in liposomes (Linke *et al.* 1986; Fiedrich *et al.*, 1989), however, the procedure had to be adapted to the polymer vesicles. The reconstitution of membrane proteins using the biobead method is still under investigation in our laboratory.

4. Proton and electron transport across the polymer membrane, results and discussions

We designed two functionality tests for complex I (Materials and Methods), in order to demonstrate the proton and electron transport via complex I after its reconstitution in the polymer membrane.

Principle of electron transfer experiments

In order to demonstrate the electron transfer via complex I, it was reconstituted in polymer vesicles using the same reconstitution method as described above. An electron acceptor was encapsulated into the vesicles whereas an electron donor was added to the outer side of the vesicles. In bacteria, the final acceptor is water ($E_{m,7} = 815$ mV). However in our system we chose the artificial electron acceptor, anthraquinone ($E_{m,7} = 154$ mV). This allowed us to monitor electron transfer using electron paramagnetic resonance spectroscopy. NADH was used as electron donor with a redox midpoint potential of ($E_{m,7} = -320$ mV) at pH 7. After addition of NADH to the solution, the formation of anthraquinone radical signal (Figure 4) due to electron transfer was recorded.

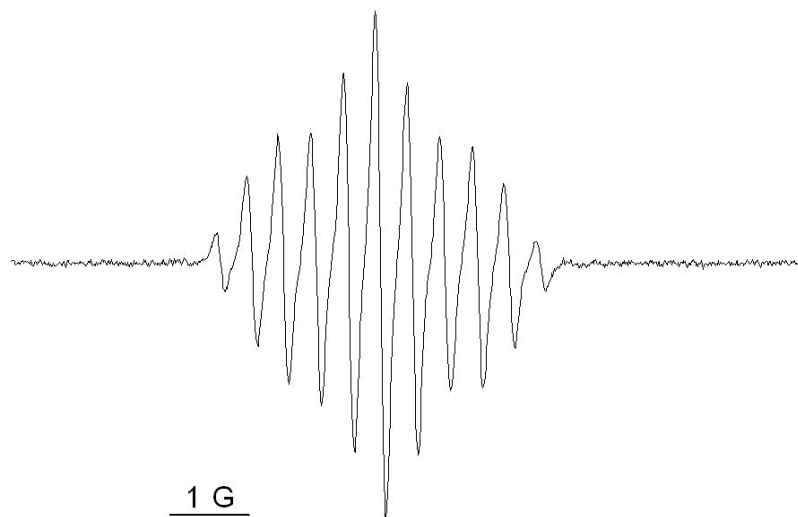


Figure 4: EPR spectra of 1 mM Anthraquinone in presence of 1mM NADH and complex I in Tris/HCl pH8 buffer containing 1% triton X-100

Electrons pathway in complex I

The pathway used by electrons during their transfer is still under investigation but some hypothesis are presented in the article of Brandt et al. (FEBS letters 545 2003 9-17). FMN (midpoint potential of $(E_{m, 7.5}) = -336$ mV) at pH 7.5 is the entry point for electrons from NADH. FMN works as an electron converter between the $n=2$ electron donor NADH and the $n=1$ electron transferring iron-sulfur clusters (N1a, N1b, etc.) (Figure 5, ref 22 de ulrich brandt). Electrons are transferred from one iron-sulfur cluster to another following the pattern of the increasing redox potential. Finally, it is assumed that the last PSST redox center is the direct electron donor for ubiquinone (Ohnishi, 1998; Sled *et al.*, 1993).

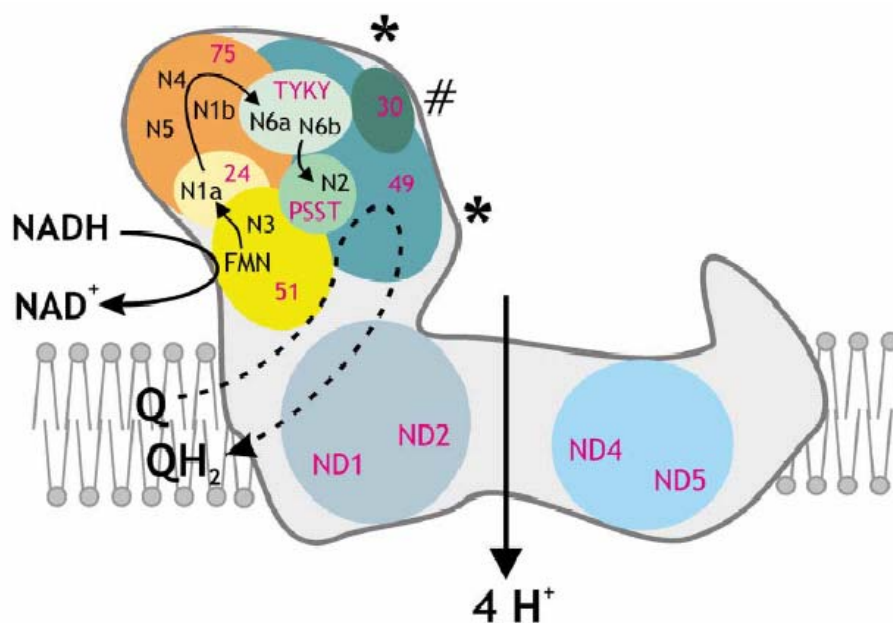


Figure 5. Cartoon of the approximate positions of central subunits and iron-sulfur clusters within L shaped complex I. The membrane arm consists of seven highly hydrophobic subunits (ND1-ND6, and ND4L). The subunit symbol is given in red and redox groups in the complex are denoted in black. The hypothetical sequence of electron transfer steps from NADH to ubiquinone (Q) is indicated by small black arrows.

In order to demonstrate the transfer of electrons was possible from NADH to the artificial electron acceptor, anthraquinone, via complex I, EPR spectroscopy measurements were done with the non-reconstituted complex I (“free” enzyme). The experiments performed are summarized in Figure 6. With complex I, electron transfer was recorded, whereas without complex I no anthraquinone radical signal was detected. The experiment has proven that the electron transfer From NADH to anthraquinone via complex was efficient. The same experiments were repeated using complex reconstituted in polymer and lipid vesicles. No anthraquinone radical signal could be recorded in the different prepared samples. After changing complex I, anthraquinone, ubiquinone, and NADH concentration still no signals were detected. Previously, we demonstrated that the reconstitution method of complex I used did not disturb its enzymatic activity. Moreover, we could prove that there was enough protein incorporated in the “right” orientation for the enzymatic activity of complex I. For this

reasons, the proteins orientation is not involved in the failure of electron transfer via complex I.

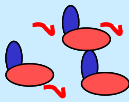
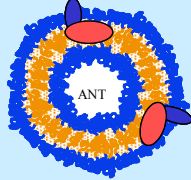
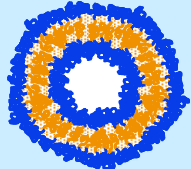
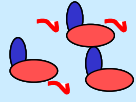
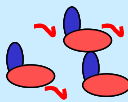
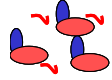
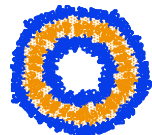
<u>Samples</u>		<u>EPR signal</u>
• Polymer		
1)	 + NADH, <u>anthraquinone</u> , ubiquinone 2	Yes (stable)
2)	 + NADH, ubiquinone 2	Not detected
3)	 + NADH, ubiquinone 2 + <u>anthraquinone</u> 	Yes (after few minutes and stable)
• Lipids		
4) Proteoliposomes	+ NADH, ubiquinone 2	Not detected
5) Liposomes	+ NADH, ubiquinone 2 + <u>anthraquinone</u> 	Yes (but signal disappeared)

Figure 6. Cartoon of the different samples prepared for the EPR spectroscopy measurements

The drawing:  represents complex I solution.

The drawing:  represents polymer vesicles

Sample 1) represents complex I in Tris/HCl pH 8 solution with 1 mM anthraquinone, and 10 μ M ubiquinone 2. Sample 2) represents proteovesicles prepared with complex I and anthraquinone (10 mM). Sample 3) was empty vesicles mixed with 1 mM anthraquinone solution and 10 μ M ubiquinone 2. Samples 4) and 5) were prepared analogously to 2) and 3), using liposomes instead of polymer vesicles. The electron transfer was recorded after the addition of 10 μ l of a 10 mM NADH solution

Another reason might be that the polymer acts as a “protective “ barrier for electron transfer. In order to demonstrate this hypothesis, lipid and polymer vesicles were prepared using the preparation procedure as described previously. The anthraquinone solution was added to the external part of the vesicles. Complex I was not incorporated into the vesicle membrane but directly added to the solution with 0.1 % Triton. This triton concentration did not disturb the vesicles integrity. Measurements were done after NADH addition described in Figure 6 and 7.

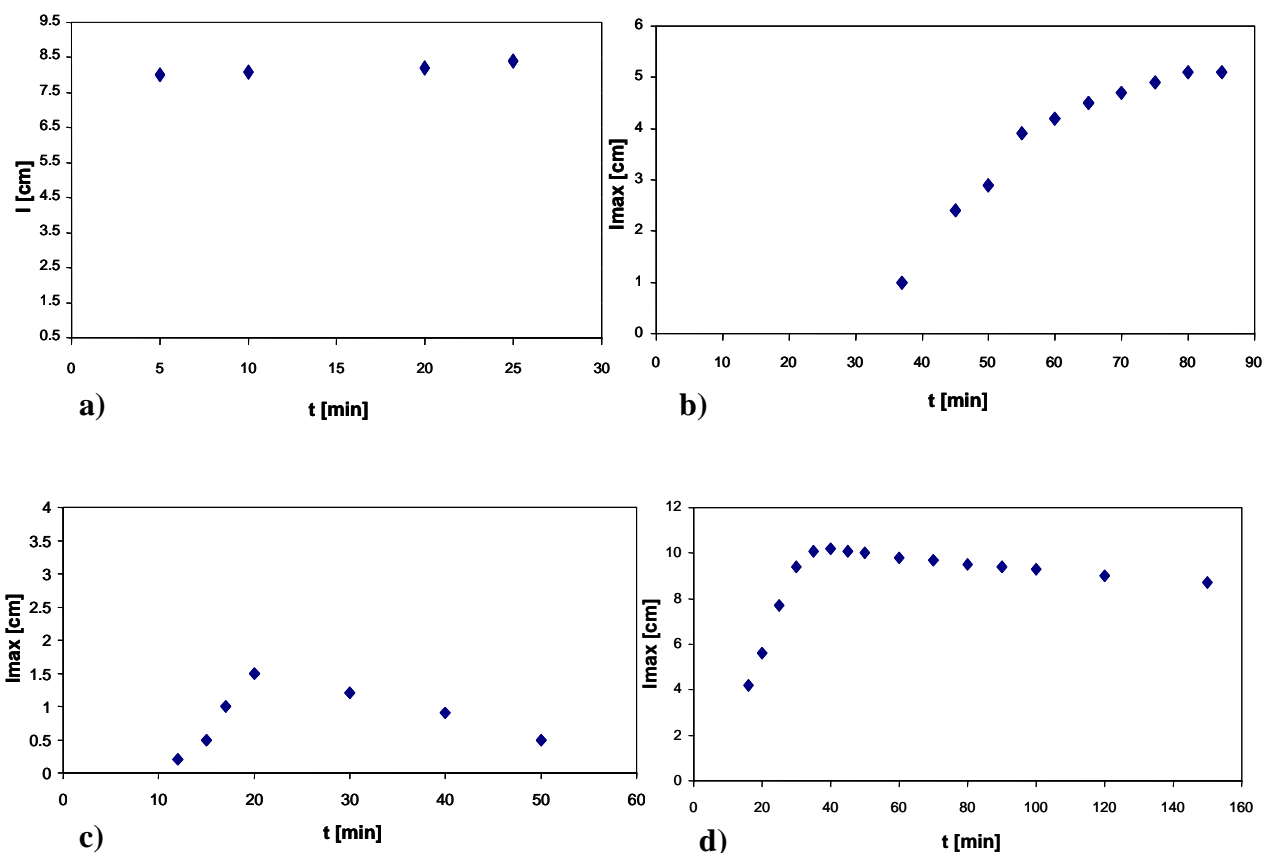


Figure 7. a), b), c), d) graphs represent EPR signals (the maximum of intensity) as a function of time. All the measurements represented by graph a), b), c), d) started after the addition of 10 μ l of a 10 mM NADH solution. Graph a) represents complex I in 1 mM anthraquinone solution with 0.1 % triton. Graph b) represents complex I in 1 mM anthraquinone solution with 1% triton. Graph c) and d) represent complex I in 1 mM anthraquinone solution containing ubiquinone 2 mixed with liposomes and polymer vesicles respectively.

The formation of anthraquinone radical signals was recorded using EPR measurements. Interestingly, EPR signal of anthraquinone radicals appeared only after few minutes in the polymer vesicle solution and were persistent for a long time, whereas in the case of lipid vesicles the signal appeared slower (Figure 7. c) and d)). Moreover, here the signal disappeared after a few minutes.

Obviously electron transfer was faster and the anthraquinone radical was more stable in the solution containing the polymer vesicles (Figure 7. d)).

In parallel, the same experiments were done with the free enzyme using increasing concentrations of Triton (Figure 7. b)). The formation of anthraquinone radical signal appeared inversely proportional to the Triton concentration in the solution. The detergent behaved as a barrier for electron transfer in the same way as polymer and lipid vesicles. This transfer mechanism is still not clear and requires further investigation.

In parallel to those experiments Chemically Induced Dynamic Nuclear Polarization (CIDNP) was performed (data not shown) on the vesicles containing the complex I. The technique demonstrated that the electrons were transferred from the NADH to the complex I iron-sulfur clusters in all cases.

However the last step, from complex I to anthraquinone, was not observed when complex I was reconstituted in both lipid and polymer vesicles.

Anthraquinone's drawbacks might be its rather low redox potential, which is not sufficient for electron acceptance in the presence of amphiphiles, like lipids, Triton, and polymers, or its rather low solubility in aqueous media. As shown by fluorescence spectra in Figure 8, the rate of anthraquinone encapsulation was low. Compared to the vesicles prepared with the ethanol method (Curve C), the vesicles prepared with the biobead method (Curve C) showed a higher fluorescence signal due to an higher rate of encapsulation. Moreover, the polymer contributes to the increase of anthraquinone fluorescence signal. Presumably anthraquinone is partially dissolved within polymer membrane.

Since we were unable to observe the electron transfer to the artificial (not occurring naturally) electron acceptor anthraquinone, we suggested to repeat the above experiments using another electron acceptor. Here we used 2-[(4-amino-3-bromo-9,10-dihydro-9,10-dioxo-1-anthracenyl)amino]-5-methyl-, monosodium salt also call blue anthraquinone was chosen for further studies, which are still in progress.

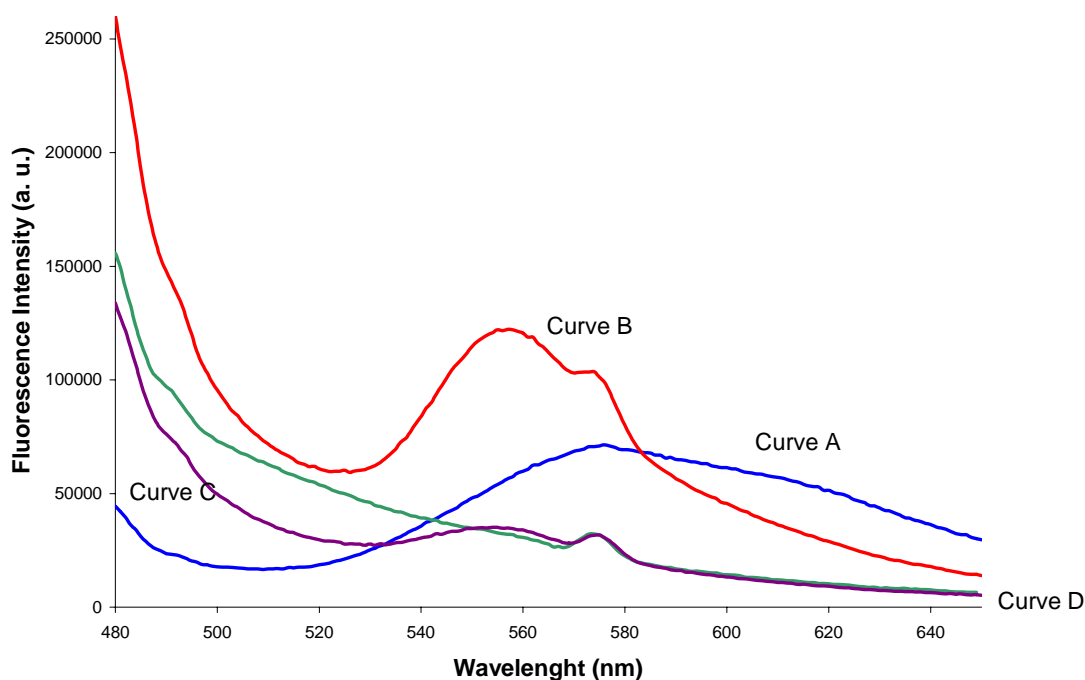


Figure 8. Fluorescence spectroscopy measurements of encapsulated anthraquinone or anthraquinone in solution. Curve A represents the free anthraquinone (1mM). Curve B, and C represent, respectively, anthraquinone (10mM) encapsulated using the biobead and ethanol methods. Curve D represents empty vesicles. Excitation wavelength was 410 nm.

Principle of proton transfer experiments

Another possibility to demonstrate functionality of complex I was to trace the transfer of protons through the polymer vesicle membrane via complex I. In these, experiments we encapsulated a fluorescent dye (HPTS), which is sensitive to the pH change in solution. The advantages of using HPTS was its high solubility in water and in buffer solution and its high sensitivity to slight pH changes. Hence the pH induced shift of the fluorescence intensity of the dye monitored directly the proton transfer from NADH to the interior of the vesicles.

Protons pathway in complex I

For the catalytic mechanism of proton translocating NADH-dehydrogenase a number of hypothetical models have been proposed over the last three decades and are discussed in the

light of recent progress on the structure and function (Brandt, 1997). In the proposed mechanism only the high-potential iron-sulfur center N-2 and ubiquinone seem to contribute to the proton-translocating machinery of complex I.

The proton transfer via complex I was demonstrated by encapsulation of HPTS, a pH-sensitive fluorescent dye. As mentioned above, HPTS is a highly water soluble molecule, even at low pH. Figure 9 shows HPTS encapsulated in the polymer vesicles prepared by both methods, “ethanol” and “direct dissolution”.

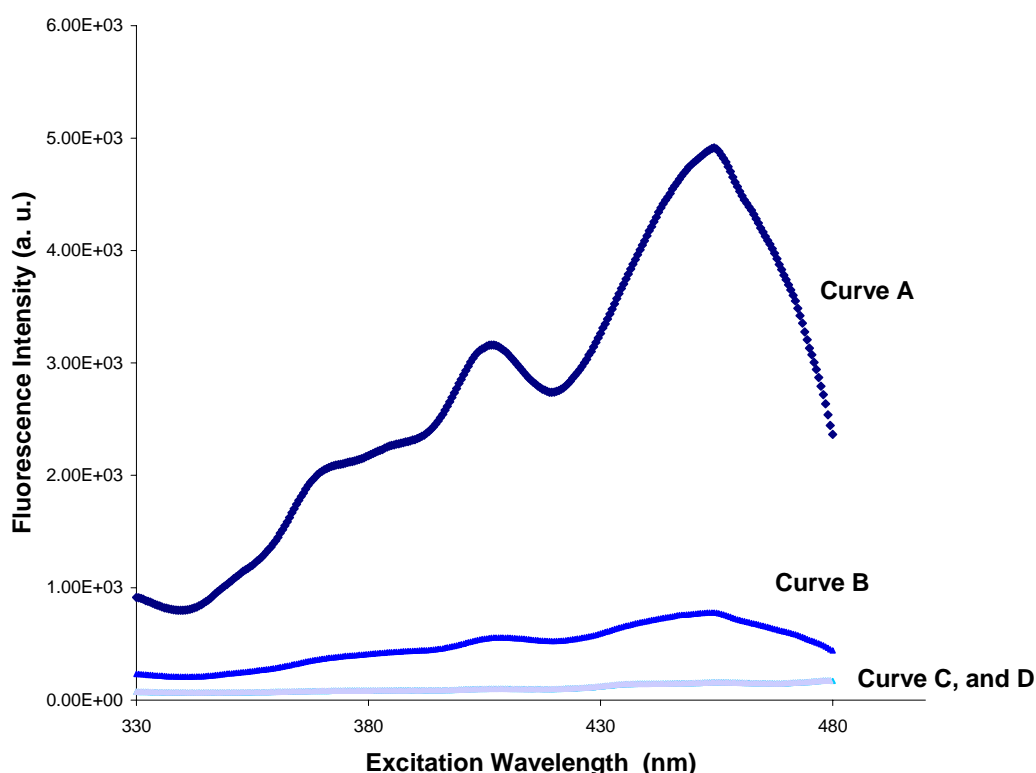


Figure 9. Fluorescence spectroscopy measurements of encapsulated HPTS from a 40 mM HPTS solution in Tris/HCl pH 8 buffer. Curve A represents HPTS encapsulated in vesicles prepared using the “direct dissolution method”, Curve B represents HPTS encapsulated in vesicles prepared using the “ethanol method”, C and D represent empty vesicles prepared using both preparation methods. Emission wavelength was 510 nm.

Compared to the non encapsulated HPTS (Figure 10) there is no significant shift in the fluorescence signal when it is encapsulated. This demonstrates that HPTS is freely dissolved in the inner aqueous cavity of the vesicles.

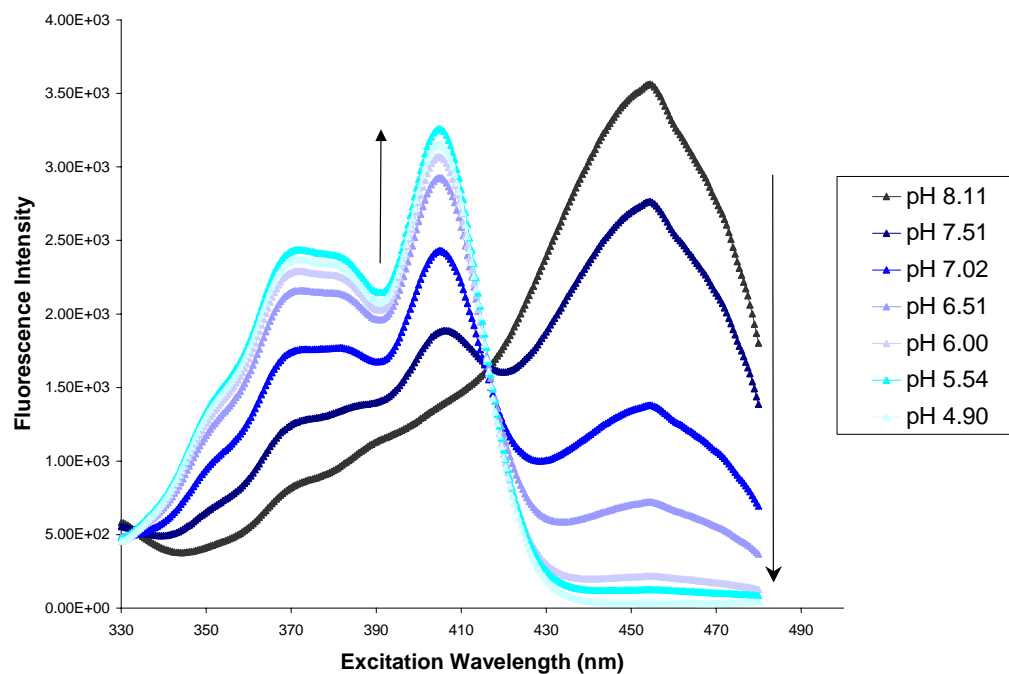


Figure 10. Excitation spectra of HPTS in the pH range 4.90-8.11. HPTS in PBS buffer was adjusted to various pHs, and the excitation wavelength was scanned over the range 330-480 nm. Fluorescence emission cutoff was set at 510 nm. The pH curve can be identified as that with the highest intensity at 450 nm and the lowest intensity at 350-400 nm. The isosbestic wavelength is 413 nm. Two arrows show the increase or decrease of the HPTS fluorescence intensity as function of the pH.

The proton transfer into the vesicle was initiated after the addition of NADH, which acts as proton donor. pH change due to proton transfer were recorded by following the fluorescence intensity increase or decrease.

Quantification of the proton transfer with the pH change can be done based on calibration curves. Solutions of fluorescent dye were prepared with different pH and the fluorescence spectra of HPTS solutions (Figure 10) were used to construct a calibration curve of emission intensity ratios as a function of pH (Figure 11). In Figure 10 the calibration curves present the

fluorescence intensity of HPTS in function of the excitation wavelength at different pH values. F_{EM} ratios from both the λ_{EX} 450/413 nm and the λ_{EX} 403/413 nm pairs are useful in reporting physiological pH. With λ_{EX} 403/413 nm, the F_{EM} ratio increases up to a constant value (2.0) below pH 6. In contrast, the F_{EM} ratio with λ_{EX} 450/413 nm decreases with pH to a small value (0.05 at pH 5.0).

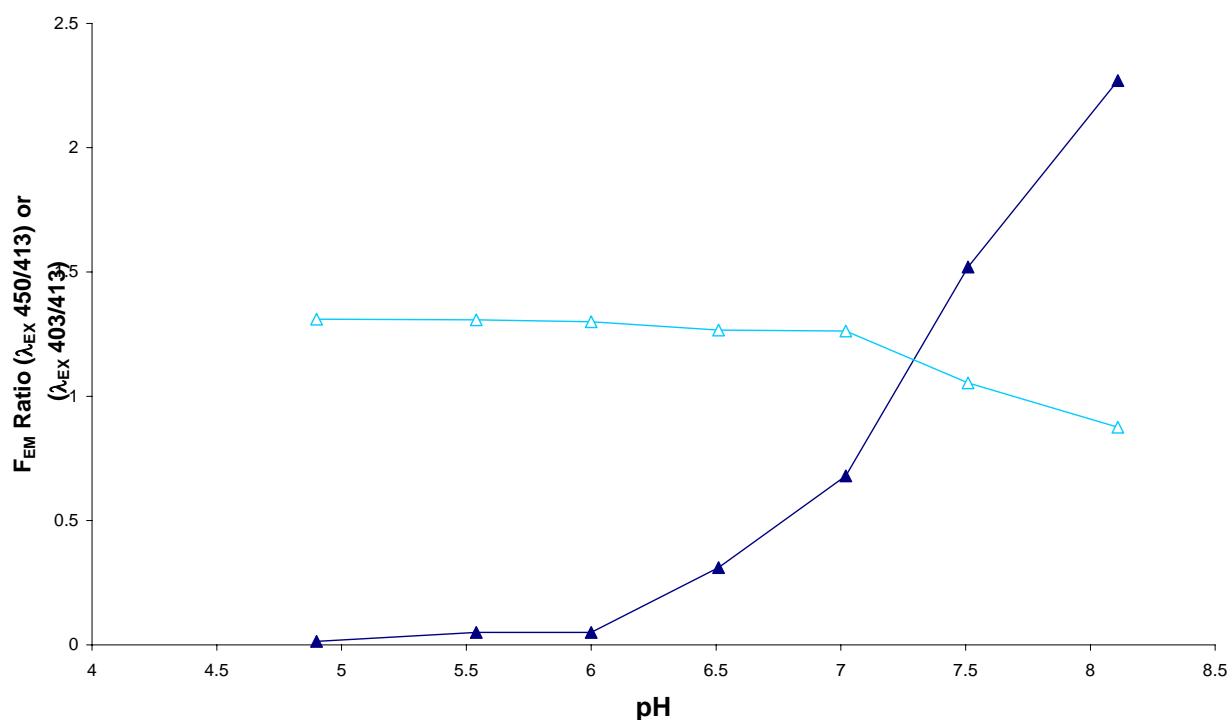


Figure 11. pH calibration curves for HPTS. Ratios were calculated for fluorescence emission intensity (F_{EM} 510) as a function of pH, with λ_{EX} 450/413 nm (filled symbols) or λ_{EX} 403/413 nm (open symbols). The data, taken from Figure 7, allow conversion of ratios to solution pH.

In practice, many wavelength combinations in the pH-sensitive excitation bands from 350-405 and 410-470 nm may be used for calculation of amount of protons after appropriate background correction and calibration. In these studies here, the λ_{EX} 450/413 nm ratio proved to be sensitive, as it changes by 2 orders of magnitude in the pH range of 4.90-8.11. By comparison, Ohkuma and Poole (Ohkuma and Poole, 1978) showed that fluorescein-based probes undergo less than a 9-fold change in the λ_{EX} 495/450 nm ratio over the same pH range.

In order to study the proton transfer through the polymer membrane via complex I and to compare them with the calibration curve, the measurements were performed using the same parameters.

Polymer vesicles were prepared with or without complex I. In both samples, HPTS was encapsulated and the non encapsulated HPTS was removed chromatographically.

The proton transfer was recorded after the NADH addition to the different vesicles solutions. The pH change were monitored using the fluorescence signal produced by the excitation scan of the different samples. The excitation scan was recorded for different incubation times and plotted in Figure 12.

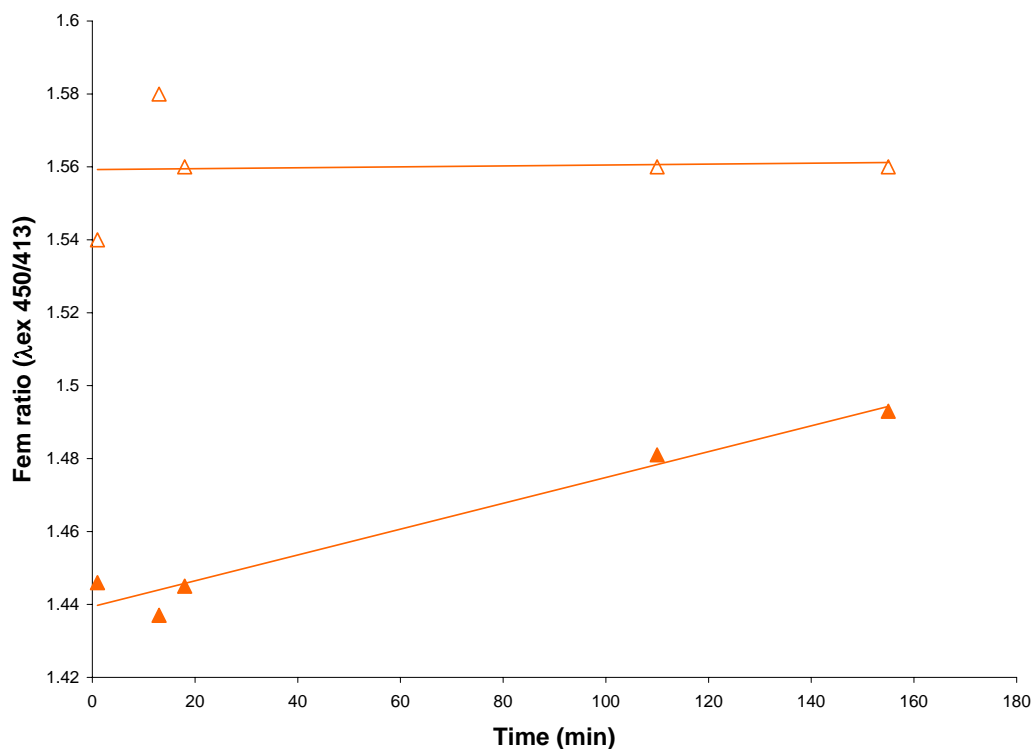


Figure 12. Fluorescence spectroscopy measurements performed on vesicles containing complex I and encapsulated HPTS (40 mM). To record the proton transfer into the vesicles, the same proteovesicle solution was incubated with 5 μ l NADH (10 mM) solution. Ratios were calculated for fluorescence emission intensity (F_{EM} 510) as a function of time, with λ_{EX} 450/413 nm for vesicles containing complex I (filled symbols) and for control vesicles (open symbols). The fluorescence signal increased in function of NADH time incubation.

As shown in Figure 12 the fluorescence signals were increasing with the NADH incubation time. Using the pH calibration curve we could extrapolate the pH change inside the proteovesicles. The pH change is on the order of 0.2 pH unit. These results were rather surprising, since we expected a decrease of the pH inside the vesicles rather than the increase. The results demonstrated that obviously protons were pumped out of the vesicles. The control measurements (vesicles without complex I) showed a constant signal. We mentioned already before that some complex I can be also incorporated in the membrane with the hydrophilic arm oriented toward the inner part of the vesicles. Hence, some protons might be transferred to the outer medium of the vesicles. If some protons were transferred in the expected manner, protons pumped inside with the complex I oriented in the right orientation, a proton equilibrium can be established and the fluorescence signal could not change.

This result was reproducible and this could explain why the signal did not supply any evidence for high step in pH change. Moreover NADH was not stable. For this reason we had to follow the fluorescent signal of a solution containing only NADH and used this as a blank for the fluorescence measurements. Such NADH calibration was also used for the graphic in Figure 12.

5. Conclusion

We could demonstrate that complex I is active after its reconstitution in polymer vesicles. The NADH: ferricyanide activity test showed that at least part of complex I was oriented in the membrane presenting its water soluble part to the external medium. This does however not exclude that part of the protein had the reverse orientation. But we have also to take in account that the protein can be inserted in the opposite way. The encountered difficulties were due to the complex I insertion as it was differing from one experiment to another, namely, for batch of polymer vesicles the ratio of complex I inserted in the “desired” way could be different, even though exactly the same procedure was applied upon sample preparation and handling. On the other hand, experiments with proteovesicles were difficult for interpretation owing to unchanging fluorescence signals. In addition, differences in complex I insertion were also noted for various proteovesicle samples, similarly to polymer vesicles.

The next step of this reconstitution will be the incorporation of complex I in asymmetric membranes (ABC triblock copolymers) in order to guide the protein in the desired orientation.

***Reconstitution of The Membrane Protein Hemagglutinin in Block
Copolymer Membranes***

Summary

In our study we proposed and demonstrated the reconstitution of a fusogenic protein, hemagglutinin, in block copolymer vesicles. The functionality of hemagglutinin has been demonstrated by fluorescence resonance energy transfer (FRET). Here, the polymer vesicles containing the hemagglutinin are mixed with fluorescently labeled liposomes to monitor the fusion event between polymer vesicles and lipid vesicles.

This opens the door to fusion of artificial polymer membranes with biological cells. Moreover, the use of nano-sized carriers to overcome the limitations in cellular uptake of highly active compounds is the focus of new drug delivery strategies. The system combining the fusion promotor, hemagglutinin, and block copolymer vesicles seems to be a very promising approach.

The combination of viral membrane proteins such as hemagglutinin with block copolymers is also promising for medical applications. This chimeric combination proposed in this study is also a potential tool for vaccination, since it can be used as adjuvant of antigenic protein vaccination to elicit humoral and/or cellular immune responses in vaccinated subjects.

1. Structure and function of the flux virus membrane protein hemagglutinin

Membrane fusion is a universal event in living organisms. It is crucial for exocytosis and endocytosis, for intracellular membrane traffic, and is also used by enveloped viruses to enter and infect cells (Jahn and Südhof, 1999). Membrane fusion is energetically unfavorable and does not occur spontaneously. In Nature, specific molecules induce biomembrane fusion. In the case of virus-membrane fusion, it was demonstrated that fusogenic proteins were directly responsible for the induction of membrane fusion. (Stegmann *et al.*, 1989). For example, Influenza virus enters its host cell by endocytosis, followed by fusion between the endosomal and the viral membrane which is mediated by the trimeric integral membrane protein hemagglutinin (HA) (Hernandez *et al.* 1996; Hughson, 1995) (Figure 1).

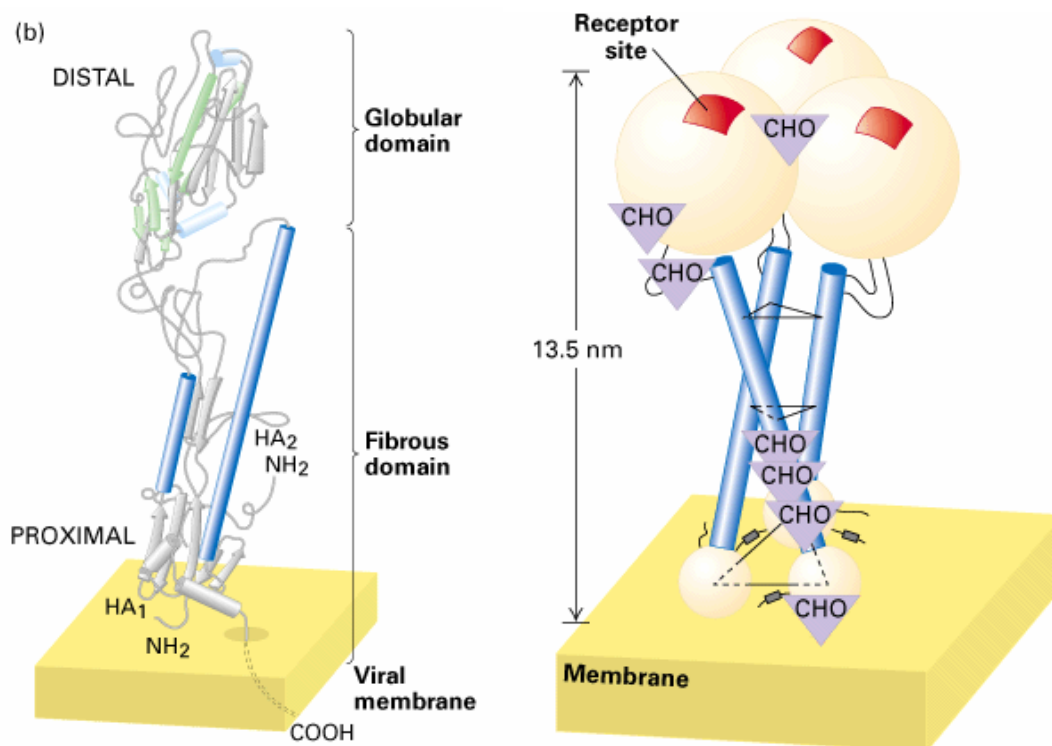


Figure 1. Representation of the tertiary structure (a) and quaternary structure of hemagglutinin (b).

It is triggered by the low endosomal pH, which induces a conformational change in the protein. Each monomer of HA consists of two disulfide-linked subunits, the smaller one, HA2, is membrane-anchored at the C-terminus. The N-terminus of this subunit consists of a hydrophobic amino-acids known as the “fusion-peptide”, which is buried in the stem of the HA trimer at neutral pH (Wilson *et al.*, 1981). The conformational change at low pH moves this peptide to the outside of the protein (Bullough, 1994), and studies of liposome-virus fusion have shown that the peptide then enters the hydrophobic interior of the target membrane for fusion (Stegmann, 1991; Tsurudome *et al.*, 1992). Insertion could perturb the target membrane locally, providing a starting point for fusion. It was found that virus (Shangguan *et al.*, 1996) or single purified trimer of the ectodomain of HA (Jiricek *et al.*, 1997), produce a pore in target membranes at low pH, allowing the leakage of water-soluble molecules across these membranes. The formation of either lipidic or proteinaceous intermediate structure has been proposed to precede the membrane merger. Lipidic intermediates could be “stalks” of fused outer membrane leaflets, formed after a local perturbation of the target membrane bilayer by the inserted viral fusion peptides (Siegel, 1993). This “hemifusion” intermediates would then expand laterally, be followed by breakthrough and merger of the inner leaflets at this point, leading to complete fusion. Although several observations are compatible with this theory (Chernomordik *et al.*, 1993; Klotz *et al.*, 1996), it follows that lipids would be the first aqueous connection between the viral and the target membrane interior, the so-called “fusion pore”. However, electrophysiological measurements have shown that fusion pores form before lipid mixing can be detected (Tse *et al.*, 1993). Thus, alternatively, it was proposed that fusion pores may be proteinaceous (Lindau and Almers, 1995) and would expand gradually, incorporating lipids as they open Figure 2. The fusion mechanism is still not completely understood and the proposed models are still under investigation.



Figure 2. “Stalk-pore” hypothesis for membrane fusion mediated with by influenza hemagglutinin (HA). Expert review in molecular medicine © Cambridge University Press.

2. Hemagglutinin (HA) insertion in block copolymer vesicles and induction of fusion with lipid membranes.

The HA was reconstituted into polymer membranes using the biobead method. It was performed using triton X100 detergent as described in materials and methods.

There are different ways of preparing the hemagglutinin (HA) protein depending on the extraction and purification procedure applied. HA can be co-extracted with the viral lipids, or extracted as a trimer (BHA), or as a complex made of different (HA) trimers (HA rosettes). They all induces pores of less than 26 Å in diameter in liposomal membranes at low pH. These pores are persistent and begin to open shortly after the low pH-induced conformational change in HA. HA rosette and virus also induce the formation of much larger pores (which are called leakage pores here to distinguish them clearly from all other pores) (Hernandez *et al.* 1996), allowing the leakage of fluorescent probes across the liposomal membrane, at time well after the conformational change. It was shown, that fusion pores and leakage pores in the case of HA are related structures (Hernandez *et al.* 1996).

Block copolymer vesicles were prepared with HA rosettes for mainly two reasons. The first reason was that this HA preparation method allowed us to use the protein immediately after its purification. The last step was performed in presence of detergent and our reconstitution method involved the reconstitution of the protein using detergent (Materials and Methods). This avoids structural changes of HA due to the detergent removal. The second reason was the size of the pore formed in the membrane. They were larger and this is an advantage for the sensitivity of the measurements. The reconstitution of HA was also performed using the “ethanol method”. This was also done to compare the incorporation efficiency of HA in the polymer using two different methods. The results are reported below.

The fusogenic activity of (HA) after reconstitution in the polymer vesicles was tested in the presence of labeled liposomes containing N-NBD-PE (*N*-(7-nitrobenz-2-oxa-1,3-diazol-4-yl)-1,2-dihexadecanoyl-*sn*-glycero-3-phosphoethanolamine, triethylammonium salt) and *N*-Rh-PE (Lissamine™ rhodamine B 1,2-dihexadecanoyl-*sn*-glycero-3-phosphoethanolamine, triethylammonium salt). The experiments were performed using fluorescence resonance energy transfer (FRET), which is a photophysical effect where energy that is absorbed by one fluorescent molecule (donor) is transferred to a second fluorescent molecule (acceptor). The efficiency of FRET depends both on the orientation of the chromophores and their distances.

The preparation of the fluorescently labeled liposomes, vesicles and also the FRET assay are described in details in “materials and methods”. The fusion is detected by an increase of the fluorescence intensity due to the lipid membrane destabilization.

2.1 Results and discussions

To demonstrate the hemagglutinin-induced fusion of block copolymer with lipid membranes we first demonstrated that the polymer vesicles without HA did not disturb the liposomes at pH 7.4 and 5. For that purpose, labeled liposomes were mixed with polymer vesicles and FRET was recorded at pH 7.4 and 5. When the labeled liposomes are not destabilized (e. g. fusion, pore formation, etc.), the fluorescent dyes inside the lipid bilayer of the liposomes can do a energy transfer because they are close enough in distance.

When the liposome membrane is solubilized the distance of the two dyes increases and hence energy transfer decreases (see in material and method the principle of FRET). The results for pH 7.4 and pH 5 were identical. Therefore only one set of experiments is shown in Figure 3.

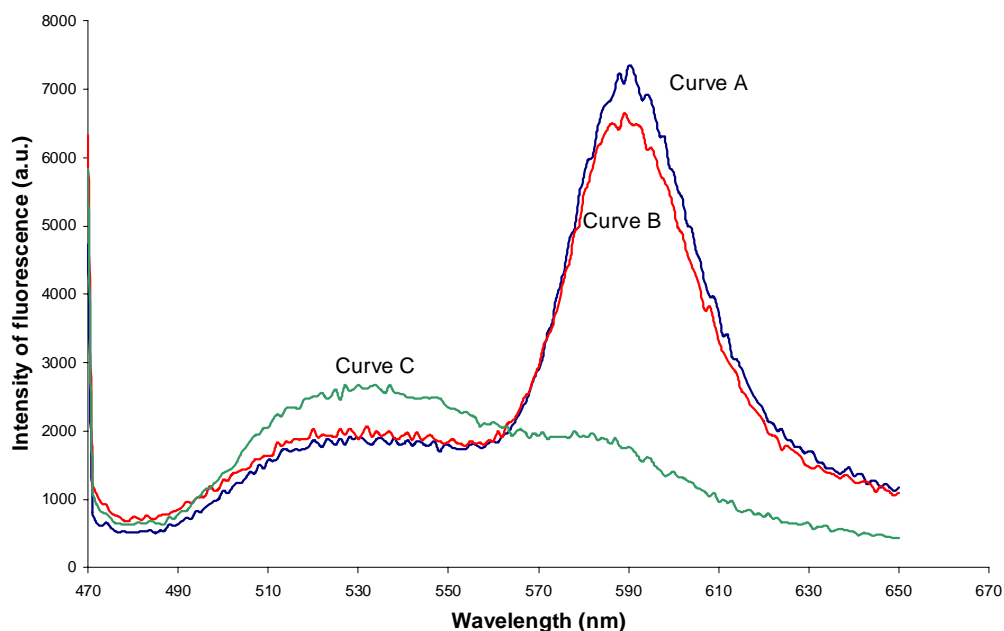


Figure 3. FRET experiments were performed at pH 5, 37 °C. Curve A represent the solution of the labeled liposomes. Curve B represent the labeled liposomes solution in presences of

polymer vesicles and curve C represent the labeled liposomes with polymer vesicles and 0.5 % triton X100. Excitation wavelength was 465 nm. The FRET did not change in the presence of the polymer vesicles at pH 7.4. At pH 5, a small increase of FRET was observed. The polymer vesicles showed a slight tendency to fuse or to perturb the lipid membrane. **This phenomena was observed by Ruyschaert et al in preliminary studies.** This decrease of FRET is subtracted during the calculation. Finally, FRET decreased after the solubilization of the liposomes with the detergent (curve C). The measurements with vesicles prepared with the “biobead” and “ethanol method” and they have shown the same behavior in the resonance energy transfer assay.

Afterwards we preformed the same measurements were performed with polymer vesicles containing hemagglutinin (prepared with the biobead and ethanol method). The HA containing vesicles were added to the solution containing the labeled liposomes and fusion was recorded as a function of time at pH 7.4 and pH 5 (Figure 4-5).

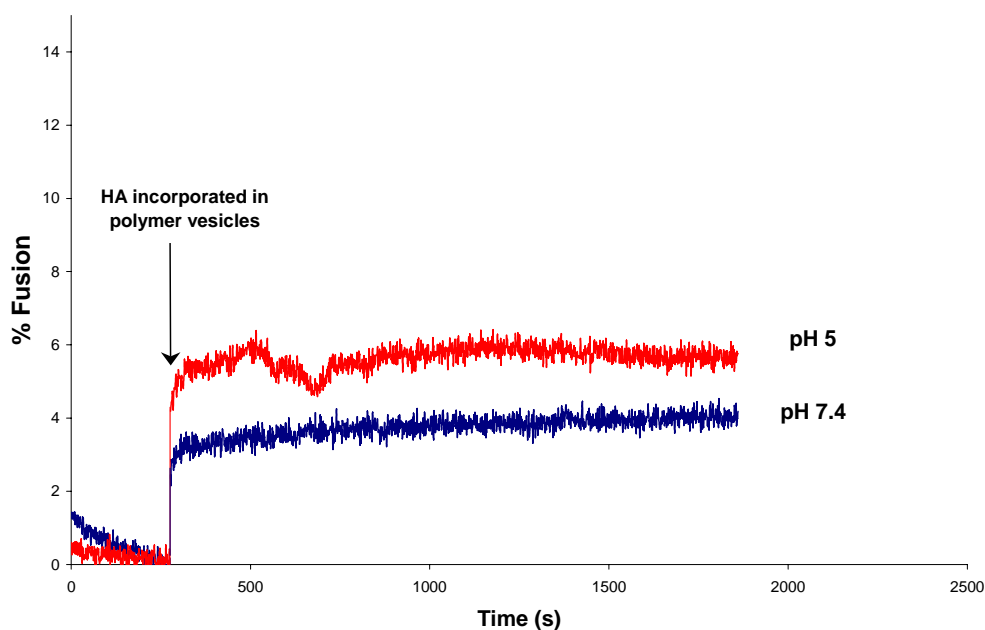


Figure 4. Kinetic measurements of the fusion of HA containing polymer vesicles (prepared with the biobead method) with liposomes containing N-NBD-PE and N-Rh-PE, at pH 5 and pH 7.4, 37 °C. Fusion was measured with a resonance energy transfer assay as described in materials and methods. Liposomes concentration was 7.5 μM and 150 μl of a 10 $\mu\text{g}.\text{ml}^{-1}$ vesicles solution was added to the liposome solution.

For both method of preparation we could detect fusion between the polymer containing HA and the liposomes membrane however the signal was very low. Fusion was even lower with the sample prepared with the “ethanol method”. Surprisingly, a fusion signal was also detected at pH 7.4 in the sample prepared with the biobead method. Moreover, the curves did not show a typical fusion time course as described for the influenza virus or for HA reconstituted in liposomes. Usually, the fusion increases slowly and continuously. In the presence of polymer vesicles, the fusion signal increase instantaneously and then a plateau is reached.

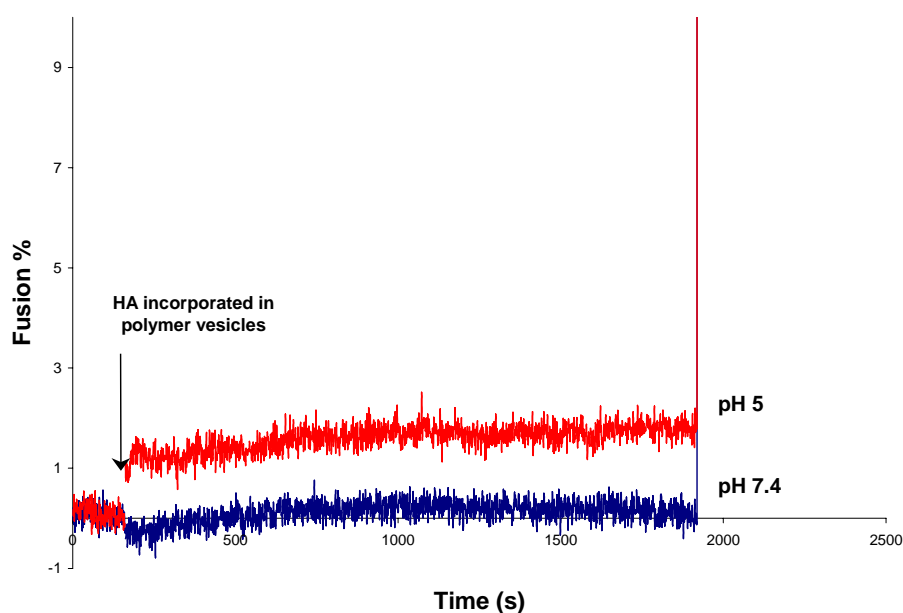


Figure 5. Kinetic measurements of the fusion of HA containing polymer vesicles (prepared with the ethanol method) with liposomes containing N-NBD-PE and N-Rh-PE, at pH 5 and pH 7.4, 37 °C. Fusion was measured with a resonance energy transfer assay as described in materials and methods. Liposomes concentration was 7.5 μM and 150 μl of a 10 $\mu\text{g}\cdot\text{ml}^{-1}$ vesicles solution was added to the liposome solution.

Different concentration of polymer vesicles containing HA were tested and different amount of HA were inserted but no qualitative phase of the fusion signal could be detected.

The fusion was not efficient and the intensity signal was very low when compared with influenza virus. The virus induced 30 % of fusion (Bonnafeous and Stegmann, 2000) whereas HA reconstituted in the polymer could induce 5-6 % fusion (Figure 4).

The low fusion presumably due to a low or non efficient incorporation of HA. It is also possible that the protein was not inserted in a functional way. This hypothesis is still under investigation. Another explanation is that the mixture of lipid and polymer membrane would require a high energy barrier to overcome. The same fusion assays have been performed with reconstituted viral membrane containing poly(ethylene glycol) grafted lipids (Chams *et al.*, 1999). Obviously, the presence of PEG at the surface of the membrane affected the fusion with the liposomes. Moreover, the inhibition of fusion was more extensive using a larger hydrophilic graft chain.

2.2 Conclusion

In this experiment the length of the hydrophilic part was a limitation factor. HA could not have access to the host membrane due to the sterical hindrance produced by the hydrophilic PEG graft chains. We deduced that the same phenomenon must occur for the polymer vesicles. The PMOXA block behaves similar to the PEG-graft. The long PMOXA chain can also inhibit and disturb the fusion mediated by HA. Thus, this explains the low fusion efficiency.

Hence, in order to overcome the sterical hindrance due to a too long hydrophilic PMOXA block, a shorter one can be used. Also, a new strategy to insert HA in the block copolymer will be developed.

Incorporation of FhuA Δ 5-160 in Block Copolymer Vesicles

Summary

The wild type of FhuA outer membrane protein, which is involved in the iron uptake in cells was genetically converted into a non specific channel, which is called FhuA Δ 5-160. We presented in this study the reconstitution and the functionality of FhuA Δ 5-160 in block copolymer vesicles.

The functionality of FhuA Δ 5-160 has been demonstrated using an enzymatic test. First, we encapsulated an enzyme which was big enough not to cross the membrane via the channel protein. In a second step the enzyme substrate was added to the external medium. The substrate could diffuse through the channel and was hydrolyzed in the internal medium. The enzymatic reaction was followed by a colorimetry test using an UV-spectrophotometer. We demonstrated that FhuA Δ 5-160 preserved its function after reconstitution in block copolymer vesicles.

The incorporation of FhuA Δ 5-160 in block copolymer membranes opens broader applications compared to membrane proteins with lower size exclusion limit, such as OmpF. A promising application is the design of new devices for DNA entrapment which is particularly well suitable for DNA size screening.

For example, during DNA sequence amplification process called, polymerase chain reaction (PCR), oligonucleotide sequences, so called primers, are required for initiating the amplification process. The size exclusion limit of FhuA Δ 5-160 allows to discriminate DNA sequences from the oligonucleotide primers. Primers can be entrapped inside the vesicles, where encapsulated positively charged polymers precipitate them. Thus, prevent them from diffusing out from the vesicles again.

1. Structure and functions of FhuA Δ 5-160 from *Escherichia coli*

The wild type of FhuA outer membrane transport protein of *E. coli* consists of 22 anti-parallel β -sheets that form a β -barrel into which a globular domain is inserted from the periplasmic side. The globular domain seems to close the β -barrel channel and prevent entry of even small molecules and was for this reason designated the “cork” (Ferguson *et al.*, 1981). Ferrichrome, the natural substrate of FhuA, binds in a cavity located well above the outer membrane lipid bilayer. Ferrichrome is a cyclic hexapeptide composed of three glycine and three modified ornithine residues that bind Fe(III) with hydroxamate groups [-N(OH)C(=O)C].

The cork domain and the β -barrel domain contribute five or six amino acid side chains to the cavity, respectively, which are less than 4 Å away from the ferrichrome (Ferguson *et al.*, 1981). It is thought that opening of the FhuA channel requires dislocation of the cork, resulting in a connection between the cavity exposed to the cell surface and the region exposed to the periplasm. Although binding of ferrichrome to FhuA moves the cork about 2 Å towards ferrichrome, this does not open the channel. The binding of ferrichrome enhances the interaction of FhuA with TonB (Moeck *et al.*, 1997), which may be facilitated by a movement of 17 Å. TonB proteins are essential components in iron-siderophore uptake in bacteria, and function as energy transducers that couple the energized state of the cytoplasmic membrane to outer-membrane receptor function. Ton B protein is located in the periplasm with the N-terminus anchored to the cytoplasmic membrane. The protonated form of TonB is able to interact with the outer membrane transporters and changes its conformation, such that Fe³⁺ and the Fe³⁺ complexes dissociate from their binding sites and diffuse through the channel which is opened at the same time. The transport mechanism of Fe³⁺ is sketched in Figure 1.

The “Cork” can be genetically removed to convert FhuA into a non-specific channel with a determined molecular size-exclusion. In Figure 2, the cork domain is represented in light color. The cork domain was deleted by removing amino acids 5 to 160. Previous investigation demonstrated that FhuA Δ 5-160 was converted into a non-specific single channel (Braun *et al.*, 2002; Braun *et al.*, 1999).

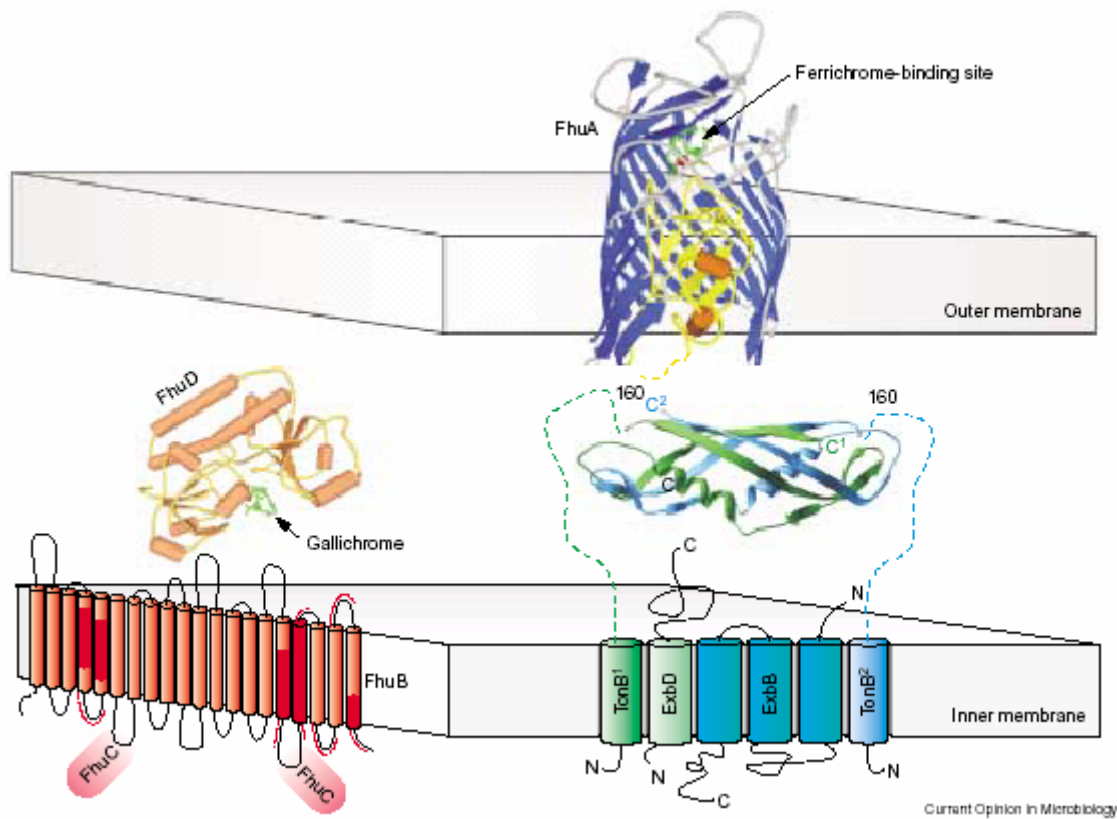


Figure 1. Illustration of the FhuA ligands and the proteins involved in ferrichrome transport. In the crystal structure of FhuA, b-strands in the front were removed to better visualize the globular domain. The TonB box of FhuA is located at the amino-terminal and binds to the region around residue 160 of TonB (marked 160). The crystal structure of the dimeric TonB fragment 164-239 is shown; the green and blue interrupted lines reflect the unknown parts of the structure. C1 indicates the carboxy-terminal end of one TonB monomer, C2 indicates the carboxy-terminal end of the other monomer in the TonB dimer fragment. The orientation of the TonB fragment in the periplasm is not known. The crystal structure of FhuA provides a static picture of the protein but does not reflect the highly dynamic structure alterations that take place upon binding and release of ferrichrome and during ferrichrome transport (Braun *et al.*, 2002).



Figure 2. FhuA crystal structure. In the side view, a portion of the β -strands (blue) was deleted to improve the view on the globular central domain (cork; yellow). The view from outside the cell (top view) illustrates the closure of the β -barrel channel by the cork domain. (Braun and Braun, 2002)

2. FhuA Δ 5-160 incorporation and functionality test: Results and discussions

Here we incorporated FhuA Δ 5-160 into polymer vesicles. In order to prove the FhuA functionality we designed a test exploiting FhuA is non-specific diffusion channel properties. The enzyme peroxydase was encapsulated into polymer vesicles containing FhuA Δ 5-160. The two reconstitution methods (Materials and Methods), “ethanol” and “direct dissolution methods”, were used to prepare the vesicles. The peroxydase-containing vesicles were prepared as described in β -lactamase experiments.

The peroxidase substrate, 3,3', 5,5'-tetramethyl-benzidine (TMB), was added to different samples: vesicles, proteovesicles and to the free enzyme. The enzyme activity was recorded by measuring the absorbance of the different samples at 450 nm.

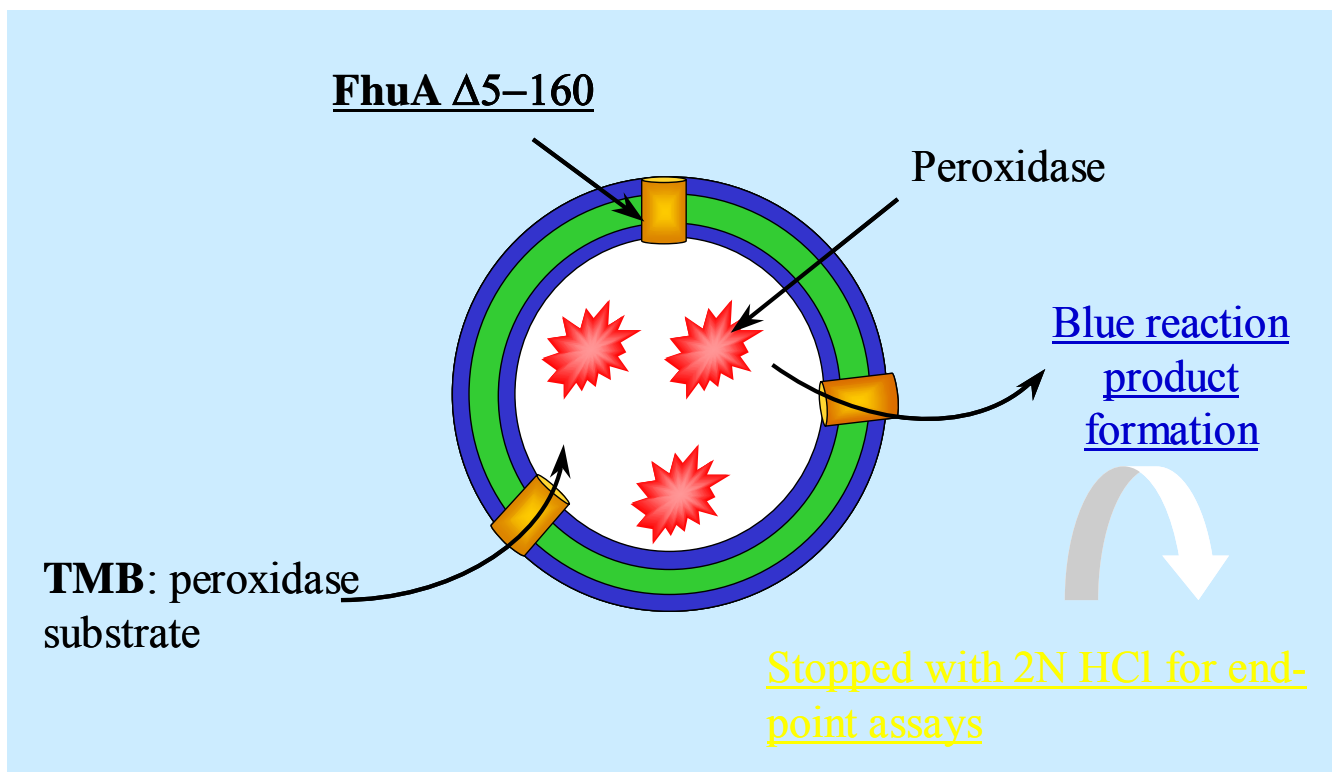


Figure 3. Cartoon of the peroxidase test.

In figure 3 we have present a sketch of the peroxidase test. The non encapsulated peroxidase and non incorporated protein were removed chromatographically. Afterwards, the vesicles containing or not FhuA were incubated with TMB, the peroxidase substrate. Due to its small molecular mass, TMB can be transferred through FhuA into the vesicles and be cleaved by the peroxidase. The substrate system developed a blue reaction product when reacted with peroxidase. For end-point assays, 2 M of hydrochloric acid was added to the reaction system. As a consequence the solution developed a stable yellow colour end product. Afterwards the absorbance was measured. All the results are reported in the figure 4. The peroxidase activity could be detected in both samples containing FhuA (Figure 4) whereas in the samples containing no FhuA no activity was detected. The absorbance for the sample prepared by

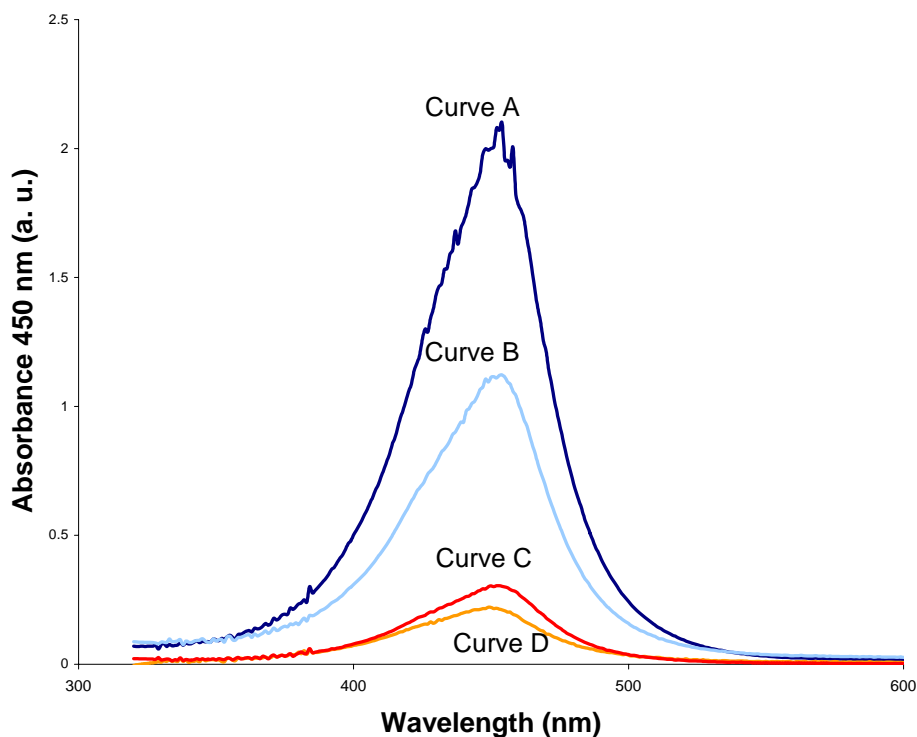


Figure 4. Peroxydase activity measured by absorbance at 450 nm using an end point assays. Curve A and C represent the proteovesicles containing FhuA prepared with “direct dissolution method” and “ethanol method” respectively. Curve B and D represent the vesicles prepared using the “direct dissolution method” and the “ethanol method” respectively.

“direct dissolution” method was higher than for the “ethanol method”. This can be explained by the fact that the samples prepared by direct dissolution method are more turbid than the ones prepared with ethanol method. This explains also why the vesicles without FhuA also absorb light. When the absorbance of the vesicles is compared to the proteovesicles in respect to the reconstitution method used, we could observe the peroxydase activity in both samples containing FhuA.

2.1 Conclusion

We can conclude that FhuA was functional as a non-specific channel. TMB could diffuse through FhuA and be further converted into a colored end product.

The next steps would be the determination of the size exclusion limit of this non-specific channel and use the protein in another polymer vesicle system. Similar to OmpF the application possibilities for FhuA are wide, mainly in the fields of drug and DNA delivery, and therefore more extensive research should be carried out in this field, to gain better understanding of both protein insertion mechanism as well as its functionality in artificial polymer membranes.

Summary

Summary

We presented in this work the design and preparation of new types of artificial and stable membranes for the reconstitution of membrane proteins. In the first part of the study we introduced a stabilization strategy for lipid membranes using hydrophobic polymers. Electroporation experiments with free-standing planar bilayers showed that after incorporation of such hydrophobic scaffold the energy to create a defect in the membrane increased by a factor of two. In liposomes the 2-D network provides considerable stabilization against lyses.

Moreover, we showed that the incorporated polymer still allowed a functional insertion of membrane proteins. As a model protein we used OmpF that preserved its full activity, as long as the cross-linking density of the polymer scaffold is not too high. For very low mesh sizes it seems that part of the protein is deactivated or expelled from the membranes.

In a different approach we used an amphiphilic triblock copolymer PMOXA-PDMS-PMOXA to form highly stable membranes. It had already been shown that this particular block copolymer behaves like typical bilayer-forming lipids, such as lecithin, and forms vesicular structures with higher mechanical and chemical stability in dilute aqueous solution (Nardin *et al.*, 2001). Moreover, it is obvious to regard the PMOXA-PDMS-PMOXA triblock copolymer membranes as a mimetic of biological membranes.

Indeed, recently it had been shown that the bacterial porin OmpF, a channel protein from the outer cell wall of gram-negative bacteria, could be reconstituted in such artificial membranes and preserved its full activity. Here we extended these reconstitution studies to other types of membrane proteins. This required the adaptation of already existing and the development of new reconstitution protocols.

As a first example we reconstituted LamB in ABA-block copolymer vesicles. LamB acts as a phage receptor, which triggers the ejection of λ phage DNA. We could show that in agreement with the natural bacteria infection process, the phage was able to infect the polymer vesicles reconstituted with LamB by DNA injection across the polymer membrane. Hence the protein remained fully active and had a physiological orientation in the membrane of the triblock copolymer vesicles.

Also, FhuA Δ 5-160, a large and non specific channel mutant of FhuA, was reconstituted into the polymer membranes. After reconstitution, we tested its functionality by controlling the membrane permeability. In fact the channel remains active and large model substrates were able to diffuse across the membrane in the presence of FhuA Δ 5-160.

In another set of experiments the fusogenic membrane protein of influenza viruses, hemagglutinin, was reconstituted into the polymer membrane. Depending on the reconstitution procedure we measured up to 5-6 % of membrane fusion which is about 20% of the activity of the virus. Nevertheless, we expect that their fusion rate can be improved by changing for example the length of the PMOXA chains.

Finally, complex I from the respiratory chain of *E. coli* bacteria was reconstituted into polymer membranes using different preparation procedures. A well-established NADH: ferricyanide activity test showed that the reconstituted protein was functional and that at least a part of the incorporated proteins inserted into the membrane by presenting their water soluble part to the external medium.

Altogether we demonstrated the functional reconstitution of different type of membrane proteins. As shown during the studies, the functional reconstitution depends mainly on the protein structure and stability and also on the reconstitution procedure itself. The combination of natural proteins properties with the one of synthetic polymer is very promising and may lead to a multitude of applications in different field, like in biotechnology, pharmacy, etc.

Materials and Methods

Materials and Methods

1. Lipids, enzymes and fluorescent probes

1.1 Commercial products

DphPC (1,2-diphytanoyl-*sn*-glycero-3-phosphocholine), POPC (1-palmitoyl-2-oleoyl-*sn*-glycero-3-phosphocholine) and Ceramide molecules were provided by Avanti Polar Lipids Company (Alabaster, AL). Egg-phosphatidylcholine molecules were provided by SIGMA Company (St.Louis, MO).

All the fluorescent probes: 5-(and- 6)-carboxyfluoresceine, HPTS (8- hydroxypyrene-1, 3, 6-trisulfonic acid, YO-PRO®- 1 iodide, NBD- PE (*N*-(7-nitrobenz-2-oxa-1,3-diazol- 4-yl)-1,2-dihexadecanoyl-*sn*- glycero-3-phosphoethanolamine, triethylammonium salt) and *N*- Rh- PE (Lissamine™ rhodamine B 1,2-dihexadecanoyl-*sn*-glycero-3- phosphoethanolamine, triethylammonium salt (or rhodamine DHPE) were purchased from Molecular Probes (JURO supply GmbH).

Acetylcholinesterase, β -lactamase were provided from SIGMA Company (St. Louis, MO).

The lipids were stored at $-20\text{ }^{\circ}\text{C}$ either in powder or in chloroform solution.

The fluorescent probes were stored either at $-20\text{ }^{\circ}\text{C}$ or at room temperature and protected from the light. The Enzymes were stored like mentioned by SIGMA Company.

1.2 β -lactamase production and purification.

β -lactamase was also produced in our laboratory using an *E. coli* strain expressing the enzyme. The bacteria were grown in LB medium in the presence of ampicillin to the “mid-log phase” ($\text{OD}_{600} \sim 0.5$) at $37\text{ }^{\circ}\text{C}$. Then the culture was harvested by centrifugation at $14\ 000\text{g}$ during 10-15 s. The pellet was washed in PBS followed by centrifugation at $14\ 000\text{ g}$ for 10-15 s. The pellet was solubilized in PBS and the solution was sonicated 3 times for 3 s on ice. The last centrifugation ($14\ 000\text{ g}$, 10-15 s) was performed in order to remove the cell envelopes. The supernatant containing β -lactamase was used directly for the experiment or stocked several days at $4\text{ }^{\circ}\text{C}$.

2. Protein and phage purifications

2.1 The Outer Membrane Protein OmpF

BL21 (DE3) competent cells were transformed with the plasmid pGompF. The plasmid coding for OmpF was prepared by using the vector pGEM®-5Zf (-) from PROMEGA company.

The vector codes for ampicilline resistance and contains the T7 RNA polymerase transcription initiation site which is necessary for the OmpF gene transcription. The strain BL21 (DE3) competent cells carry the genotype *E. coli* B F dcm ompT hsdS (r_B m_B) gal λ (DE3) which allows high-level protein expression and an easy IPTG induction. These strains are general protein expression strains that lack both the protease and the OmpT outer membrane protease, which would both degrade proteins during purification. The strain was provided from Stratagene company.

The transformation of the competent cells was performed by using the following protocol: 100 µl of competent cells were incubated with DNA (1-2 µl plasmid preparation) on ice for 30 min. Then the cells were incubated at 37 °C for 5min. Again the cells were incubated on ice for 20 min., and then the cells were mixed with 1 ml of LB medium and incubated at 37°C for 1 hour. The transfected cells were plate out on antibiotic (100 µg·ml⁻¹) agar plates, and next colonies were taken and mixed with 10 ml of antibiotic-containing LB medium to prepare a preculture the other day. The preculture was then mixed with 1 L. of LB medium and incubated at 37 °C over-night . The induction was performed during the night with 1 mM IPTG as final concentration. The culture was then centrifuged at 5000 rpm for 30 min at 4 °C. The formed pellet was mixed with the “ breaking buffer “ (20mM Tris/HCl pH 8 and 2% SDS). After homogenization (ultraturax), the mixture was incubate at 60 °C for 1h. with shaking. Then the mixture was spun for 40 min. at 28 000 rpm. The preextraction step was then performed by adding 0.125% octyl-POE (ALEXIS company), 20mM NaH₂PO₄ pH 7.3 to the pellet. The mixture was homogenized, incubated at 37 °C for 45 min. and spun for 40 min. at 28 000 rpm. The extraction of OmpF was done by homogenization with 3% octyl-POE, 20mM NaH₂PO₄ pH 7.3 followed by additional shaking at 37 °C for 45 min. and centrifugation at 28 000 rpm for 40 min.

10 mM EDTA was then added to the OmpF-containing supernatant.

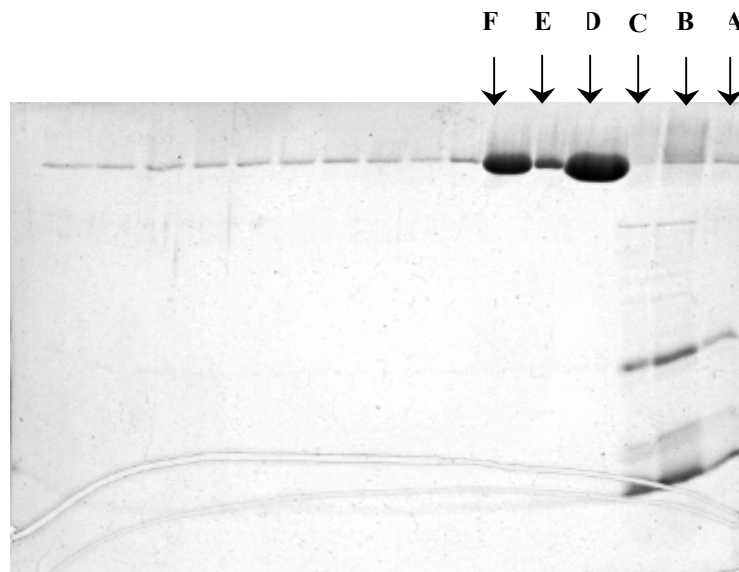


Figure 1. Purity analysis of OmpF by 12 % SDS-Page. After each purification steps an aliquot is analysed (**A**, **B**, **C**, **E**). **D** is the sample **E** concentrated 10 times. **F** represents purified OmpF (99 kDa).

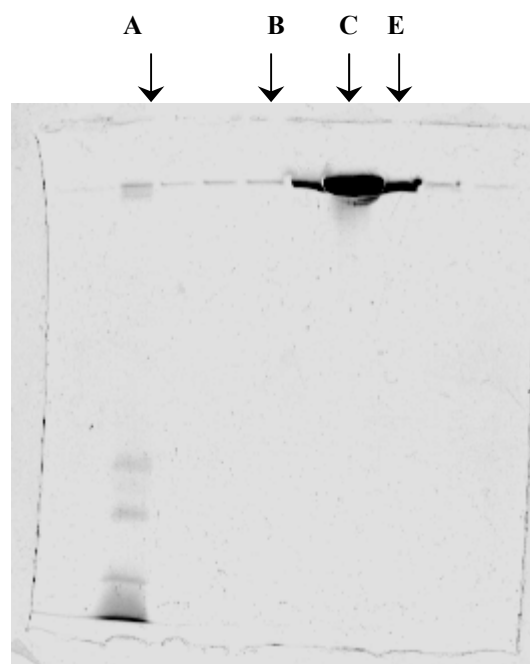


Figure 2. Purity analysis of LamB by 12 % SDS-Page. After the last purification step the supernatant containing LamB is loaded on an affinity column. Aliquots are analysed before elution (**A**) and after elution of LamB (**B**, **C**, **E**). The contaminants do not bind the column and are eluted (**A**). The LamB elution is performed using maltose (**B**, **C**, **E**).

The OmpF purity was examined by a 12% SDS-Page gel (Figure 1) and the concentration was determined after dialysis against 1% octyl-POE, 20 mM Tris/HCl, 100 mM NaCl pH 8 by UV-Vis spectrometry at 280 nm against 1% octyl-POE, 20 mM Tris/HCl, 100 mM NaCl pH 8 buffer.

The measured concentration was $1.6 \text{ mg} \cdot \text{ml}^{-1}$.

A further purification step can be performed by using PBE 94 chromatography.

2. 1. 1 Purification of plasmid DNA

The plasmid pGOmpF was purified by using the QIAprep® Miniprep kit from QIAGEN company.

2. 2 LamB membrane protein

The LamB from *S. Sonnei* was produced using *E. coli* strain pop 154, a derivative of *E. coli* K12, carrying the *malB* gene of *S. Sonnei* 3070 (Roa and Scandella, 1976).

LamB was solubilized from the outer membrane by using octyl-polyoxyethylene (octyl-POE, Alexis, Laufelfingen, Switzerland) as detergent and purified following the procedure analogous to that used for *E. coli* porins (Prilipov *et al.*, 1998).

The purity of the protein was examined by 12% SDS-page gel (Figure 2). The protein concentration was determined by UV-Vis spectrometry at 280 nm against 20mM phosphate buffer and 1% octyl-POE. The measured concentration was $3 \text{ mg} \cdot \text{ml}^{-1}$.

2. 3 NADH:oxydo-reductase (Complex I)

E. coli Complex I was isolated from a strain overproducing Complex I (Spehr and Friedrich, 1999) and kindly provided by Thorsten Friedrich. The protein was stored in 50mM MES/NaOH pH 6, 50mM NaCl, 0.15% Dodecyl-maltoside. The NADH/ferricyanide reductase activity was measured at 410 nm as described above. The enzymatic activity of the NADH:Q reductase was measured at 25 °C by following the reduction of the ferricyanide by NADH at 410 nm. The assays contained 0.300 ml of the vesicles or proteovesicles solution, 0.185 ml of Tris/HCl pH 8 buffer and 5 µl of a 0.1 M

ferricyanide solution. The enzymatic activity was recorded after the addition of 10 μl of a 10 mM NADH solution. The NADH stock solution was prepared freshly for each experiments set. The same measurement was done with the “free” complex I. 5 μl of a 10 $\text{mg}\cdot\text{ml}^{-1}$ stock solution was mixed with 0.485 ml Tris/HCl pH 8 buffer containing 0.1 % Triton X100. (Friedrich *et al.*, 1989).

2. 4 Hemagglutinin (HA)

2. 4. 1 Virus

Hemagglutinin was extracted from the viral recombinant strain X31 of influenza A virus (from plaque C-[Doms, R. W.] which was kept at $-80\text{ }^{\circ}\text{C}$. The virus was grown by the Schweizerisches Serum- und Impfinstitut (Bern, Switzerland) in allantoic cavity of embryonated eggs, and purified, handled and stored as described before (Nebel *et al.*, 1995). The virus stock solution was provided by Toon Stegmann.

2. 4. 2 Preparation of HA Rosettes

After defreezing, the virus suspension was centrifuged at 100 000 g during 30 min. at $4\text{ }^{\circ}\text{C}$. The pellet was resuspended in a buffer containing 145 mM NaCl, 1 mM EDTA, 2.5 mM Hepes pH 7.4 (buffer A) and 2% Triton X100 for 20 min. at $0\text{ }^{\circ}\text{C}$. In order to disaggregate the viruses, the suspension was passed through needles with decreasing sizes (26G, 25G, 22G, and 21G). The procedure was repeated several times. Additional centrifugation at 100 000 g was done for 30 min at $4\text{ }^{\circ}\text{C}$. The supernatant was then applied on a Lectin column (Lectin from *Ricinus communis* (Castor bean) Agglutinin RCA₁₂₀; Matrix: Cross-linked 4% beaded agarose). Extreme precautions were used when using this Lectin column. All eluats of no interest were neutralized by 1 N NaOH solution. The Lectin column was rinsed several times with buffer A containing 2 % Triton X100. The supernatant containing the viral membrane solubilized was applied to the column. The column was then washed 5 times (column volume) to remove the viral lipids. Finally, hemagglutinin was eluted with buffer A containing 0.2 M D(+) galactose. The supernatant was passed through the column several times according to described procedure (Nebel *et al.*, 1995).

In order to obtain the rosette of hemagglutinin the fractions containing hemagglutinin were dialyzed against 1000 X volume of buffer A for 24 h at 4 °C.

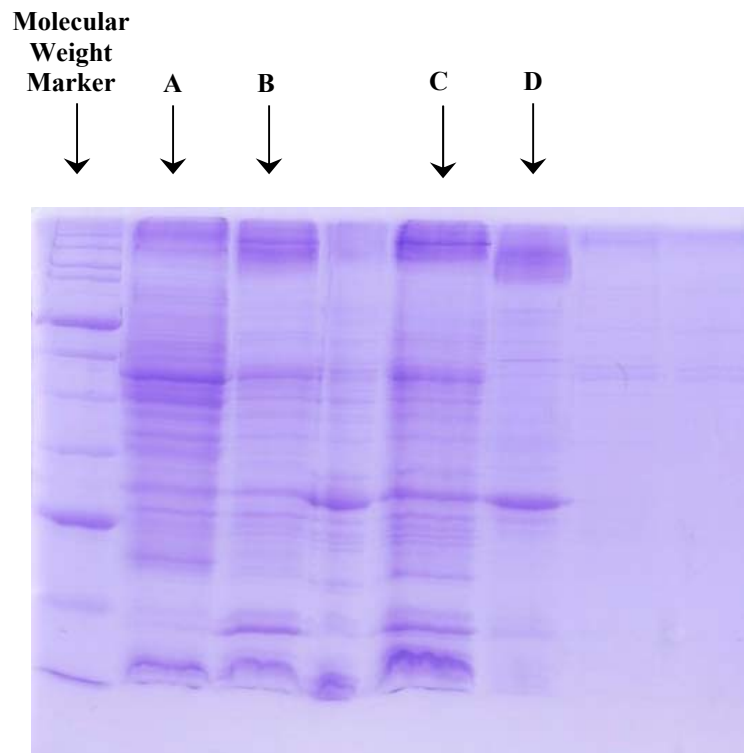


Figure 3. Purity analysis of FhuA Δ 5-160 by 10 % SDS-Page. After each purification steps an aliquot is analysed (**A**, **B**, **C**, **D**). **F** represents purified FhuA Δ 5-160 (61 kDa).

The protein purity was examined on a 12 % SDS-page gel. The protein concentration was determined by the Bradford assay at 595nm by using the Bradford reagent from SIGMA company. Bovine serum albumine (BSA) with known concentration was used as a standard for the titration curve.

2. 5 FhuA Δ 5-160 purification and functionality test

The pellet of the bacteria culture was given by the Ulrich Schwanenberg from the international university of Bremen. We used the same purification procedure than for the FhuA wild type (Locher *et al.*, 1998) (Figure 3). The functionality was tested by the encapsulation of the peroxydase enzyme. The vesicles and proteovesicles were prepared in a 10 mM peroxydase solution in PBS buffer. The non encapsulated enzyme was removed by gel permeation chromatography using a sepharose 4B. After cleaning 0.500 ml of each samples were mixed to 0.250 ml of non-diluted TMB solution (provided by SIGMA company). The reaction was stopped after few minutes by the addition of 0.750 ml of a 2 N HCl solution. Then, the samples were measured by absorbance measurements at 410 nm. The experiments were performed at room temperature.

2. 6 Preparation of λ phages

λ phages were isolated from an infected culture of *E. coli* JM109, which was grown in LB medium supplemented with 0.5 % maltose. After infection overnight, uninfected *E. coli* cells and cell fragments were removed as described (Maniatis).

Phages were collected from the cleared supernatant by ultracentrifugation at 75 000 g for 3 h at 4 °C. The obtained glassy pellet was resuspended in a buffer containing 10 mM MgCl₂ and 10 mM Tris/HCl, pH 8. Typically, this method yields concentrated phage stock solution of 10¹¹-10¹² plaque-forming units·ml⁻¹.

3. PMOXA-PDMS-PMOXA triblock copolymer synthesis and characteristics

3. 1 Polymer used

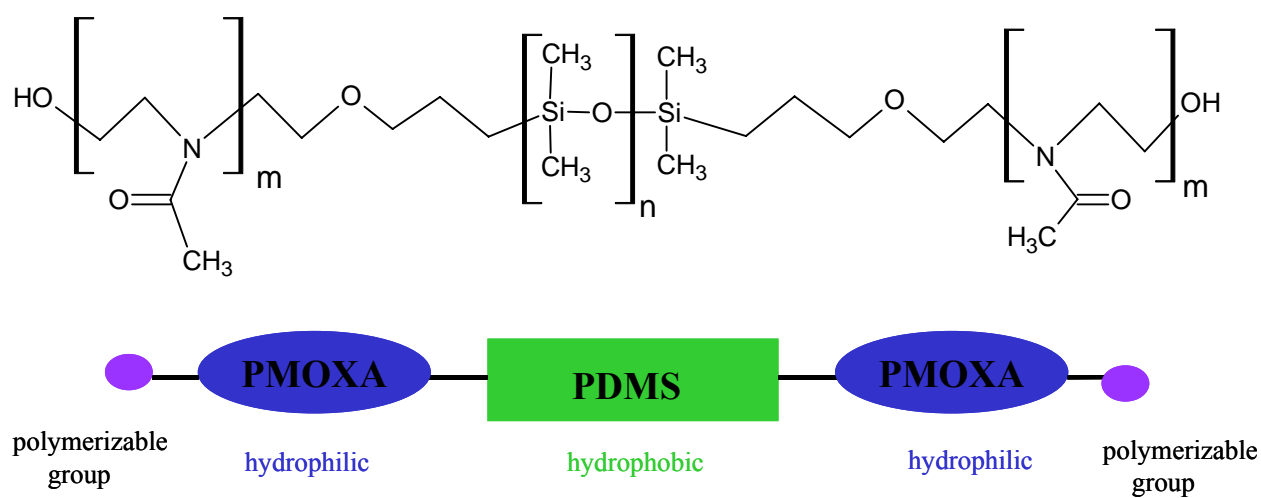


Figure 4. PMOXA-PDMS-PMOXA general chemical formula (without polymerizable end-groups) and its schematical representation

Two batches of triblock copolymer have been used in these studies: HP708 and TDO2. The block composition of both polymer was similar. The HP708 was synthesized by CIBA vision and TDO2 was synthesized in our laboratory.

The middle block PDMS of the HP708 triblock copolymer (α , ω -bis(3-hydroxypropyl) poly(dimethylsiloxane)) was purchased from Wacker Chemie Company and the PDMS middle block of TDO2 came from Aldrich company.

3. 2 Polymer characteristic

Gel permeation chromatography (GPC) in THF revealed the molecular weight of the first triblock copolymer of $M_n = 9000 \text{ g.mol}^{-1}$ and polydispersity of $M_w/M_n = 1.7$. Consequently, the molecular weight of the two poly-dimethylsiloxane blocks was $M_n = 1800 \text{ g.mol}^{-1}$, respectively. The molecular weight of the second triblock copolymer used was of $M_n = 8667 \text{ g.mol}^{-1}$, the molecular weight of the two poly-dimethylsiloxane blocks was $M_n = 1534 \text{ g.mol}^{-1}$. Additionally, both triblock copolymers contain polymerizable methacrylate end groups.

For comparison in the article 3 (chapter 2), another polymer was used: JW03. The molecular weight of the two poly-dimethylsiloxane blocks is $M_n = 1105 \text{ g.mol}^{-1}$, the middle block PDMS (dimethylsiloxane) is $M_n = 1941 \text{ g.mol}^{-1}$.

4. Membrane protein reconstitution in liposomes and triblock copolymer vesicles

4.1 Liposomes, proteoliposomes preparation

4.1.1 OmpF and LamB reconstitution

For both proteins, OmpF and LamB the same reconstitution procedure was performed. 20 mg of a lipid-chloroform stock solution of 10 mg.ml^{-1} was evaporated under high vacuum with rotary evaporation in a glass flask. To remove the traces of chloroform from the lipid film, additional exposure to high vacuum was performed over-night. Afterwards, 20-80 μl of a $1\text{-}3 \text{ mg.ml}^{-1}$ stock solution of OmpF or LamB in 1 % detergent octyl-POE (o-POE) was dispersed on the film and then vortexed to yield a homogeneous mixture, and dried

again for a short period under vacuum. The dry mixed lipid/protein film was dispersed in 1 ml of buffer containing 10 mM Hepes, 100 mM NaCl, pH 7.4. The above procedure results in a dispersion containing multilamellar, polydisperse liposomes. A freeze-thaw cycle was applied to the dispersion, consisting of five cycles of freezing in liquid nitrogen and thawing in water bath at 30 °C.

To obtain unilamellar liposomes of more uniform size, the dispersion was repeatedly extruded through polycarbonate filters (Nucleopore filters (Millipore)) with a pore size of 0.45 µm and 0.22 µm. The size and the polydispersity of the liposome solutions were examined by dynamic light scattering at 90 °.

4. 1. 2 Complex I reconstitution

The reconstitution of Complex I was performed by using biobeads SM2 from BIORAD company. These biobeads absorb detergents (o-POE, Triton X100, etc.) and facilitate the formation of proteoliposomes (Rigaud *et al.*, 1998; Rigaud *et al.*, 1995). The reconstitution of complex I was inspired by method of the Rigaud and al. and by the method used in the group of Weiss, H. (Linke *et al.*, 1986).

The protein solubilized in detergent was admixed to a liposome solution (prepared as described above) in order to obtain the desired protein/ lipid ratio. In a first step the lipid/protein solution was mixed for 2-3 hours at 4 °C before the addition of biobeads. Prior to the biobeads addition these were first cleaned two times with methanol and then washed several times with water (Holloway, 1973). The biobeads amount depends on the choice of detergent (Rigaud *et al.*, 1998). The amount of biobeads was added in three 1 hours steps then the sample was stirred for 6-8 h at 4 °C. The supernatant containing the proteoliposomes was then centrifuged (Heraeus, 5000 rpm during 20 min.) to remove biobeads dust. Gel permeation chromatography was performed to remove the non incorporated proteins.

4. 1. 3 Preparation of fluorescent labelled liposomes

The fluorescent liposomes were prepared in order to test the fusion properties of hemagglutinin when it is reconstituted in polymer vesicles (see § 4. 2. 3).

A chloroformic solution containing respectively egg-phosphatidylcholine, egg-phosphatidylethanolamine, ganglioside in molar ratio (6: 3: 1) and the fluorescent probe NBD-

PE(*N*-(7-nitrobenz-2-oxa-1,3-diazol-4-yl)-1,2-dihexadecanoyl-*sn*-glycero-3-phosphoethanolamine, triethylammonium salt) and *N*-Rh-PE (Lissamine™ rhodamine B 1,2-dihexadecanoyl-*sn*-glycero-3-phosphoethanolamine, triethylammonium salt (or rhodamine DHPE) was evaporated under high vacuum and the obtained lipid film was processed like previously described previously (§ 4. 1. 1).

The solution of fluorescent liposomes was then ready to use for the fusion assays (§ 7. 2. 3. 2.).

4. 2 Protein reconstitution in triblock copolymer vesicles

4. 2. 2 Triblock copolymer vesicles preparation and reconstitution of LamB

4. 2. 2. 1 Triblock copolymer vesicles preparation

Two different methods were applied to prepare the vesicles and the protein-containing vesicles. The first is called “ethanol method” and it is described in the following chapter (§ 4. 2. 2. 2).

The “direct dispersion method”, which is the second method applied here, is based on the “dispersion” of the triblock copolymer (50 mg) directly in buffer solution (4.950 g). This is performed without previous dissolution in organic solvent, like described for the ethanol method. The mixture, polymer + buffer solution, was stirred over-night. The mixture was then extruded through Millipore filters (0.45µm and 0.22 µm) to obtain a monodisperse solution of vesicles and to remove big aggregates.

4. 2. 2. 2 Reconstitution of LamB

The formation of small, unilamellar vesicles from the triblock copolymer could be achieved according to the following procedure. The polymer was dissolved in ethanol to yield a clear, homogeneous solution containing 17 wt % polymer. The solution was then added dropwise under vigorous stirring to the 100 mM KCl, 5 mM MgCl₂, 1 mM CaCl₂, 10 mM Tris/HCl, pH 7.4 buffer solution. This procedure leads to a dispersion of triblock copolymer vesicles of a rather broad size distribution. The vesicle size can be controlled (like liposomes) by applying several extrusion cycles through 0.45 µm and 0.22 µm Nucleopore filters (Millipore). The vesicles containing the LamB porin were prepared by mixing the stock solution of the purified

protein (3 mg.ml⁻¹, 1 % octyl-POE, 100 mM NaCl, 20 mM NaH₂PO₄ pH 7.4) with the 17 wt % solution of the triblock copolymer in ethanol. Afterwards, this mixture was added to the buffer solution as described previously. The non incorporated proteins were removed by gel filtration chromatography on a 1 X 55 cm Sepharose 4B (SIGMA) column.

4. 2. 3 Complex I reconstitution and functionality tests

The biobeads method (Rigaud *et al.*,1995) was applied to reconstitute Complex I in triblock copolymer vesicles. The vesicles were prepared using the “direct dissolution method” (§ 4. 2. 2. 1). The detergent (Triton X 100 0.5 % final concentration) was then added to the solution containing the preformed vesicles. The mixture containing triblock copolymer and detergent was stirred for 1h. Subsequently two sonication cycles of 10 s were performed. Afterwards, the protein (80 µl of a 1mg.ml stock solution) was added to the mixture polymer/ detergent and stirred during 3-6 hrs. Finally, the biobeads were added to the mixture as previously described for the reconstitution in liposomes. The same treatment (centrifugation, gel permeation chromatography) was then applied to obtain the solution of proteovesicles and vesicles.

4. 2. 4 Hemagglutinin reconstitution

The reconstitution of hemagglutinin was inspired by the biobeads method. 30 mg of HP708 ABA triblock copolymer was dissolved in 6 ml of “fusion” buffer pH 7.4 (135 mM NaCl, 15 mM Na citrate, 10 mM MES, 5 mM HEPES, 1 mM EDTA) and 2 % Triton X100. The biobeads were added after complete “dispersion” of the polymer. Hemagglutinin (0.7 mg.ml⁻¹) was added (80 µl) before the addition of bio-beads and incubated with the polymer for 2-3 hrs. The control (vesicles without Hemagglutinin) was prepared in the same way as the sample the protein.

4. 2. 5 FhuAΔ5-160 reconstitution and functionality test

The reconstitution of FhuA was performed following the same procedure as for complex I. FhuA was also reconstituted by using the “ ethanol method “. In this method the protein was not dissolved directly in the polymer-ethanol mixture but injected at the same time as the polymer-ethanol solution into the buffer. The resulting solution was then stirred for few hours at 4 °C.

The vesicles and proteovesicles were prepared in a 10 mM peroxydase solution in PBS. The non encapsulated enzyme was removed by gel permeation chromatography on a sepharose 4B column. After the cleaning step, 0.5 ml of the vesicle or the proteovesicle solutions were mixed with 0.25 ml of TMB (TMB was used without dilution and was provided from SIGMA company). The mixtures were incubated for a given time and the reaction was stopped by the addition of 0.750 ml of a 2 N HCl solution. The samples were the ready for the absorbance measurements at 410 nm. The reaction were performed at room temperature.

5. Dynamic light scattering (DLS)

The dynamic light scattering experiments were performed using a commercial goniometer (ALV-Langen) equipped with a frequency-doubled Nd:YAG laser (ADLAS, wavelength $\lambda=532$ nm) The measurements can be performed at scattering angles between 30 ° and 150 °. The angle of 90 ° was usually chosen for the experiments An ALV-5000/E correlator calculates the photon intensity autocorrelation function $g^2(t)$. The samples were prepared by filtering the solution through Millipore filters (HN 0.45 μm) into 10 mm diameter quartz cells. Cells were further mounted in a thermostated optical matching vat with a temperature accuracy of $T= 0.02$ K. The experiments were performed at $T= 293$ K.

The refractive index increment dn/dc was obtained at the temperature and wavelength corresponding to the light scattering experiments by using a commercial ALV-DR-1 differential refractometer.

The data of DLS were analysed using a Williams-Watts function (Nardin *et al.*, 2000). The size polydispersity of the vesicles was determined according to references of Nardin *et al.*, 2000

6. Langmuir film experiments

The set-up was provided by NIMA company. All the experiments were performed with a Langmuir balance (series 601 BAM). The trough is made of Teflon[®] and has a volume of 300 ml.

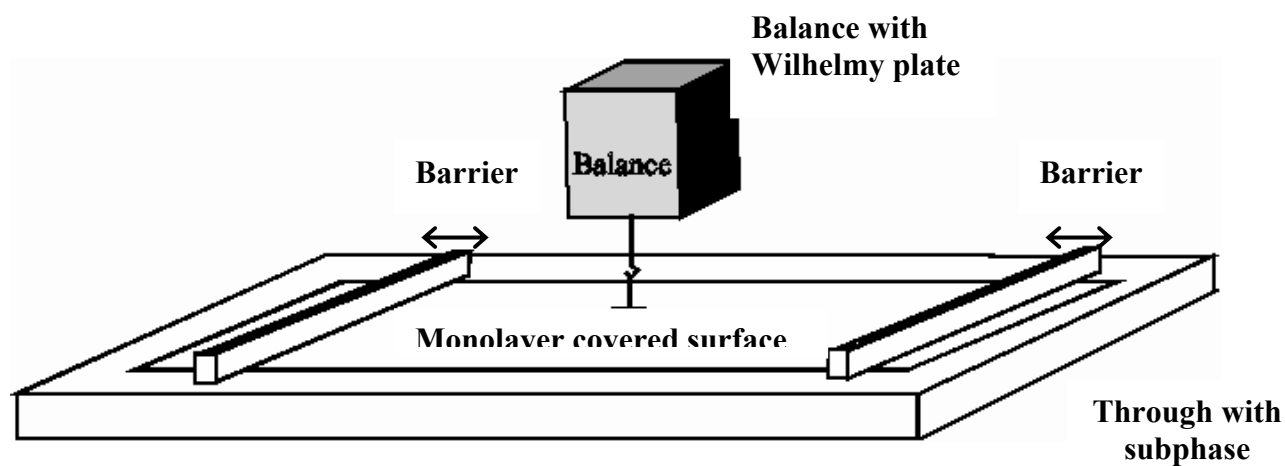
6.1 Surface pressure measurements

Figure 5 a). Schematic illustration of a Langmuir film balance with a Wilhelmy plate (Figure 5 b)) electrobalance measuring the surface pressure, and barriers for reducing the available surface area.

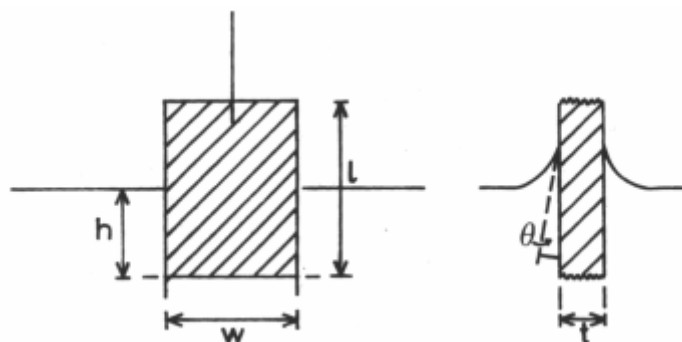


Figure 5 b). A Wilhelmy plate partially immersed in a water surface.

The surface pressure on Nima trough was measured by the Wilhelmy plate-method (Figure 5). The Wilhelmy plate is a strip of chromatography paper (Whatman's Chr 1) which, when suspended at an air-water interface, is pulled down into the bulk of the subphase by the surface tension of the water.

Basic investigation method in the studies of insoluble monolayers at the liquid-air interface involves the measurements of surface pressure (Π) as the function of area per molecule in the film (A) at constant temperature and external pressure. In the equilibrium conditions, surface pressure is defined as difference between surface tension of liquid (water), γ_0 , and the surface tension of liquid covered with a monomolecular film (γ):

$$\Pi = \gamma_0 - \gamma$$

Surface pressure, Π , is often considered as two-dimensional analogue of pressure, ρ .

6.2 Amphiphile spreading

Water-insoluble amphiphilic substances might form monomolecular, insoluble films at the free surface of water or aqueous solution (liquid-air interface). Such films referred to as Langmuir monolayers, are forming after a small volume of the amphiphile solution in a volatile and preferably water-immiscible solvent is spread dropwise on liquid surface. Subsequent solvent evaporation leads to a uniform layer, in which amphiphilic molecules are anchored towards liquid phase with their hydrophilic parts, whereas hydrophobic fragments are exposed towards air.

In these studies, a typical amphiphilic concentration of 1 mg. ml⁻¹ was used. A part from chloroform, various solvents were also studied to get insight into polymer's spreading behaviour.

6.3 Isotherm measurements

We monitored the surface pressure as a function of the area occupied per molecule at the interface. The characteristic of the monolayer on the water surface were studied by measuring the changes in the surface tension upon monolayer compression.

In the case of Langmuir films, surface pressure (Π) is plotted as the function of area per molecule (A), giving Π - A isotherms. The pattern of Π - A depends on the chemical structure

of the amphiphilic substance and on a number of experimental conditions (spreading solvent, compression rate, subphase composition, etc).

The isotherms were recorded at room temperature and with a barrier speed of 100 cm²/ min.

7. Fluorescence spectroscopy

7.1 Steady-state fluorescence

All steady-state fluorescence measurements (emission and excitation spectra, time scan, fluorescence resonance energy transfer (FRET)) were performed using a spectrofluorimeter JASCO F-P-773. In general, the fluorescence intensity measured by the instrument is proportional to the concentration of the fluorophore and this can be expressed as:

$$I_{\text{obs}} = \Phi I_0 (1 - 10^{-\epsilon c \ell})$$

Where I_{obs} is the observed fluorescence, Φ is the quantum yield, ϵ is the molar extinction coefficient, c is the fluorophore concentration and ℓ is the pathlength. However, the total signal from the sample could also be expressed as:

$$S_T = S_F + S_B$$

Where S_T is the total observed light, S_F is the fluorescence signal and S_B is the signal from background and scattered light. As a preliminary experiment the optical density of the solutions was measured in the range from 300 to 800 nm to determine if the scattered light has to be taken in account. The scattered light is considered insignificant under 0.1 in absorbance for fluorescence measurements. For the measurements, slits for emission and excitation were adjusted at 2, 5, 10 or 20 nm, depending on the sample. Sample temperature was controlled by a thermostated bath with a temperature range from 15°C to 60°C. Most of the experiment were done at room temperature (20°C) or at 37°C.

7. 2 Fluorescence resonance energy transfer (FRET)

7. 2. 1 Principle of FRET

Fluorescence resonance energy transfer (FRET) is a distance-dependent interaction between the electronic excited states of two different dye molecules in which excitation transferred from a donor molecule to an acceptor molecule without emission of a photon. The principle of the energy transfer is illustrated figure 1.1.

Figure 1.1: FRET between two molecules.

Föster (Föster, 1959) showed that the efficiency of this process (**E**) depend on the inverse sixth-distance between donor and acceptor:

$$E = 1 / \{1 + (R / R_0)^6\},$$

where **R₀** is the distance at which half of the energy is transferred, and depends on the spectral characteristic of the dyes and their relative orientation. (Stryer and Haugland, 1967) then showed that this could be used as a spectroscopic ruler- that is, by measuring E and knowing or calculating R₀, the distance could be inferred. Because R₀ is typically 20-60 Å, distances on this order can be measured. In general, FRET is better suited for detecting changes in distance (conformation) rather than absolute distance, because E depends on the orientation of the dye molecules, which is often poorly measured. Additionally, E is influenced by the finite probe size and the position at which the probe is attached to biomolecular backbone. FRET is then usually used for investigating a variety of biological phenomena that produce changes in molecular

proximity. Like structure an conformation of proteins, spatial distribution and assembly of protein complexes, distribution and transport of lipids, membrane fusion assays, etc.

7. 2. 2 Prerequisites for FRET

Both donor and acceptor molecules must be in close proximity (10-100 Å).

The absorption spectrum of the acceptor must overlap the fluorescence emission spectrum of the donor (Figure 6).

The donor and acceptor transition dipole orientations must be approximately parallel.

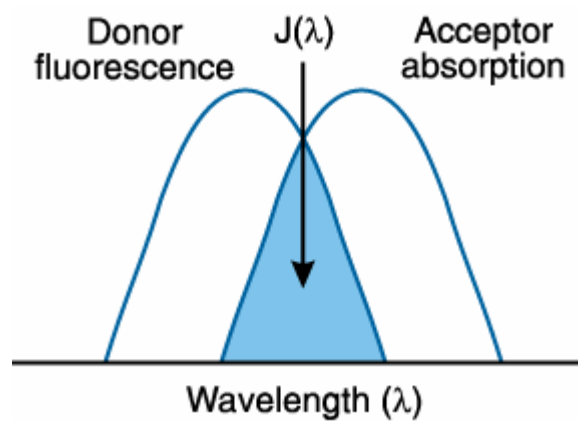


Figure 6: Schematic representation of the FRET spectral overlap integral (www.probes.com).

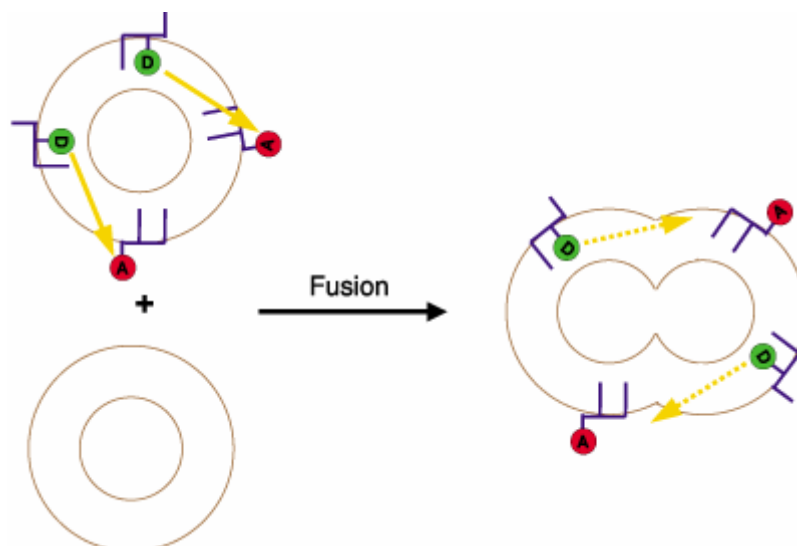


Figure 7: Pictorial representation of a lipid-mixing assay based on fluorescence resonance energy transfer (FRET). The average spatial separation of the donor (D) and acceptor (A) lipid probes increases upon fusion of labelled membranes with unlabeled membranes, resulting in decreased efficiency of proximity-dependent FRET (represented by yellow arrows). Decreased FRET efficiency is registered by increased donor fluorescence intensity and decreased acceptor fluorescence intensity (www.probes.com).

7. 2. 3 Membrane fusion

7. 2. 3. 1 General principle

Struck, Hoekstra and Pagano introduced lipid-mixing assays based on NBD–rhodamine energy transfer. In this method (Figure 7), membranes labelled with a combination of fluorescence energy transfer donor and acceptor lipid probes — typically NBD-PE and *N*-Rh-PE, respectively — are mixed with unlabeled membranes. Fluorescence resonance energy transfer (FRET), detected as rhodamine emission at ~585 nm resulting from NBD excitation at ~470 nm, decreases when the average spatial separation of the probes is increased upon fusion of labelled membranes with unlabelled membranes. The reverse detection scheme, in which FRET increases upon fusion of membranes that have been separately labelled with donor and acceptor probes, has also proven to be a useful lipid-mixing assay.

7. 2. 3. 2 Fusion assays

Fluorescent labelled liposomes were prepared for membrane fusion assays like described previously (§ 4. 1. 3)

8. *Transmission electron microscopy (TEM)*

The samples were examined using a Phillips EM 4000 (100kV) electron microscope with different magnifications.

8.1 Sample preparation

The samples (~ 5 µl) were adsorbed on carbon parlodion composite film on copper grids and negatively stained with 2 % uranyl acetate solution as described by Engel and coworkers (Ringler *et al.*, 2000)

References

- P. W. Anderson, D. L. Stein, in *Self-organization systems* **1987**, (Eds.: I. Yates, F. Eugene), Plenum, New York.
- M. Akeson, D. Branton, J. J. Kasianowicz, E. Brandin, D. W. Deamer, *Biophysical Journal* **1999**, *77*, 3227.
- P. Alexandridis, *Current Opinion in Colloid & Interface Science* **1996**, *1*, 490.
- Y. Anraku, R. B. Gennis, *Trends in Biochemical Sciences* **1987**, *12*, 262.
- Y. Anraku, *Annual Review of Biochemistry* **1988**, *57*, 101.
- M. Antonietti, S. Forster, *Advanced Materials* **2003**, *15*, 1323.
- T. Azzam, A. Raskin, A. Makovitzki, H. Brem, P. Vierling, M. Lineal, A. J. Domb, *Macromolecules* **2002**, *35*, 9947.
- H. Bader, H. Ringsdorf, *Journal of Polymer Science Part a-Polymer Chemistry* **1982**, *20*, 1623.
- G. Bahr, A. Diederich, G. Vergeres, M. Winterhalter, *Biochemistry* **1998**, *37*, 16252.
- P. Bonnafous, T. Stegmann, *Journal of Biological Chemistry* **2000**, *275*, 6160.
- K. A. Borden, K. M. Eum, K. H. Langley, D. A. Tirrell, *Macromolecules* **1987**, *20*, 454.
- C. Branden and J. Tooze, *Introduction to protein Structure*, **1991**, Garland, New York.
- U. Brandt, J. G. Okun, *Biochemistry* **1997**, *36*, 11234.
- U. Brandt, *Biochimica Et Biophysica Acta-Bioenergetics* **1997**, *1318*, 79.
- M. Braun, H. Killmann, V. Braun, *Molecular Microbiology* **1999**, *33*, 1037.
- V. Braun, M. Braun, *Febs Letters* **2002**, *529*, 78.
- M. Braun, H. Killmann, E. Maier, R. Benz, V. Braun, *European Journal of Biochemistry* **2002**, *269*, 4948.
- P. A. Bullough, F. M. Hughson, J. J. Skehel, D. C. Wiley, *Nature* **1994**, *371*, 37.
- K. N. J. Burger, *Traffic* **2000**, *1*, 605.
- V. Chams, P. Bonnafous, T. Stegmann, *Febs Letters* **1999**, *448*, 28.

- A. Charbit, C. Andersen, J. A. Wang, B. Schiffler, V. Michel, R. Benz, M. Hofnung, *Molecular Microbiology* **2000**, 35, 777.
- L. V. Chernomordik, S. S. Vogel, A. Sokoloff, H. O. Onaran, E. A. Leikina, J. Zimmerberg, *Febs Letter* **1993**, 318, 71.
- J. Chiefari, Y. K. Chong, F. Ercole, J. Krstina, J. Jeffery, T. P. T. Le, R. T. A. Mayadunne, G. F. Meijs, C. L. Moad, G. Moad, E. Rizzardo, S. H. Thang, *Macromolecules* **1998**, 31, 5559.
- B. Chu, *Langmuir* **1995**, 11, 414.
- S. W. Cowan, T. Schirmer, G. Rummel, M. Steiert, R. Ghosh, R. A. Pauptit, J. N. Jansonius, J. P. Rosenbusch, *Nature (London, United Kingdom)* **1992**, 358, 727.
- J. Dennig, E. Duncan, *Reviews in Molecular Biotechnology* **2002**, 90, 339.
- F. Devesa, V. Chams, P. Dinadayala, A. Stella, A. Ragas, H. Auboiron, T. Stegmann, Y. Poquet, *European Journal of Biochemistry* **2002**, 269, 5163.
- A. Diederich, G. Bahr, M. Winterhalter, *Physical Review E* **1998**, 58, 4883.
- A. Diederich, G. Bahr, M. Winterhalter, *Langmuir* **1998**, 14, 4597.
- A. Diederich, M. Strobel, W. Meier, M. Winterhalter, *Journal of Physical Chemistry B* **1999**, 103, 1402.
- B. M. Discher, Y.-Y. Won, D. S. Ege, J. C. M. Lee, F. S. Bates, D. E. Discher, D. A. Hammer, *Science (Washington, D. C.)* **1999**, 284, 1143.
- S. Drose, K. Zwicker, U. Brandt, *Biochimica et Biophysica Acta* **2002**, 1556, 65.
- A. Dupuis, I. Prieur, J. Lunardi, *Journal of Bioenergetics and Biomembranes* **2001**, 33, 159.
- M. Engler, T. Anke, O. Sterner, U. Brandt, *Journal of Antibiotics* **1997**, 50, 325.
- J. Falbe, M. Regitz, *Römpf Lexikon Chemie* **1996**, Thieme, Stuttgart
- A. D. Ferguson, E. Hofmann, J. W. Coulton, K. Diederichs, W. Welte, *Science FIELD Publication* Date:1998 Dec 18, 282, 2215.
- S. Foerster, M. Zisenis, E. Wenz, M. Antonietti, *Journal of Chemical Physics* **1996**, 104, 9956.

- T. Forster, *Discussions of the Faraday Society* **1959**, No. 27, 7.
- S. Forster, T. Plantenberg, *Angewandte Chemie, International Edition* **2002**, 41, 688.
- W. Frey, J. Schneider, H. Ringsdorf, E. Sackmann, *Macromolecules* **1987**, 20, 1312.
- T. Friedrich, G. Hofhaus, W. Ise, U. Nehls, B. Schmitz, H. Weiss, *European Journal of Biochemistry* **1989**, 180, 173.
- T. Friedrich, P. Vanheek, H. Leif, T. Ohnishi, E. Forche, B. Kunze, R. Jansen, W. Trowitzschkienast, G. Hofle, H. Reichenbach, H. Weiss, *European Journal of Biochemistry* **1994**, 219, 691.
- T. Friedrich, *Biochimica Et Biophysica Acta-Bioenergetics* **1998**, 1364, 134.
- J. H. Fuhrhop, K. Ellermann, H. H. David, J. Mathieu, *Angewandte Chemie-International Edition in English* **1982**, 21, 440.
- J. H. Fuhrhop, J. Mathieu, *Journal of the Chemical Society-Chemical Communications* **1983**, 144.
- J. H. Fuhrhop, H. H. David, J. Mathieu, U. Liman, H. J. Winter, E. Boekema, *Journal of the American Chemical Society* **1986**, 108, 1785.
- J. H. Fuhrhop, D. Fritsch, *Accounts of Chemical Research* **1986**, 19, 130.
- Garofano, K. Zwicker, S. Kerscher, P. Okun, U. Brandt, *Journal of Biological Chemistry* **2003**, 278, 42435.
- A. Gast, *NATO ASI Ser. Ser. E* **1998**, 303, 311
- A. Graff, M. Winterhalter, W. Meier, *Langmuir* **2001**, 17, 919.
- A. Graff, M. Sauer, P. Van Gelder, W. Meier, *Proceedings of the National Academy of Sciences of the United States of America* **2002**, 99, 5064.
- D. G. Hawthorne, G. Moad, E. Rizzardo, S. H. Thang, *Macromolecules* **1999**, 32, 5457.
- L. D. Hernandez, L. R. Hoffman, T. G. Wolfsberg, J. M. White, *Annual Review of Cell and Developmental Biology* **1996**, 12, 627.

- M. Hofnung, *An Intelligent Channel*, *Science* **1995**, 267, 473
- P. W. Holloway, *Analytical Biochemistry* **1973**, 53, 304.
- F. M. Hughson, *Current Biology* **1995**, 5, 265.
- S. T. Hyde, I. S. Barnes, B. W. Ninham, *Langmuir* **1990**, 6, 1055.
- R. Jahn, T. C. Sudhof, *Annual Review of Biochemistry* **1999**, 68, 863.
- M. K. Jain and R. C. Wagner, *Introduction to biological membrane* **1980**, Wiley, New York.
- R. Jiricek, G. Schwarz, T. Stegmann, *Biochimica Et Biophysica Acta-Biomembranes* **1997**, 1330, 17.
- K.-H. Klotz, I. Bartoldus, T. Stegmann, *Journal of Biological Chemistry* **1996**, 271, 2383.
- P. Kraiczy, U. Haase, S. Gencic, S. Flindt, T. Anke, U. Brandt, G. Von Jagow, *European Journal of Biochemistry* **1996**, 235, 54.
- W. Krebs, J. Steuber, A. C. Gemperli, P. Dimroth, *Molecular Microbiology* **1999**, 33, 590.
- A. Laschewsky, H. Ringsdorf, J. Schneider, *Angewandte Makromolekulare Chemie* **1986**, 145, 1.
- A. Laschewsky, H. Ringsdorf, G. Schmidt, J. Schneider, *Journal of the American Chemical Society* **1987**, 109, 788.
- H. Leif, V. D. Sled, T. Ohnishi, H. Weiss, T. Friedrich, *European Journal of Biochemistry* **1995**, 230, 538.
- M. Lindau, W. Almers, *Current Opinion in Cell Biology* **1995**, 7, 509.
- P. Linke, G. Bechmann, A. Gothe, H. Weiss, *European Journal of Biochemistry* **1986**, 158, 615.
- K. P. Locher, B. Rees, R. Koebnik, A. Mitschler, L. Moulinier, J. P. Rosenbusch, D. Moras, *Cell (Cambridge, Massachusetts)* **1998**, 95, 771.
- P. L. McNeil, R. Khakee, *American Journal of Pathology* **1992**, 140, 1097.
- P. L. McNeil, S. Ito, *Journal of Cell Science* **1990**, 96, 549.

-
- P. L. McNeil, R. A. Steinhardt, *Journal of Cell Biology* **1997**, 137, 1.
- W. Meier, C. Nardin, M. Winterhalter, *Angewandte Chemie, International Edition* **2000**, 39, 4599.
- W. Meier, A. Graff, A. Diederich, M. Winterhalter, *Physical Chemistry Chemical Physics* **2000**, 2, 4559.
- B. Meunier, C. Ortwein, U. Brandt, P. R. Rich, *Biochemical Journal* **1998**, 330, 1197.
- G. S. Moeck, J. W. Coulton, K. Postle, *Journal of biological chemistry FIELD Publication Date:1997 Nov 7*, 272, 28391.
- M. Moffitt, K. Khougaz, A. Eisenberg, *Accounts of Chemical Research* **1996**, 29, 95.
- A. J. Moody, U. Brandt, P. R. Rich, *FEBS Letters* **1991**, 293, 101.
- A. J. Moody, M. Richardson, J. P. E. Spencer, U. Brandt, P. R. Rich, *Biochemical Journal* **1994**, 302, 821.
- J. D. Moroz, P. Nelson, *Biophysical Journal* **1997**, 72, 2211.
- P. Mueller, W. C. Wescott, D. O. Rudin, H. T. Tien, *Journal of Physical Chemistry* **1963**, 67, 534.
- C. Nardin, W. Meier, *Journal of Biotechnology* **2002**, 90, 17.
- C. Nardin, S. Thoeni, J. Widmer, M. Winterhalter, W. Meier, *Chemical Communications (Cambridge)* **2000**, 1433.
- C. Nardin, M. Winterhalter, W. Meier, *Langmuir* **2000**, 16, 7708.
- C. Nardin, T. Hirt, J. Leukel, W. Meier, *Langmuir* **2000**, 16, 1035.
- C. Nardin, W. Meier, *Chimia* **2001**, 55, 142.
- C. Nardin, W. Meier, *Reviews in Molecular Biotechnology* **2002**, 90, 17.
- S. Nebel, I. Bartoldus, T. Stegmann, *Biochemistry* **1995**, 34, 5705.
- R. Neumann, H. Ringsdorf, *Journal of the American Chemical Society* **1986**, 108, 487.
- R. Neumann, H. Ringsdorf, E. V. Patton, D. F. O'Brien, *Biochimica Et Biophysica Acta* **1987**, 898, 338.

-
- H. Nikaido, E. Y. Rosenberg, *Journal of Bacteriology* **1983**, 153, 241.
- H. Nikaido, M. Vaara, *Microbiological Reviews* **1985**, 49, 1.
- S. Ohkuma, B. Poole, *Proceedings of the National Academy of Sciences of the United States of America Publication* ,**1978**, 75, 3327.
- T. Ohnishi, U. Brandt, G. Von Jagow, *European Journal of Biochemistry* **1988**, 176, 385.
- T. Ohnishi, *Biochimica Et Biophysica Acta-Bioenergetics* **1998**, 1364, 186.
- Y. Okahata, T. Kunitake, *Journal of the American Chemical Society* **1979**, 101, 5231.
- J. G. Okun, P. Lummen, U. Brandt, *Journal of Biological Chemistry* **1999**, 274, 2625.
- C. Ortwein, T. A. Link, B. Meunier, A.-M. Colson-Corbisier, P. R. Rich, U. Brandt, *Biochimica et Biophysica Acta* **1997**, 1321, 79.
- K. Pfeiffer, V. Gohil, A. Stuart Rosemary, C. Hunte, U. Brandt, L. Greenberg Miriam, H. Schagger, *Journal of biological chemistry FIELD Publication Date:2003 Dec 26*, 278, 52873.
- A. Prilipov, P. S. Phale, P. Van Gelder, J. P. Rosenbusch, R. Koebnik, *FEMS Microbiology Letters* **1998**, 163, 65.
- D. Raucher, M. P. Sheetz, *Journal of Cell Biology* **2000**, 148, 127.
- D. Raucher, T. Stauffer, W. Chen, K. Shen, S. L. Guo, J. D. York, M. P. Sheetz, T. Meyer, *Cell* **2000**, 100, 221.
- J. L. Rigaud, D. Levy, G. Mosser, O. Lambert, *European Biophysics Journal* **1998**, 27, 305.
- J. L. Rigaud, B. Pitard, D. Levy, *Biochimica et Biophysica Acta* **1995** 1231, 223.
- P. Ringler, B. Heymann, A. Engel, *Membrane Transport* **2000**, 229.
- H. Ringsdorf, B. Schlarb, *Abstracts of Papers of the American Chemical Society* **1986**, 192, 117.
- H. Ringsdorf, G. Schmidt, J. Schneider, in *Thin Solid Films, Vol. 152*, **1987**, pp. 207.
- H. Ringsdorf, B. Schlarb, *Makromolekulare Chemie-Macromolecular Chemistry and Physics* **1988**, 189, 299.

- H. Ringsdorf, B. Schlarb, P. N. Tyminski, D. F. O'Brien, *Macromolecules* **1988**, *21*, 671.
- H. Ringsdorf, B. Schlarb, J. Venzmer, *Angewandte Chemie-International Edition in English* **1988**, *27*, 113.
- T. K. Rostovtseva, T. T. Liu, M. Colombini, V. A. Parsegian, S. M. Bezrukov, *Proceedings of the National Academy of Sciences of the United States of America* **2000**, *97*, 7819.
- D. Scheide, R. Huber, T. Friedrich, *Febs Letters* **2002**, *512*, 80.
- T. Schirmer, T. A. Keller, Y.-F. Wang, J. P. Rosenbusch, *Science (Washington, D. C.)* **1995**, *267*, 512.
- K. Seki, D. A. Tirrell, *Macromolecules* **1984**, *17*, 1692.
- J. Selb, Y. Gallot, in *Developments in Block Copolymers* **1985**, Vol. 2, p. 27 (Ed.: I Goodman), Elsevier, Amsterdam
- T. Segura, L. D. Shea, *Annual Review of Materials Research* **2001**, *31*, 25.
- T. Shanguan, D. Alford, J. Bentz, *Biochemistry* **1996**, *35*, 4956.
- H. Simonnet, J. Demont, K. Pfeiffer, L. Guenaneche, R. Bouvier, U. Brandt, H. Schaeffer, C. Godinot, *Carcinogenesis* **2003**, *24*, 1461.
- V. D. Sled, T. Friedrich, H. Leif, H. Weiss, S. W. Meinhardt, Y. Fukumori, M. W. Calhoun, R. B. Gennis, T. Ohnishi, *Journal of Bioenergetics and Biomembranes* **1993**, *25*, 347.
- V. D. Sled, N. I. Rudnitsky, Y. Hatefi, T. Ohnishi, *Biochemistry* **1994**, *33*, 10069.
- V. Spehr, A. Schlitt, D. Scheide, V. Guenebaut, T. Friedrich, *Biochemistry* **1999**, *38*, 16261.
- T. Stegmann, R. W. Doms, A. Helenius, *Annual Review of Biophysics and Biophysical Chemistry* **1989**, *18*, 187.
- T. Stegmann, J. M. Delfino, F. M. Richards, A. Helenius, *Journal of Biological Chemistry* **1991**, *266*, 18404.
- R. A. Steinhardt, G. Q. Bi, J. M. Alderton, *Science* **1994**, *263*, 390.

-
- L. Stryer, R. P. Haugland, *Proceedings of the National Academy of Sciences of the United States of America* **1967**, *58*, 719.
- M. Takada, T. Yuzuriha, K. Katayama, K. Iwamoto, J. Sunamoto, *Biochimica Et Biophysica Acta* **1984**, *802*, 237.
- D. Y. Takigawa, D. A. Tirrell, *Makromolekulare Chemie-Rapid Communications* **1985**, *6*, 653.
- C. Taupin, M. Dvolaitzky, C. Sauterey, *Biochemistry* **1975**, *14*, 4771.
- D. A. Tirrell, A. B. Turek, D. A. Wilkinson, T. J. McIntosh, *Macromolecules* **1985**, *18*, 1512.
- T. Togo, J. M. Alderton, G. Q. Bi, R. A. Steinhardt, *Journal of Cell Science* **1999**, *112*, 719.
- T. Togo, T. B. Krasieva, R. A. Steinhardt, *Molecular Biology of the Cell* **2000**, *11*, 4339.
- V. P. Torchilin, A. L. Klibanov, N. N. Ivanov, H. Ringsdorf, B. Schlarb, *Makromolekulare Chemie-Rapid Communications* **1987**, *8*, 457.
- F. W. Tse, A. Iwata, W. Almers, *Journal of Cell Biology* **1993**, *121*, 543.
- M. Tsurudome, R. Gluck, R. Graf, R. Falchetto, U. Schaller, J. Brunner, *Journal of Biological Chemistry* **1992**, *267*, 20225.
- Z. Tuzar, P. Kratochvil, in *Surface and Colloid Science* **1993**, (Ed.: E. Matijevic), Plenum, New York
- D. M. Vriezema, J. Hoogboom, K. Velonia, K. Takazawa, P. C. M. Christianen, J. C. Maan, A. E. Rowan, R. J. M. Nolte, *Angewandte Chemie, International Edition* **2003**, *42*, 772.
- G. M. Whitesides, B. Grzybowski, *Science (Washington, DC, United States)* **2002**, *295*, 2418.
- C. Wilhelm, M. Winterhalter, U. Zimmermann, R. Benz, *Biophysical Journal* **1993**, *64*, 121.
- I. A. Wilson, J. J. Skehel, D. C. Wiley, *Nature* **1981**, *289*, 366.
- P. Wingfield, T. Arad, K. Leonard, H. Weiss, *Nature* **1979**, *280*, 696.
- D. V. Zhelev, D. Needham, *Biochimica Et Biophysica Acta* **1993**, *1147*, 89.